論文 / 著書情報
Article / Book Information

題目(和文)	量子アニーリングにおけるスピン系の相転移に対する非疑似古典効果
Title(English)	Non-Stoquastic Effects on Phase Transitions in Spin Systems for Quantum Annealing
著者(和文)	高田珠武己
Author(English)	Kabuki Takada
出典(和文)	学位:博士(理学), 学位授与機関:東京工業大学, 報告番号:甲第11366号, 授与年月日:2020年3月26日, 学位の種別:課程博士, 審査員:西森 秀稔,齋藤 晋,笹本 智弘,古賀 昌久,相川 清隆
Citation(English)	Degree:Doctor (Science), Conferring organization: Tokyo Institute of Technology, Report number:甲第11366号, Conferred date:2020/3/26, Degree Type:Course doctor, Examiner:,,,,
学位種別(和文)	博士論文
Type(English)	Doctoral Thesis

Dissertation

Non-Stoquastic Effects on Phase Transitions in Spin Systems for Quantum Annealing

Kabuki Takada
Department of Physics, Tokyo Institute of Technology

February 27, 2020

Abstract

Quantum annealing is a metaheuristic, a generic approximate algorithm, for solving a combinatorial optimization problem, i.e., the problem of determining the arguments which minimize a function of discrete variables. In quantum annealing, we control the quantum Ising model in a time-dependent manner to obtain the ground state of the Ising Hamiltonian which encodes the solution to a given combinatorial optimization problem. Traditionally, a transverse field has been used as a quantum fluctuation appended to the Ising Hamiltonian.

The presence of a first-order phase transition is a bottleneck of quantum annealing, because it makes the required annealing time exponentially long as a function of the system size. One of the possible candidates for avoidance of first-order transitions is introduction of non-stoquasticity. Here, a Hamiltonian whose every off-diagonal matrix element is real and non-positive is called to be stoquastic, while a non-stoquastic Hamiltonian has a positive or imaginary off-diagonal element. Although non-stoquastic Hamiltonians are known to be difficult to classically simulate due to the sign problem, it does not necessarily mean a speedup of quantum annealing.

In this thesis, we study three models to reveal effects of non-stoquastic interactions on phase transitions and to compare them with those of stoquastic interactions and inhomogeneity in the transverse field. First, we analyze the mean-field weak-strong cluster model using a semi-classical method. We show that a non-stoquastic or stoquastic transverse interaction and inhomogeneous driving of the transverse field can eliminate the first-order transition which exists in the traditional quantum annealing, if appropriately implemented. Second, we analyze the weak-strong cluster model with sparse intercluster interactions by evaluating the partition function in the thermodynamic limit and the zero-temperature limit. We clarify which type of transverse interaction or field removes the first-order transition, as compared with the mean-field case. Third, we perform the real-space renormalization group analysis to study the frustrated Ising ladder in a transverse field with non-stoquastic or stoquastic transverse interactions. The resulting phase diagram is in agreement with numerical methods at the qualitative level and shows that a first-order transition is unavoidable in the presence of the large frustration. We also make a rough prediction that the Hamiltonian with the optimal non-stoquastic transverse interaction might have a slight advantage over stoquastic Hamiltonians in quantum annealing of the frustrated Ising ladder, in the sense that the former possibly reduces the exponential decay rate of the energy gap at the first-order transition as a function of the system size. The analyses presented in this thesis may lead to a better understanding of when and how non-stoquastic interactions enhance the performance of quantum annealing.

Acknowledgments

First of all, I would like to thank my supervisor Prof. Hidetoshi Nishimori for guidance on my researches. The discussion with him has been indispensable for carrying out the study through the three years in the doctoral course. I am very grateful to Prof. Kazutaka Takahashi for comments and discussions on my research works. I thank Prof. Masayuki Ohzeki and Prof. Todd Tilma for comments and discussions in seminars. I also thank the current and previous members of the Nishimori group. My life at Tokyo Institute of Technology has been supported by them.

I am deeply indebted to Prof. Daniel A. Lidar for his support and discussions at the University of Southern California. Studying the frustrated Ising ladder, one of the main topics in this thesis, in his group for about three months was a precious experience. I am grateful to Miriam Snyder for her arrangement of the lodging and her support during my stay. I also thank the members of the Lidar group.

I feel honored to collaborate with Dr. Seiji Yunoki and Dr. Shigetoshi Sota on the project of the frustrated Ising ladder. I acknowledge the financial support through the Research Fellowships of Japan Society for the Promotion of Science for Young Scientists. Finally, I would like to express my gratitude to my family for their continuing support.

Contents

1 Introduction **1**

2 Quantum annealing **9**
2.1 Combinatorial optimization problems 9
2.2 Quantum annealing and phase transition 10
2.3 Introduction of non-stoquasticity 14
2.4 Avoidance of the first-order transition in the ferromagnetic p-spin model . 16

3 Mean-field weak-strong cluster model **19**
3.1 Analysis of an infinite-range system consisting of several subsystems 19
3.1.1 Classical limit 19
3.1.2 Quantum fluctuation 20
3.2 Results for the mean-field weak-strong cluster model 25
3.3 Summary 30

4 Weak-strong cluster model with sparse intercluster interactions **33**
4.1 Analysis of a system with sparse interactions between subsystems 33
4.2 Results for the weak-strong cluster model with sparse intercluster interactions 37
4.3 Summary 39

5 Frustrated Ising ladder **43**
5.1 Introduction to the frustrated Ising ladder 44
5.2 Mapping onto the quantum dimer model 46
5.3 Preliminary analysis 51
5.4 Renormalization group transformation 54
5.4.1 Hamiltonian 54
5.4.2 Block partition and introduction of a projector 55
5.4.3 Construction of the projector 56
5.4.4 Projection of the Hamiltonian 59
5.4.5 Hamiltonian operator on the coarse-grained space 64
5.4.6 Determination of the variational parameters 65
5.4.7 Renormalization group equations 67

5.4.8 Repeat of the renormalization group transformation 68
5.5 Results and their implications for quantum annealing 69
5.6 Summary 76

6 Conclusion **79**

List of publications **83**

References **85**

Chapter 1

Introduction

Spin systems have attracted attention in experimental and theoretical physics. Let us focus on the Ising model as a simple spin system. The Ising model is composed of many spin-1/2 particles and has the energy produced by interactions between the spins and actions of external magnetic fields on the spins. In this model, the interactions and the magnetic fields apply only to the single direction of the spins. The strengths of the interactions and the magnetic fields can depend on the locations of the spins.

It is important that the Ising model expresses not only a spin system but also any system formed by degrees of freedom taking two values with two-body interactions and one-body terms. Not confined to physics, the Ising model has practical applications to computer science. We can regard the problem of finding the ground state of the Ising model as that of seeking the choice which minimizes the cost. Here, the cost is the energy of the Ising model and a number of choices correspond to configurations of the Ising spins.

The problem of finding the optimal choice, or more precisely the problem of determining the arguments which minimize a function of discrete variables, is called a combinatorial optimization problem in computer science [1]. We can represent the cost function (i.e., the function to be minimized) as the energy of the Ising model by transforming the set of discrete variables into a sequence of binary variables. Although the cost function generally has terms of third or more order in the binary variables, it can be reduced to a function containing up to second-order terms [2].

In most real-world applications, the cost function has an extremely complicated structure with many local minima in the configuration space of the variables, which makes it difficult to efficiently solve the combinatorial optimization problem. In terms of the Ising model, there can be a large number of metastable states depending on the coupling constants and the magnetic fields determined by the original cost function.

Quantum annealing [3–9] is a metaheuristic for solving combinatorial optimization problems. A metaheuristic is an algorithm which is generic (i.e., problem-independent) but has no guarantee that the global optimum is output in a fixed time interval. In quantum annealing, we control the transverse-field Ising model in a time-dependent manner to obtain the ground state of the Ising Hamiltonian which is equivalent to a given cost

function. A strong transverse field is appended at the beginning of quantum annealing and then decreased toward zero, while the strength of the Ising Hamiltonian is increased from zero to a finite value. Finally we measure the state of the system, which is a candidate of the ground state of the Ising Hamiltonian. A quantum annealing machine with superconducting flux qubits was implemented several years ago [10].

Although there is no guarantee that quantum annealing yields the true ground state in a fixed computation time, it is possible in the framework of adiabatic quantum computation [11, 12] to estimate the annealing time required to obtain the ground state of a given Ising Hamiltonian. Adiabatic quantum computation is a class of quantum computation in which an adiabatic evolution along the instantaneous ground state is utilized. If the present time-dependent Hamiltonian varies sufficiently slowly, the adiabatic approximation holds. Setting the initial state to the trivial ground state of the initial Hamiltonian, we can make the system adiabatically follow the instantaneous ground state. Then, the final state is nothing but the non-trivial ground state of the final Hamiltonian. The required computation time of adiabatic quantum computation is evaluated as an inverse polynomial of the minimum energy gap between the ground state and the first excited state [8, 12].

In the setting of quantum annealing, only the transverse field constitutes the initial Hamiltonian, which has the trivial ground state (all spins pointing in the transverse direction). The final Hamiltonian is the Ising Hamiltonian, whose ground state corresponds to the solution to the combinatorial optimization problem. Since we need the annealing time which is an inverse polynomial of the minimum energy gap, a rapidly closing gap as a function of the system size is harmful to successfully obtaining the ground state of the Ising Hamiltonian. In particular, the presence of a phase transition is crucial because it involves a vanishing energy gap. It is known from the finite-size scaling theory that the energy gap at a second-order transition decays polynomially as the system size grows [13]. On the other hand, there is empirical evidence that the energy gap at a first-order transition closes exponentially [13]. These facts indicate that a second-order transition imposes only polynomial annealing time, while a first-order transition demands exponentially diverging annealing time. Therefore, the presence of a first-order transition is one of the bottlenecks of quantum annealing.

In the adiabatic quantum computing paradigm, it is significant to find an optimization problem for which the minimum energy gap in the time evolution is at worst an inverse polynomial of the problem size while classical algorithms take exponential time to solve the problem. A possible existence of such a problem means a quantum speedup for that problem. To define classes of quantum speedup, we should be careful what classical algorithms are compared with a quantum algorithm. Let us introduce three types of quantum speedup which are applicable to general quantum algorithms [14,15]: A provable quantum speedup means that there is a rigorous proof that any classical algorithm cannot outperform a given quantum algorithm (Grover's search algorithm [16] belongs to this class). A strong quantum speedup is a speedup over the best classical algorithm, whether

such an algorithm is known or not (Shor's factoring algorithm [17, 18] is in this class). A limited quantum speedup is a speedup over a classical counterpart of a given quantum algorithm. The last type of quantum speedup is often used in the context of quantum annealing. As a classical counterpart of quantum annealing, simulated annealing (the classical Monte Carlo method in which temperature is lowered gradually) [19] or simulated quantum annealing (the quantum Monte Carlo method with the Hamiltonian varied along the schedule of quantum annealing) [5, 20] is usually used.

The limited quantum speedup is the weakest of the three types of speedup; nevertheless, even finding a problem for which quantum annealing has a computational advantage over the quantum Monte Carlo method may be difficult. The reason is that the Hamiltonian in the traditional quantum annealing, namely the transverse-field Ising Hamiltonian, belongs to the class of stoquastic Hamiltonians. Here, a Hamiltonian whose every off-diagonal matrix element is real and non-positive is said to be stoquastic (we typically take the standard basis, in which the Pauli operators have the ordinary matrix elements) [21]. The fact that all the matrix elements of the Gibbs density operator for a stoquastic Hamiltonian are non-negative (i.e., there is no sign problem) allows us to map the system onto a classical system [22] and to apply the quantum Monte Carlo method. This suggests a possibility that quantum annealing with the transverse-field Ising Hamiltonian can be simulated classically. Indeed, there is much evidence that simulated quantum annealing captures essential features of quantum annealing such as computational power and tunneling through energy barriers [5, 20, 23–29].

It should be of course noticed that the absence of the sign problem does not necessarily mean a classical simulatability, since the equilibration time of the quantum Monte Carlo method could be longer than polynomials of the system size. In fact, there is an example of a transverse-field Ising model for which topological obstructions prevent the path-integral quantum Monte Carlo algorithm from equilibrating despite the presence of the energy gap opening inverse polynomially [30]. In addition, an example of a stoquastic Hamiltonian with an inverse polynomial gap which cannot be simulated efficiently by the diffusion quantum Monte Carlo algorithm due to non-topological obstructions is known [31]. In these examples, the adiabatic evolution of quantum annealing takes only polynomial time whereas the quantum Monte Carlo method cannot efficiently simulate its dynamics. This results in at least a limited quantum speedup over simulated quantum annealing. Furthermore, it was shown that quantum annealing for the glued-trees problem [32] with a perturbed tight-binding Hamiltonian, which is stoquastic, can achieve a provable quantum speedup through explicitly utilizing diabatic transitions between the ground and first excited states [33].

Here we introduced examples of quantum annealing with stoquastic Hamiltonians which does not allow classical simulations. However, they are still likely to be exceptional cases. The fact that stoquastic Hamiltonians have no sign problem generally makes it difficult to find a problem for which quantum annealing with a stoquastic Hamiltonian outperforms simulated quantum annealing.

Under the above circumstances, introduction of non-stoquasticity has been suggested as a possible candidate for enhancing the efficiency of quantum annealing. A non-stoquastic Hamiltonian has a positive or imaginary off-diagonal matrix element. The quantum Monte Carlo simulation of a non-stoquastic Hamiltonian is difficult due to the sign problem [34], in which the Gibbs density matrix has a negative or imaginary element. The presence of the sign problem in classical simulation has raised the expectation that non-stoquastic Hamiltonians have stronger quantum effects than stoquastic ones and might achieve increased performance of quantum annealing.

Let us introduce several previous studies on quantum annealing with non-stoquastic Hamiltonians. An example of a bit-permutation symmetric cost function for which a non-stoquastic interaction turns exponentially long annealing time into polynomial time was provided [35]. Numerical simulations of the time-dependent Schrödinger equation for finite-size systems indicated that adding non-stoquastic terms increases the success probability in a small subset of instances of the maximum 2-satisfiability problem (MAX 2-SAT) [36] and of a long-range Ising spin glass problem [37]. Analytical studies of the ferromagnetic p-spin model and the Hopfield model (both of which are infinite-range many-body interacting spin systems, the former containing ferromagnetic interactions and the latter random ones) showed that a transverse antiferromagnetic interaction (which makes the Hamiltonian non-stoquastic) is effective in removing a first-order transition [38–41], leading to an exponential speedup over the traditional quantum annealing. In a recent paper, Albash [42] introduced a mean-field version of the weak-strong cluster problem (also known as the large-spin tunneling problem) [15, 27, 43, 44], which has been used as a benchmark problem in the context of quantum annealing. He carried out numerical diagonalization of the finite-size systems and showed that a non-stoquastic interaction between the two clusters can remove the first-order transition which exists in the traditional quantum annealing. He also constructed a geometrically local Ising model formed by two rings and showed numerically for the small-size systems that a non-stoquastic Hamiltonian has an advantage over stoquastic Hamiltonians.

Another motivation for implementing non-stoquastic Hamiltonians lies in the connection with universal quantum computation [45]. It is known that adiabatic quantum computation with arbitrary Hamiltonians is equivalent to the quantum circuit model in the sense that the latter can efficiently simulate the former [46, 47] and vice versa [48]. Significantly, the Ising Hamiltonian with a transverse field and a transverse interaction in which the magnetic fields and the interactions have spatially inhomogeneous and time-dependent coefficients is sufficient for universal adiabatic quantum computation [49]. On the other hand, adiabatic quantum computation with stoquastic Hamiltonians is thought to be insufficient for universal quantum computation [12, 21] except that utilizing excited states [50] or adaptive single-qubit measurements in non-standard bases [51] enables universal adiabatic quantum computation with stoquastic Hamiltonians.

Toward possible improvements of quantum annealing and realization of universal adiabatic quantum computation, efforts have been put into hardware implementation of tun-

able non-stoquastic interactions. Experimental demonstration of a non-stoquastic Hamiltonian was recently provided on a system of coupled superconducting flux qubits [52].

Of course, there remains a possibility that the efficiency of quantum annealing is enhanced with stoquastic but non-traditional Hamiltonians. Now we introduce two non-traditional protocols with stoquastic Hamiltonians. The first is inhomogeneous transverse-field driving, in which the transverse field is applied inhomogeneously depending on the spatial position of the spin, in contrast to the traditional protocol with the uniform transverse field. A number of previous studies have predicted improvements of the performance of quantum annealing with the inhomogeneous transverse field [53–57]. In addition, analytical studies revealed that inhomogeneous transverse-field driving can eliminate the first-order transition for the ferromagnetic p-spin model [58, 59] and for the Lechner–Hauke–Zoller model [60]. Inhomogeneous transverse-field driving is partly available on the current quantum annealing machine and yielded increased performance for several problems [61, 62].

The second is reverse annealing [63, 64], in which a classical state is initially prepared and then a transverse field is increased from zero to a finite value and decreased to zero. The initial classical state is a candidate for the solution to a combinatorial optimization problem and should be obtained in advance, for example by a classical heuristic. This is in contrast to the traditional quantum annealing, which starts from the uniform superposition of all classical states. The concept of reverse annealing lies in deriving a better solution from the first candidate through quantum fluctuations. For the ferromagnetic p-spin model, studies on the equilibrium statistical mechanics [65] and the dynamics [66] showed that reverse annealing achieves an exponential speedup over the traditional quantum annealing. Reverse annealing has been implemented on the current quantum annealing machine and was used for quantum simulation of a many-body quantum system [67], though the implemented protocol is different from the framework of adiabatic quantum computation in the strict sense [66].

It is worth continuing to explore the effectiveness of these two protocols. However, it may be difficult in a future direction to find a problem for which one of these protocols exhibits a quantum speedup while the traditional quantum annealing does not, since any stoquastic Hamiltonian does not have a sign problem. This implies that studying effects of non-stoquasticity on quantum annealing is still important toward the long-term goal of solving hard optimization problems which cannot be solved by classical algorithms.

In spite of such an implication, when non-stoquastic Hamiltonians achieve increased performance compared to the traditional quantum annealing and/or classical algorithms and what types of non-stoquastic interaction enhance the efficiency of quantum annealing are open problems. Although the transverse-field Ising model with transverse interactions is universal in the sense of quantum computation [49], the optimal values of transverse interactions are highly non-trivial when adiabatic quantum computation is regarded as a metaheuristic solver of combinatorial optimization problems.

Needless to say, one of the obstacles to investigate non-stoquastic effects is the sign

problem in the quantum Monte Carlo scheme [34]. This motivates analytical approaches to phase transitions of spin systems with non-stoquastic Hamiltonians, which are strongly connected with the efficiency of quantum annealing as explained above. In this direction, it is noteworthy that quantum annealing with a non-stoquastic transverse interaction [38,39, 41] as well as inhomogeneous transverse-field driving [58,59] and reverse annealing [65,66] gains an exponential speedup over the traditional quantum annealing for the ferromagnetic p-spin model. However, the energy landscape of this model is extremely simple thanks to its mean-field nature and does not represent a realistic situation. In addition, this model has infinite-range many-body interactions, which are far from implementation on real devices.

Hence, it is desirable in the next stage to analyze effects of non-stoquastic interactions on phase transitions for a problem with few-body interactions of sparse connectivity. This thesis ultimately aims to take a step toward understanding of non-stoquastic effects on phase transitions of such spin systems.

To achieve this purpose, we study three models. All of them have only two-body interactions and magnetic fields. For the third model, interactions are spatially local, which means sparse connectivity. These models have transverse-field Ising Hamiltonians with transverse interactions. We consider the Hamiltonians with non-stoquastic (antiferromagnetic) transverse interactions and also compare them with the stoquasticized Hamiltonians, which have stoquastic (ferromagnetic) transverse interactions (here, "stoquasticizing" means replacing the off-diagonal matrix elements with their absolute values times minus one). In addition, we partly include inhomogeneity in the transverse field for comparison.

The first model is the mean-field weak-strong cluster model formulated in Ref. [42]. This model is a two-body interacting quantum Ising model which consists of the weak cluster and the strong cluster. There are longitudinal fields and infinite-range ferromagnetic interactions. The longitudinal fields in the two clusters point in opposite directions and the longitudinal field in the weak cluster has a smaller strength than that in the strong cluster. We analyze the model by a semi-classical method and confirm the numerical conclusion [42] that a non-stoquastic interaction between the clusters with an appropriate strength eliminates the first-order transition which occurs in the traditional quantum annealing. We also calculate the energy gap between the ground and first excited states and find the result which is consistent with the numerical result [42]. In addition, we see that the removal of the first-order transition is achieved either by a non-stoquastic or stoquastic interaction depending on whether the interaction is introduced within the weak cluster, within the strong cluster, or between the clusters. We further demonstrate that inhomogeneous driving of the transverse field is effective in avoiding the first-order transition. Here, inhomogeneity means that the transverse field is driven more quickly in one of the clusters than in the other.

The second model is the weak-strong cluster model in which the interactions between the clusters are replaced with sparse (not all-to-all) interactions. We analyze the

model using the imaginary-time path-integral formulation of the partition function and the saddle-point method with the static ansatz. Then, we show that a non-stoquastic or stoquastic interaction can remove the first-order transition if appropriately implemented. In the case of the inhomogeneous transverse field, we find results which are similar to those in the mean-field weak-strong cluster model.

The third model is the frustrated Ising ladder in a transverse field with transverse interactions. The version without the transverse interactions was proposed by Laumann *et al.* [68], who showed by numerical diagonalization of the small-size systems that varying the transverse field causes a first-order transition which originates in the topological nature of the model. The model is a quasi-one-dimensional system and has only spatially local two-body interactions and magnetic fields. Thus, this model is much closer to experimental realization than the former two models, though no quantum annealing machine with a transverse interaction is available to us at the present time. The Ising Hamiltonian consists of interactions and a magnetic field which lead to frustration, and another field which splits the energy level between different topological sectors. We analyze the model with the transverse field and the transverse interactions by the real-space renormalization group method. Instead of using the standard method [69], we propose a way to correctly keep contributions of the low-energy states to the coarse-grained space in the present system with large frustration. We unfortunately find that neither non-stoquastic nor stoquastic transverse interactions eliminate the first-order transition at least in the limit of the large frustration. The resulting phase diagram is compared with the result of numerical diagonalization [68] and that of the density-matrix renormalization group (DMRG) method [70]. We finally make a rough prediction that the case of the non-stoquastic transverse interactions might have a slight advantage in quantum annealing over the case of no transverse interactions and that of the stoquastic transverse interactions, though the energy gap in all of the cases is most likely to be exponentially small as a function of the system size.

This thesis is organized as follows: Chapter 2 gives fundamentals of quantum annealing. In Chapter 3, we analyze the mean-field weak-strong cluster model after describing a semi-classical method for an infinite-range system formed by several clusters. In Chapter 4, we provide the method of analyzing a system with sparse interactions between clusters and apply it to the weak-strong cluster model with sparse intercluster interactions. Chapter 5 is devoted to the real-space renormalization group analysis of the frustrated Ising ladder as well as a review of its basic properties. Chapter 6 concludes the thesis.

Chapters 3–5 play principal roles in this thesis. Chapters 3 and 4 are based on the author's work with Yu Yamashiro and Hidetoshi Nishimori [71]. Chapter 5 is grounded on the author's work with Hidetoshi Nishimori and Daniel A. Lidar.

In this thesis, we set the velocity of light c, the reduced Planck constant $\hbar$, and the Boltzmann constant k_{B} to unity.

Chapter 2

Quantum annealing

We provide basics of quantum annealing in this chapter. In Section 2.1, we introduce a combinatorial optimization problem and demonstrate how to map the problem onto the problem of finding the ground state of the Ising Hamiltonian using a well-known example. In Section 2.2, we explain the traditional quantum annealing and its relationship to phase transitions, in which the way to experimentally realize quantum annealing is briefly mentioned. Section 2.3 gives the background of non-stoquasticity from the viewpoint of quantum annealing and adiabatic quantum computation. In Section 2.4, we review how to avoid the first-order transition in the ferromagnetic p-spin model as a simple example.

2.1 Combinatorial optimization problems

Determining the arguments which minimize a given function of discrete variables has central importance in computer science. This sort of problem is referred to as a combinatorial optimization problem [1]. The function to be minimized is called the cost function. For most practical combinatorial optimization problems, the cost function has a highly complicated structure with many local minima, so that one will experience tremendous difficulty finding the global minimum of the cost function, i.e. the optimal solution.

Let us represent the set of the discrete variables as an N-bit binary number, which is translated into a sequence of N Ising variables taking the values ± 1. Although the cost function is generally written as an expansion up to Nth order in the Ising variables, we can reduce it to the sum of first- and second-order terms [2]. Then, we can regard the cost function as the energy of the Ising model. This means that solving the combinatorial optimization problem is nothing but the task of finding the ground state of the Ising model with coupling constants and local magnetic fields depending on the problem.

To see the difficulty of a combinatorial optimization problem caused by a complicated structure of the cost function, let us consider the traveling salesperson problem as a well-known example. This problem is the question of which the shortest course is, on the condition that a salesperson visits n cities and finally goes back to the starting point. We

show an example of the case of $n = 4$ in Fig. 2.1(a). Since there are $n!/(2n)$ courses except for the choices of the starting point and the direction in which the salesperson goes, the number of the possible courses diverges factorially with an increase in n.

The cost function of the traveling salesperson problem is given by [72, 73]

$$H_{\rm p}(\{x_{ij}\}) = A \sum_{i,i',j=1}^{n} d_{ii'} x_{ij} x_{i',j+1} + B \sum_{i=1}^{n} \left(\sum_{j=1}^{n} x_{ij} - 1 \right)^2 + C \sum_{j=1}^{n} \left(\sum_{i=1}^{n} x_{ij} - 1 \right)^2 , \quad (2.1)$$

where $x_{ij} = 0, 1$ $(i, j = 1, \ldots, n)$ are binary variables on which the periodic boundary conditions $x_{i,n+1} = x_{i1}$ are imposed for all i, $d_{ii'}$ are the distances between the cities i and i', and A, B, and C are positive parameters. The variable x_{ij} is one if the salesperson visits the city i at the jth time and zero otherwise. We show in Fig. 2.1(b) the schematic diagram of the matrix (x_{ij}) in the case where the salesperson visits the cities 1, 4, 3, and 2 in order (we denote this itinerary by $1 \to 4 \to 3 \to 2$ and the others by similar symbols). By converting the binary variables into the Ising variables $Z_{ij} = 1 - 2x_{ij} = \pm 1$, we can regard this cost function as the Ising Hamiltonian with the system size $N = n^2$.

The first term of the Hamiltonian (2.1) is the distance through the whole of the course. The second term represents the condition that the salesperson visits each city only once, because this term is minimized when $\sum_j x_{ij} = 1$ for all i. Minimizing the third term means that $\sum_i x_{ij} = 1$ for all j and imposes the condition that the salesperson can visit only one city at the same time. Since the constraints imposed by the second and third terms must be satisfied at any cost, the parameters B and C should be sufficiently larger than A.

We depict in Fig. 2.1(c) the cost function (2.1) for the example defined by Fig. 2.1(a), where we set $A = 1$, $B = 10$, and $C = 10$ and converted a sequence of the binary variables $x_{11} \cdots x_{14} x_{21} \cdots x_{24} x_{31} \cdots x_{34} x_{41} \cdots x_{44}$ to a decimal number x. The eight red lines in Fig. 2.1(c) indicate $2n = 8$ itineraries which minimize the cost function.

Figure 2.1(d) is an enlargement of Fig. 2.1(c) near $x = 33{,}060 = 2^{15}+2^8+2^5+2^2$, which corresponds to the binary number 1000 0001 0010 0100 and the itinerary $1 \to 4 \to 3 \to 2$ depicted in Fig. 2.1(b). There are many local minima in Fig. 2.1(d) in spite of much narrower region of x than the whole region depicted in Fig. 2.1(c). This complicated structure of the cost function makes it difficult to solve the combinatorial optimization problem.

2.2 Quantum annealing and phase transition

Quantum annealing [3–9] is a metaheuristic which solves combinatorial optimization problems and was first proposed as a quantum version of simulated annealing [19]. To find the optimal solution, quantum annealing utilizes quantum fluctuations while simulated annealing uses thermal fluctuations controlled by temperature. Before quantum annealing is applied, a given combinatorial optimization problem is converted to the problem

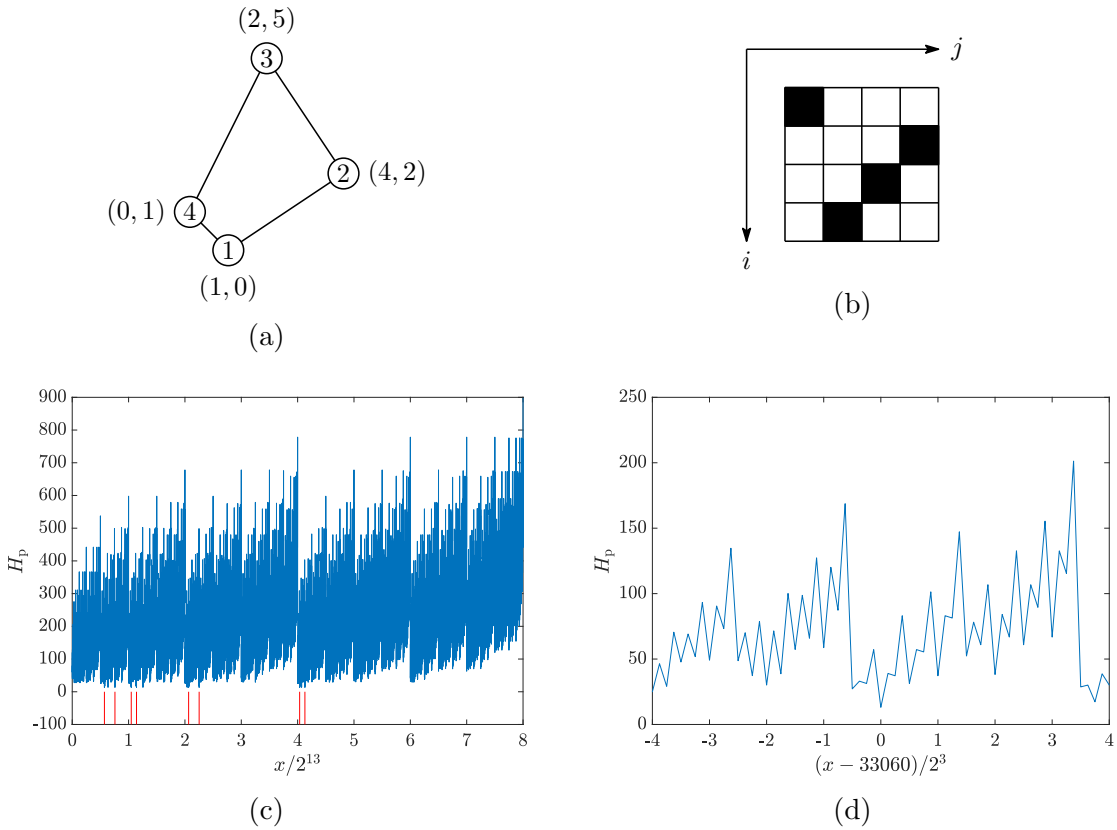

Figure 2.1: The traveling salesperson problem for four cities. (a) Cities are located at the coordinates denoted by the sets of numbers in the parentheses. The numbers in the circles indicate the city numbers i. The four line segments constitute the shortest course. (b) Schematic diagram of the matrix (x_{ij}). The white and black squares stand for $x_{ij} = 0$ and $x_{ij} = 1$, respectively. This example represents the itinerary $1 \to 4 \to 3 \to 2$. (c) The blue line indicates the cost function H_p of the decimal variable x for the example defined by (a). We set $A = 1$, $B = 10$, and $C = 10$. The red lines denote the values of x minimizing the cost function and correspond to the itineraries $4 \to 3 \to 2 \to 1$, $2 \to 3 \to 4 \to 1$, $3 \to 4 \to 1 \to 2$, $3 \to 2 \to 1 \to 4$, $4 \to 1 \to 2 \to 3$, $2 \to 1 \to 4 \to 3$, $1 \to 4 \to 3 \to 2$, and $1 \to 2 \to 3 \to 4$ from left to right. (d) Enlargement of (c) near $x = 33{,}060$, which corresponds to the itinerary $1 \to 4 \to 3 \to 2$.

of determining the ground state of the Ising Hamiltonian in the manner explained in the previous section. In the traditional quantum annealing, we append at the initial time a strong transverse magnetic field to make the state of the system an equally weighted superposition of all eigenstates of the Ising Hamiltonian, and decrease the transverse field for the system to tunnel potential barriers in the cost function and to reach the ground state of the Ising Hamiltonian.

Suppose that the cost function is written as the Ising Hamiltonian

$$\hat{H}_{\rm p} = \sum_{i,j=1}^{N} J_{ij}\hat{Z}_i\hat{Z}_j + \sum_{i=1}^{N} h_i\hat{Z}_i. \tag{2.2}$$

Here, J_{ij} and h_i denote coupling constants and longitudinal fields, respectively, and $\hat{X}_i$, $\hat{Y}_i$, and $\hat{Z}_i$ are the Pauli operators at site $i = 1, \ldots, N$. The traditional quantum annealing Hamiltonian is given by the time-dependent transverse-field Ising model

$$\hat{H}(s) = K(s)\hat{H}_{\rm p} - \Gamma(s)\sum_{i=1}^{N}\hat{X}_i, \tag{2.3}$$

where $s = t/t_{\rm f} \in [0, 1]$ is the dimensionless time and $t_{\rm f}$ is the computation time of quantum annealing. The system obeys the time-dependent Schrödinger equation

$$i\frac{d\,|\psi(s)\rangle}{ds} = t_{\rm f}\hat{H}(s)\,|\psi(s)\rangle\,, \tag{2.4}$$

where $|\psi(s)\rangle$ denotes the state of the system at dimensionless time s.

At the beginning of quantum annealing $s = 0$, we apply the transverse field $\Gamma(0) > 0$ and set $K(0) = 0$, which makes all the spins point in the x-direction. Then, we decrease the transverse field $\Gamma(s)$ and increase the strength of the problem Hamiltonian $K(s) \geq 0$ with time s. At the end of the computation $s = 1$, we remove the transverse field, i.e., set $\Gamma(1) = 0$. The Ising Hamiltonian $\hat{H}_{\rm p}$ (or $K(s)\hat{H}_{\rm p}$) is called the problem Hamiltonian, while the transverse field $-\Gamma(s)\sum_i \hat{X}_i$ is called the driver Hamiltonian. In the next section, we will consider a driver Hamiltonian including other terms than the transverse field.

A quantum annealing machine (to be called a quantum annealer) was experimentally implemented several years ago [10]. The quantum annealer is formed by rf SQUIDs (radio-frequency superconducting quantum interference devices) [74,75], which are superconducting rings with Josephson junctions mounted [76] as shown in Fig. 2.2(a). An rf SQUID has a double-well potential $V(\Phi)$ as a function of the magnetic flux Φ through the ring and can be used as a qubit (quantum bit) because we can effectively regard the state space of this system as a two-state space spanned by the low-energy states localized at the two wells [77], as depicted in Fig. 2.2(b). A qubit is a quantum two-state system and allows a superposition of the states $\alpha\,|0\rangle + \beta\,|1\rangle$ ($\alpha, \beta \in \mathbb{C}$) unlike a classical bit constituted only by the two states $|0\rangle$ and $|1\rangle$. Although the actual rf-SQUID qubit

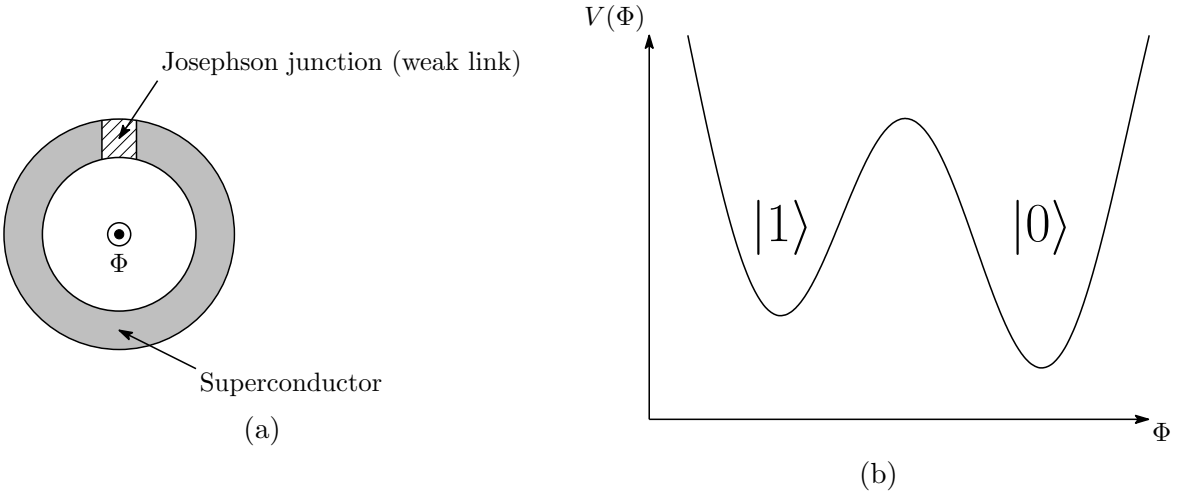

Figure 2.2: (a) An rf SQUID, a superconducting ring which includes a single Josephson junction as a weak link. The magnetic flux through the ring is denoted by Φ. (b) Double-well potential of an rf SQUID. The ground states $|0\rangle$ and $|1\rangle$ for the two wells span an effective two-state space.

used for the quantum annealer includes two superconducting loops and there are two flux degrees of freedom per qubit, we can approximately treat this rf-SQUID qubit as a one-dimensional system with the flux Φ for a sufficiently small inductance of the second loop (see Supplementary information of Ref. [10]).

How long do we need to perform quantum annealing to solve a combinatorial optimization problem? Now we consider the closed spin system with the transverse-field Ising Hamiltonian (2.3) at zero temperature. Then, we can estimate the required computation time $t_{\rm f}$ for quantum annealing in its implementation as adiabatic quantum computation [11, 12]. The adiabatic approximation for the time-dependent Schrödinger equation is valid, provided that the changes of the coefficients $\Gamma(s)$ and $K(s)$ are sufficiently slow. In particular, the adiabatic time evolution of the system follows the instantaneous ground state of $\hat{H}(s)$ when we set the initial state to the trivial ground state of $-\sum_i \hat{X}_i$ (all spins pointing in the x-direction). At the end of annealing $s = 1$, the system is in the ground state of $\hat{H}_{\rm p}$, which is the solution to the combinatorial optimization problem.

The traditional condition for adiabaticity is written as [8]

$$t_{\rm f} \gg \frac{1}{\Delta_n(s)^2} \left| \left\langle n(s) \left| \frac{d\hat{H}(s)}{ds} \right| 0(s) \right\rangle \right| \quad (\forall n > 0, \quad \forall s \in [0,1]), \tag{2.5}$$

where $|n(s)\rangle$ are the instantaneous eigenstates of $\hat{H}(s)$ with the eigenvalues $\varepsilon_n(s)$ (assumed to be in ascending order $\varepsilon_0(s) < \varepsilon_1(s) < \cdots$) and $\Delta_n(s) = \varepsilon_n(s) - \varepsilon_0(s)$ are the energy gaps between the ground state and the excited states (see, e.g., Ref. [12] for more strict adiabatic conditions). The adiabatic condition implies that a phase transition of the

system is detrimental to quantum annealing, because the energy gap between the ground and first excited states $\Delta_1(s)$ vanishes at the transition point and the computation time $t_{\rm f}$ diverges.

In the application to combinatorial optimization problems, the number of spins N is finite and a positive value of the energy gap remains. Hence, how rapidly the minimum energy gap $\Delta = \min_s \Delta_1(s)$ decays as a function of N is used for evaluating the required computation time $t_{\rm f}$. For a second-order phase transition, the minimum gap obeys the power law $\Delta \sim N^{-a}$ with a constant a [13] and the computation time $t_{\rm f}$ increases polynomially as N increases. Even worse, it is empirically known that a first-order phase transition imposes an exponential decrease on the minimum gap as $\Delta \sim \exp(-bN)$ (b is a constant) [13] and an exponential increase on the computation time $t_{\rm f}$, though there are a few exceptions [78–80]. This indicates that the presence of a first-order phase transition is a bottleneck of quantum annealing.

2.3 Introduction of non-stoquasticity

In the previous section, we explained that a first-order transition of the spin system causes a drop in the efficiency of quantum annealing. One of the possible candidates for improving the performance of quantum annealing is the use of a non-stoquastic Hamiltonian. Let us define a stoquastic Hamiltonian: If a Hamiltonian obeys the condition that all off-diagonal matrix elements in a product basis of local states are real and non-positive, then the Hamiltonian is stoquastic [21]. Conversely, a non-stoquastic Hamiltonian has a positive or imaginary off-diagonal element. Notice that we have the arbitrariness with the choice of the product basis because we can change the local basis at each site unitarily. This means that the concept of stoquasticity is dependent on what basis is chosen.

The transverse-field Ising Hamiltonian given by Eq. (2.3) is stoquastic in the standard basis $\{\,|\{Z_i\}\rangle\,; Z_i = \pm 1\}$. Here, $|\{Z_i\}\rangle = \bigotimes_{i=1}^{N} |Z_i\rangle$ is the product state of the local states $|Z_i\rangle$ in which the Pauli operators have the matrix elements

$$\hat{X}_i \doteq \begin{pmatrix} 0 & 1 \\ 1 & 0 \end{pmatrix}, \quad \hat{Y}_i \doteq \begin{pmatrix} 0 & -i \\ i & 0 \end{pmatrix}, \quad \hat{Z}_i \doteq \begin{pmatrix} 1 & 0 \\ 0 & -1 \end{pmatrix}, \tag{2.6}$$

where $\doteq$ denotes the correspondence between an operator and a matrix. How can we construct a non-stoquastic Hamiltonian for quantum annealing? One of the simplest ways is to append the transverse antiferromagnetic interaction $+\hat{X}_i\hat{X}_j$ to the transverse-field Ising model, which changes the Hamiltonian into a non-stoquastic one. To emphasize that this interaction makes the Hamiltonian non-stoquastic, we call the transverse antiferromagnetic interaction the non-stoquastic XX interaction, while the transverse ferromagnetic interaction $-\hat{X}_i\hat{X}_j$ is called the stoquastic XX interaction. Experimental implementation of non-stoquastic interactions was recently demonstrated [52].

Let us explain why it has been suggested that non-stoquasticity enhances the efficiency of quantum annealing. We are first aware that every matrix element of the Gibbs density

operator $\hat{\rho} = e^{-\beta\hat{H}}/\operatorname{Tr} e^{-\beta\hat{H}}$ for a stoquastic Hamiltonian $\hat{H}$ and any inverse temperature $\beta \geq 0$ is non-negative [21]. This is because we can choose a sufficiently large constant C such that all of the matrix elements of $C - \beta\hat{H}$ are non-negative and we find that the operator

$$Z\hat{\rho} = e^{-\beta\hat{H}} = e^{-C}e^{C-\beta\hat{H}} = e^{-C}\sum_{k=0}^{\infty}\frac{(C-\beta\hat{H})^k}{k!} \tag{2.7}$$

has non-negative matrix elements, where $Z = \operatorname{Tr} e^{-\beta\hat{H}} > 0$ denotes the partition function. Then, we derive the classical expression of the partition function Z by the Suzuki-Trotter decomposition [22] if the Hamiltonian $\hat{H}$ is stoquastic:

$$\begin{aligned} Z &= \operatorname{Tr} e^{-\beta\hat{H}} = \lim_{M\to\infty}(e^{-\beta\hat{H}/M})^M \\ &= \lim_{M\to\infty}\sum_{\{Z_{i,\mu}=\pm1\}}\prod_{\mu=1}^{M}\langle\{Z_{i,\mu+1}\}_i|e^{-\beta\hat{H}/M}|\{Z_{i,\mu}\}_i\rangle = \lim_{M\to\infty}\sum_{\{Z_{i,\mu}=\pm1\}} e^{-S}, \end{aligned} \tag{2.8}$$

where we inserted the resolution of the identity in the basis $\{\,|\{Z_i\}\rangle\,\}$ between the Boltzmann factors $e^{-\beta\hat{H}/M}$, imposed the periodic boundary condition $Z_{i,\mu} = Z_{i,\mu+M}$, and defined

$$e^{-H_{\rm cl}(\{Z_{i,\mu+1}\}_i,\{Z_{i,\mu}\}_i)} = \langle\{Z_{i,\mu+1}\}_i|e^{-\beta\hat{H}/M}|\{Z_{i,\mu}\}_i\rangle\,, \tag{2.9}$$

$$S = \sum_{\mu=1}^{M} H_{\rm cl}(\{Z_{i,\mu+1}\}_i, \{Z_{i,\mu}\}_i). \tag{2.10}$$

Since the action S is expressed in terms of the classical Ising variables $Z_{i\mu} = \pm1$ at site $i = 1, \ldots, N$ and discrete imaginary time $\mu = 1, \ldots, M$, we can use the quantum Monte Carlo method to investigate the properties of the system determined by the quantum Hamiltonian $\hat{H}$. We should notice that it is only when $\hat{H}$ is stoquastic that we can simulate the quantum system classically in the above manner, because the matrix elements of the Boltzmann factor $e^{-\beta\hat{H}/M}$ need to be non-negative in order to represent the elements as the exponential functions of the real classical Hamiltonian $H_{\rm cl}$ as in Eq. (2.9). The term "stoquastic" comes from the fact that stochastic processes such as the Metropolis algorithm [81] can efficiently simulate the quantum Hamiltonian $\hat{H}$ [21].

For a non-stoquastic Hamiltonian $\hat{H}$, the Boltzmann factor $e^{-\beta\hat{H}/M}$ has matrix elements with negative signs, or more generally complex elements. This is called the sign problem. The sign problem makes it difficult to classically simulate the quantum system [34], which implies that non-stoquastic Hamiltonians, in some sense, yield stronger quantum effects than stoquastic ones. For this reason, it has been expected that introduction of non-stoquasticity improves the efficiency of quantum annealing.

As described in the previous chapter, there are a number of previous studies on advantages of non-stoquastic Hamiltonians in quantum annealing [35–42]. In particular, the avoidance of the first-order transition in the ferromagnetic p-spin model [38, 39, 41] will

be reviewed in the next section. In addition, the mean-field weak-strong cluster model which was formulated and numerically studied in Ref. [42] is the main topic in the next chapter.

From the viewpoint of quantum computation, introduction of non-stoquasticity is important in connection with universal quantum computation [45]. Since adiabatic quantum computation can efficiently simulate the quantum circuit model [48] (and vice versa [46, 47]), we can perform universal quantum computation in the framework of adiabatic quantum computation. Furthermore, it is known that the Ising Hamiltonian with the transverse field and the XX interaction

$$\hat{H}(s) = \sum_{i,j=1}^{N} J_{ij}(s)\hat{Z}_i\hat{Z}_j + \sum_{i,j=1}^{N} \Xi_{ij}(s)\hat{X}_i\hat{X}_j + \sum_{i=1}^{N} h_i(s)\hat{Z}_i + \sum_{i=1}^{N} \Gamma_i(s)\hat{X}_i \tag{2.11}$$

is sufficient for universal adiabatic quantum computation [49]. Here, the coefficients $J_{ij}(s)$, $\Xi_{ij}(s)$, $h_i(s)$, and $\Gamma_i(s)$ are spatially inhomogeneous and time-dependent. The universality of this Hamiltonian motivates implementation of the non-stoquastic and stoquastic XX interactions as well as the inhomogeneous transverse field.

2.4 Avoidance of the first-order transition in the ferromagnetic p-spin model

We review the avoidance of the first-order transition in the ferromagnetic p-spin model following Refs. [38, 39, 41]. The model is a mean-field-type p-body interacting ferromagnetic system. The problem Hamiltonian is given by

$$\hat{H}_{\mathrm{p}} = -N\left(\frac{1}{N}\sum_{i=1}^{N}\hat{Z}_i\right)^p. \tag{2.12}$$

Although this problem Hamiltonian includes many-body interactions, the ferromagnetic p-spin model is a good example to illustrate how to remove a first-order transition for its simplicity. It is clear that the ground state of the ferromagnetic p-spin model for odd p is the state $\bigotimes_{i=1}^{N}|Z_i = +1\rangle$, in which all the spins point in the $(+z)$-direction (we focus only on the case of odd p, where the ground state is non-degenerate). Nevertheless, the ferromagnetic p-spin model in a transverse field

$$\hat{H}(s) = s\hat{H}_{\mathrm{p}} - (1-s)\sum_{i=1}^{N}\hat{X}_i \tag{2.13}$$

for $p \geq 3$ has a first-order phase transition from the quantum paramagnetic phase to the ferromagnetic phase at $s \in (0, 1)$ and the energy gap between the ground and first excited states at the transition point is exponentially small as a function of the system

size N [82, 83]. This means that quantum annealing to derive the ground state of the ferromagnetic p-spin model involves exponentially long computation time.

Let us add the non-stoquastic XX interaction to the Hamiltonian:

$$\hat{H}(s) = s\lambda(s)\hat{H}_{\rm p} - (1-s)\sum_{i=1}^{N}\hat{X}_i + s(1-\lambda(s))N\left(\frac{1}{N}\sum_{i=1}^{N}\hat{X}_i\right)^2, \tag{2.14}$$

where $s \in [0,1]$ is the dimensionless time and $\lambda(s)$ is a function of the time satisfying $\lambda(1) = 1$. The third term is the infinite-range non-stoquastic XX interaction in the standard basis $\{\,|\{Z_i\}\rangle\,\}$ (notice that the basis transformation interchanging z- and x-directions turns the Hamiltonian into a stoquastic one). The time evolution of quantum annealing starts from $s = 0$ and arbitrary $\lambda(0)$, at which the Hamiltonian contains only the transverse field $-\sum_i \hat{X}_i$, and finishes at the point where the Hamiltonian is equal to $\hat{H}_{\rm p}$, i.e., $s = \lambda(1) = 1$.

We show the phase diagram of the model (2.14) for $p = 11$ in Fig. 2.3(a). There are a quantum paramagnetic phase (P) and two ferromagnetic phases (F and F$'$). The P-F and F$'$-F transitions are of first order and the P-F$'$ transition is of second order. Notice that the phase boundary between the F$'$ and F phases ends at non-zero λ. We can confirm this behavior by examining the magnetization in the z-direction m^z depicted in Fig. 2.3(b). As we fix λ and increase s, for $0.45 \leq \lambda \leq 1$ the first-order P-F transition takes place and for $0.25 \leq \lambda \leq 0.45$ the first-order F$'$-F transition occurs after the second-order P-F$'$ transition. The two ferromagnetic phases join at $\lambda = 0.25$ and for $0 \leq \lambda \leq 0.25$ there is only a second-order paramagnet-ferromagnet transition.

We can determine the first-order phase boundary by the method described in Section 3.1.1, which is identical to that used in Ref. [39, 41] except that our method will contain a system consisting of several subsystems. On the other hand, we can analytically derive the expression of the second-order phase boundary $s = 1/(3-2\lambda)$ [38, 39, 41] by the Landau theory [69].

It turns out from the phase diagram that we can avoid the first-order phase transition in quantum annealing as indicated by the red solid arrow in Fig 2.3(a). This path cannot be implemented in the traditional quantum annealing (the Hamiltonian given by Eq. (2.13), or Eq. (2.14) with $\lambda(s)$ fixed to one), which is indicated by the blue dashed arrow. Introducing the non-stoquastic XX interaction allows the system to exhibit only the second-order phase transition and reduces the computation time to a polynomial of the system size N. This means an exponential enhancement of the efficiency of quantum annealing. The avoidance of the first-order phase transition with the infinite-range non-stoquastic XX interaction works for $5 \leq p < \infty$. The first-order transition is unavoidable in the exceptional cases $p = 3, \infty$ [38], though there is a size-dependent path on which the minimum energy gap in quantum annealing decays polynomially as a function of the system size N for $p = 3$ [84].

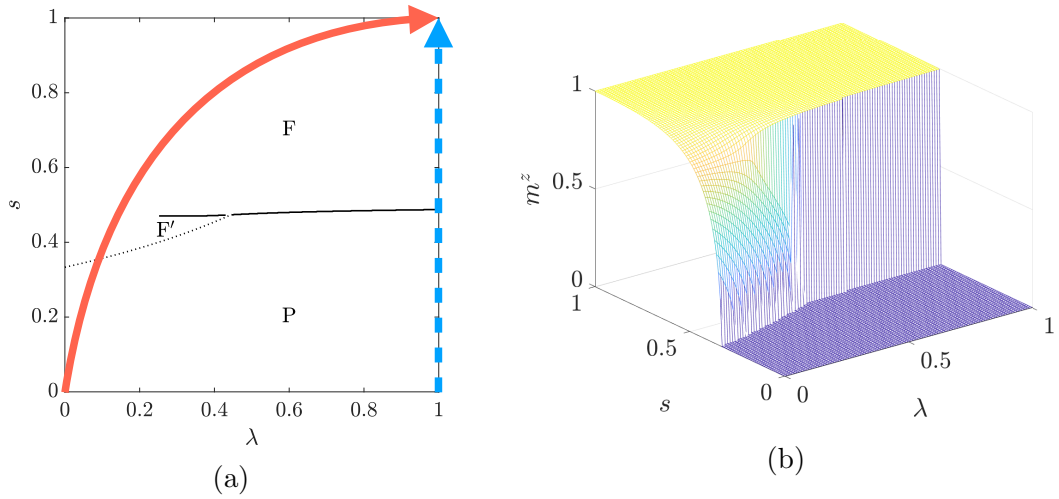

Figure 2.3: (a) Phase diagram of the ferromagnetic p-spin model with a transverse field and a non-stoquastic XX interaction for $p = 11$. F and F$'$ are the two ferromagnetic phases and P is the quantum paramagnetic phase. The solid and dotted lines in black denote the first- and second-order phase transitions, respectively. The blue dashed arrow indicates the path of the traditional quantum annealing without the XX interaction, on which there is a first-order transition. The red solid arrow shows one of the paths on which the system experiences only a second-order transition. This diagram is identical with those in Refs. [38,39,41]. (b) The z-component of the magnetization m^z for the same model as (a).

Chapter 3

Mean-field weak-strong cluster model

The weak-strong cluster problem (the large-spin tunneling problem) [15,27,43,44] is known as a benchmark problem in the context of quantum annealing and adiabatic quantum computation. This problem was used to demonstrate how tunneling effects lead to a computational advantage on a quantum annealer [27]. We consider a mean-field version of the weak-strong cluster problem formulated by Albash [42]. Section 3.1 provides a semi-classical method of analyzing an infinite-range system formed by several subsystems. We show results for the mean-field weak-strong cluster model in Section 3.2. Section 3.3 summarizes the chapter. This chapter is based on Ref. [71].

3.1 Analysis of an infinite-range system consisting of several subsystems

We analyze an infinite-range system consisting of several subsystems. Although the mean-field weak-strong cluster model analyzed in Section 3.2 has two subsystems, we develop a general argument here for possible future convenience.

3.1.1 Classical limit

Let us consider a spin system consisting of several subsystems. Let N be the number of spins and $A = \mathcal{O}(N^0)$ be the number of subsystems. Suppose that each subsystem has an equal number of spins. We denote the Pauli operator at site (a, r) by $\hat{\boldsymbol{\sigma}}_{ar} = (\hat{\sigma}^{\alpha}_{ar})_{\alpha=x,y,z} = (\hat{X}_{ar}, \hat{Y}_{ar}, \hat{Z}_{ar})^{\mathrm{T}}$, where $a = 1, \ldots, A$ is the subsystem index and $r = 1, \ldots, N/A$ is the site index in each subsystem.

We consider the Hamiltonian $\hat{H}$ which is written as a function of the total spin operators for the subsystems $\hat{\boldsymbol{S}}_a = \frac{1}{2}\sum_r \hat{\boldsymbol{\sigma}}_{ar}$. The operators $\hat{\boldsymbol{S}}_a$ satisfy the commutation

relations $[\hat{S}_a^\alpha, \hat{S}_b^\beta] = i\delta_{ab}\sum_\gamma \epsilon^{\alpha\beta\gamma}\hat{S}_a^\gamma$, where δ_{ab} is the Kronecker delta and $\epsilon^{\alpha\beta\gamma}$ is the Levi-Civita symbol. Since $[\hat{H}, \hat{\boldsymbol{S}}_a^2] = 0$ and the initial state of quantum annealing is the state in which all the spins point in the x-direction, the time evolution of quantum annealing occurs in the eigenspace of $\hat{\boldsymbol{S}}_a^2$ with $S_a = \frac{N}{2A} =: S$, where $S_a(S_a+1)$ are the eigenvalues of $\hat{\boldsymbol{S}}_a^2$. Therefore, we consider that $\hat{\boldsymbol{S}}_a$ are spin-($S = \frac{N}{2A}$) operators and the system consists of A interacting large spins.

Defining the magnetization operator for each subsystem as

$$\hat{\boldsymbol{m}}_a = (\hat{m}_a^\alpha)_{\alpha=x,y,z} = \frac{A}{N}\sum_r \hat{\boldsymbol{\sigma}}_{ar} = \frac{\hat{\boldsymbol{S}}_a}{S}, \tag{3.1}$$

we can write the Hamiltonian $\hat{H}$ as $\hat{H} = Nh(\{\hat{\boldsymbol{m}}_a\})$. We assume that $h(\{\hat{\boldsymbol{m}}_a\})$ is a polynomial of degree $P = \mathcal{O}(N^0)$, i.e. a linear combination of $\hat{m}_{a_1}^{\alpha_1}\cdots\hat{m}_{a_p}^{\alpha_p}$ $(p = 0, 1, \ldots, P)$, and the coefficients are of $\mathcal{O}(N^0)$. Now we take the thermodynamic limit $N \to \infty \iff S \to \infty$. In this limit, the non-commutativity of the components of $\hat{\boldsymbol{m}}_a$ is negligible and $\hat{\boldsymbol{m}}_a^2$ approaches unity:

$$[\hat{m}_a^\alpha, \hat{m}_b^\beta] = \frac{1}{S}i\delta_{ab}\sum_\gamma \epsilon^{\alpha\beta\gamma}\hat{m}_a^\gamma \to 0, \tag{3.2}$$

$$\hat{\boldsymbol{m}}_a^2 = \frac{\hat{\boldsymbol{S}}_a^2}{S^2} = \frac{S(S+1)}{S^2} \to 1. \tag{3.3}$$

These equations mean that we can regard the operators $\hat{\boldsymbol{m}}_a$ as classical unit vectors $\boldsymbol{m}_a$ in the limit $S \to \infty$. Since the eigenvalues of the operator $\hat{m}_a^\alpha$ are $-1, -1+1/S, \ldots, +1$, each component m_a^α of the vector $\boldsymbol{m}_a$ takes continuous values in $[-1, 1]$.

Accordingly, the ground state of $\hat{H}$ in the limit $S \to \infty$ is given by the vectors $\boldsymbol{m}_a$ which minimize the energy density $h(\{\boldsymbol{m}_a\})$ subject to the constraints $\boldsymbol{m}_a^2 = 1$. The partial derivatives of the function $h(\{\boldsymbol{m}_a\}) + \sum_a \frac{\mu_a}{2}(\boldsymbol{m}_a^2 - 1)$ vanish at the minimum point, where μ_a are the Lagrange multipliers:

$$\frac{\partial h}{\partial \boldsymbol{m}_a} = -\mu_a \boldsymbol{m}_a. \tag{3.4}$$

3.1.2 Quantum fluctuation

In order to derive the energy gap, we extend the method used in Refs. [39, 85] to the system of several large spins. First we wish to expand the spin operators $\hat{\boldsymbol{S}}_a$ around the classical limit. We introduce rotated spin operators $\hat{\boldsymbol{S}}'_a$ whose z-components are the spin operators in the directions of $\boldsymbol{m}_a =: \boldsymbol{e}_a'^z$. We choose unit vectors $\boldsymbol{e}_a'^x$ and $\boldsymbol{e}_a'^y$ such that $\{\boldsymbol{e}_a'^\alpha\}_{\alpha=x,y,z}$ is an orthonormal set and $\boldsymbol{e}_a'^x \times \boldsymbol{e}_a'^y = \boldsymbol{e}_a'^z$. Defining the components of $\hat{\boldsymbol{S}}'_a$ as $\hat{S}_a'^\alpha = \boldsymbol{e}_a'^\alpha \cdot \hat{\boldsymbol{S}}_a$, we obtain

$$\hat{\boldsymbol{S}}'_a = T_a^{\mathrm{T}}\hat{\boldsymbol{S}}_a \iff \hat{\boldsymbol{S}}_a = T_a\hat{\boldsymbol{S}}'_a, \tag{3.5}$$

where $T_a = (T_a^{\alpha\beta})_{\alpha,\beta=x,y,z} = (\boldsymbol{e}_a'^x, \boldsymbol{e}_a'^y, \boldsymbol{e}_a'^z) \in \mathrm{SO}(3)$ is a special orthogonal matrix. Then, $\hat{\boldsymbol{S}}_a'$ satisfy the commutation relations $[\hat{S}_a'^\alpha, \hat{S}_b'^\beta] = i\delta_{ab}\sum_\gamma \epsilon^{\alpha\beta\gamma}\hat{S}_a'^\gamma$.

Let $\hat{\boldsymbol{m}}_a' = \hat{\boldsymbol{S}}_a'/S$ and $\hat{m}_a'^\pm = \hat{m}_a'^x \pm i\hat{m}_a'^y$. We perform the Holstein–Primakoff transformation [86]

$$\hat{m}_a'^+ = \sqrt{\frac{2}{S}}\sqrt{1 - \frac{1}{2S}\hat{b}_a^\dagger\hat{b}_a}\,\hat{b}_a, \tag{3.6}$$

$$\hat{m}_a'^- = \sqrt{\frac{2}{S}}\,\hat{b}_a^\dagger\sqrt{1 - \frac{1}{2S}\hat{b}_a^\dagger\hat{b}_a}, \tag{3.7}$$

$$\hat{m}_a'^z = 1 - \frac{1}{S}\hat{b}_a^\dagger\hat{b}_a, \tag{3.8}$$

where $\hat{b}_a$ are bosonic operators satisfying $[\hat{b}_a, \hat{b}_b^\dagger] = \delta_{ab}$ and $[\hat{b}_a, \hat{b}_b] = 0$.

The fact that $\hat{m}_a'^z = \boldsymbol{m}_a \cdot \hat{\boldsymbol{m}}_a$ approach unity in the classical limit $S \to \infty$ implies that the number operators $\hat{n}_a = \hat{b}_a^\dagger\hat{b}_a$ take values sufficiently smaller than S in the low-energy states for large S. Expanding the operators in S^{-1} results in

$$\hat{m}_a'^+ = \sqrt{\frac{2}{S}}\,\hat{b}_a + \mathcal{O}(S^{-3/2}), \tag{3.9}$$

$$\hat{m}_a'^- = \sqrt{\frac{2}{S}}\,\hat{b}_a^\dagger + \mathcal{O}(S^{-3/2}). \tag{3.10}$$

We thus obtain

$$\hat{m}_a'^x = \frac{1}{\sqrt{S}}\hat{q}_a + \mathcal{O}(S^{-3/2}), \tag{3.11}$$

$$\hat{m}_a'^y = \frac{1}{\sqrt{S}}\hat{p}_a + \mathcal{O}(S^{-3/2}), \tag{3.12}$$

$$\hat{m}_a'^z = 1 - \frac{1}{S}\hat{n}_a, \tag{3.13}$$

where $\hat{q}_a = (\hat{b}_a + \hat{b}_a^\dagger)/\sqrt{2}$ and $\hat{p}_a = (\hat{b}_a - \hat{b}_a^\dagger)/(\sqrt{2}\,i)$ are the coordinate and momentum operators for the ath harmonic oscillator, respectively. The operators $\hat{q}_a$ and $\hat{p}_a$ satisfy the canonical commutation relations $[\hat{q}_a, \hat{p}_b] = i\delta_{ab}$.

Then, we find that the original magnetization operators $\hat{\boldsymbol{m}}_a = T_a\hat{\boldsymbol{m}}_a'$ are expanded as

$$\hat{\boldsymbol{m}}_a = \boldsymbol{m}_a + \frac{1}{\sqrt{S}}(\boldsymbol{e}_a'^x\hat{q}_a + \boldsymbol{e}_a'^y\hat{p}_a) - \frac{1}{S}\boldsymbol{m}_a\hat{n}_a + \mathcal{O}(S^{-3/2}). \tag{3.14}$$

The Hamiltonian density operator has the expansion

$$\begin{aligned} h(\{\hat{\boldsymbol{m}}_a\}) = h(\{\boldsymbol{m}_a\}) &+ \sum_a \frac{\partial h}{\partial \boldsymbol{m}_a}\cdot\left(\frac{1}{\sqrt{S}}(\boldsymbol{e}_a'^x\hat{q}_a + \boldsymbol{e}_a'^y\hat{p}_a) - \frac{1}{S}\boldsymbol{m}_a\hat{n}_a\right) \\ &+ \frac{1}{2S}\sum_{ab}(\boldsymbol{e}_a'^x\hat{q}_a + \boldsymbol{e}_a'^y\hat{p}_a)^{\mathrm{T}}\frac{\partial^2 h}{\partial \boldsymbol{m}_a\,\partial \boldsymbol{m}_b^{\mathrm{T}}}(\boldsymbol{e}_b'^x\hat{q}_b + \boldsymbol{e}_b'^y\hat{p}_b) + \frac{1}{S}c + \mathcal{O}(S^{-3/2}), \end{aligned} \tag{3.15}$$

where we defined the Hessian matrix as $\frac{\partial^2 h}{\partial \boldsymbol{m}_a \, \partial \boldsymbol{m}_b^{\mathrm{T}}} := \left(\frac{\partial}{\partial \boldsymbol{m}_a}\right)\left(\frac{\partial}{\partial \boldsymbol{m}_b}\right)^{\mathrm{T}} h$. In the above equation, the c-number c arises from the non-commutativity of $\boldsymbol{e}_a'^x \hat{q}_a + \boldsymbol{e}_a'^y \hat{p}_a$ and $\boldsymbol{e}_b'^x \hat{q}_b + \boldsymbol{e}_b'^y \hat{p}_b$:

$$\begin{aligned}[(\boldsymbol{e}_a'^x \hat{q}_a + \boldsymbol{e}_a'^y \hat{p}_a)^\alpha, (\boldsymbol{e}_b'^x \hat{q}_b + \boldsymbol{e}_b'^y \hat{p}_b)^\beta] &= i\delta_{ab}((\boldsymbol{e}_a'^x)^\alpha (\boldsymbol{e}_a'^y)^\beta - (\boldsymbol{e}_a'^y)^\alpha (\boldsymbol{e}_a'^x)^\beta) \\ &= i\delta_{ab}(T_a^{\alpha x} T_a^{\beta y} - T_a^{\alpha y} T_a^{\beta x}). \end{aligned} \tag{3.16}$$

However, the value of c is not needed for determining the energy gap.

Since the magnetizations $\boldsymbol{m}_a$ in the ground state satisfy Eq. (3.4) and $\boldsymbol{e}_a'^x$ and $\boldsymbol{e}_a'^y$ are orthogonal to $\boldsymbol{m}_a$, we find the expansion of the Hamiltonian density operator

$$h(\{\hat{\boldsymbol{m}}_a\}) = h(\{\boldsymbol{m}_a\}) + \frac{1}{S}\hat{\varepsilon} + \mathcal{O}(S^{-3/2}), \tag{3.17}$$

where

$$\hat{\varepsilon} = \sum_a \mu_a \hat{n}_a + \frac{1}{2}\sum_{ab}[h_{ab}^{xx}\hat{q}_a\hat{q}_b + h_{ab}^{yy}\hat{p}_a\hat{p}_b + h_{ab}^{xy}(\hat{q}_a\hat{p}_b + \hat{p}_b\hat{q}_a)] + c \tag{3.18}$$

and

$$\mu_a = -\frac{\partial h}{\partial \boldsymbol{m}_a} \cdot \boldsymbol{m}_a, \tag{3.19}$$

$$h_{ab}^{\alpha\beta} := (\boldsymbol{e}_a'^\alpha)^{\mathrm{T}} \frac{\partial^2 h}{\partial \boldsymbol{m}_a \, \partial \boldsymbol{m}_b^{\mathrm{T}}} \boldsymbol{e}_b'^\beta. \tag{3.20}$$

For $\alpha = \beta$, $h_{ab}^{\alpha\alpha}$ is symmetric under the exchange of the lower indices: $h_{ab}^{\alpha\alpha} = h_{ba}^{\alpha\alpha}$.

Let us diagonalize the operator $\hat{\varepsilon}$. We perform the Bogoliubov transformation

$$\hat{b}_a' = \sum_b (U_{ab}\hat{b}_b + V_{ab}\hat{b}_b^\dagger), \tag{3.21}$$

$$\hat{b}_a'^\dagger = \sum_b (V_{ab}^*\hat{b}_b + U_{ab}^*\hat{b}_b^\dagger) \tag{3.22}$$

and assume that the new bosonic operators $\hat{b}_a'$ diagonalize $\hat{\varepsilon}$:

$$\hat{\varepsilon} = \sum_a \varepsilon_a \hat{b}_a'^\dagger \hat{b}_a' + c'. \tag{3.23}$$

Here, ε_a and c' should be real numbers for $\hat{\varepsilon}$ to be Hermitian and $\hat{b}_a'$ should satisfy the commutation relations

$$[\hat{b}_a', \hat{b}_b'^\dagger] = \delta_{ab}, \quad [\hat{b}_a', \hat{b}_b'] = 0. \tag{3.24}$$

It follows from Eq. (3.18) that

$$[\hat{q}_a, \hat{\varepsilon}] = i \sum_b [(\mu_a \delta_{ab} + h_{ab}^{yy}) \hat{p}_b + h_{ba}^{xy} \hat{q}_b]$$
$$= \frac{1}{\sqrt{2}} \sum_b [(\mu_a \delta_{ab} + h_{ab}^{yy} + i h_{ba}^{xy}) \hat{b}_b - (\mu_a \delta_{ab} + h_{ab}^{yy} - i h_{ba}^{xy}) \hat{b}_b^\dagger], \tag{3.25}$$
$$[\hat{p}_a, \hat{\varepsilon}] = -i \sum_b [(\mu_a \delta_{ab} + h_{ab}^{xx}) \hat{q}_b + h_{ab}^{xy} \hat{p}_b]$$
$$= \frac{1}{\sqrt{2}\, i} \sum_b [(\mu_a \delta_{ab} + h_{ab}^{xx} - i h_{ab}^{xy}) \hat{b}_b + (\mu_a \delta_{ab} + h_{ab}^{xx} + i h_{ab}^{xy}) \hat{b}_b^\dagger]. \tag{3.26}$$

Combining these equations with Eq. (3.21), we derive

$$[\hat{b}'_a, \hat{\varepsilon}] = \sum_b (U_{ab} [\hat{b}_b, \hat{\varepsilon}] + V_{ab} [\hat{b}_b^\dagger, \hat{\varepsilon}])$$
$$= \frac{1}{\sqrt{2}} \sum_b \{(U_{ab} + V_{ab}) [\hat{q}_b, \hat{\varepsilon}] + i (U_{ab} - V_{ab}) [\hat{p}_b, \hat{\varepsilon}]\}$$
$$= \sum_c \sum_b \{[U_{ab} (\mu_b \delta_{bc} + Z_{bc}^+) - V_{ab} Z_{bc}^-] \hat{b}_c + [U_{ab} Z_{bc}^{-*} - V_{ab} (\mu_b \delta_{bc} + Z_{bc}^{+*})] \hat{b}_c^\dagger\}, \tag{3.27}$$

where

$$Z_{ab}^\pm := \frac{h_{ab}^{xx} \pm h_{ab}^{yy} - i (h_{ab}^{xy} \mp h_{ba}^{xy})}{2} \tag{3.28}$$

and $Z_{ab}^{\pm *} := (Z_{ab}^\pm)^*$. On the other hand, Eq. (3.23) yields the commutation relation

$$[\hat{b}'_a, \hat{\varepsilon}] = \varepsilon_a \hat{b}'_a = \varepsilon_a \sum_c (U_{ac} \hat{b}_c + V_{ac} \hat{b}_c^\dagger). \tag{3.29}$$

Comparing the coefficients of $\hat{b}_c$ and $\hat{b}_c^\dagger$ in Eqs. (3.27) and (3.29) results in

$$\varepsilon_a U_{ac} = \sum_b [U_{ab} (\mu_b \delta_{bc} + Z_{bc}^+) - V_{ab} Z_{bc}^-], \tag{3.30}$$
$$\varepsilon_a V_{ac} = \sum_b [U_{ab} Z_{bc}^{-*} - V_{ab} (\mu_b \delta_{bc} + Z_{bc}^{+*})]. \tag{3.31}$$

Notice that we can derive the equivalent equations by calculating $[\hat{b}_a'^\dagger, \hat{\varepsilon}]$ with Eqs. (3.18), (3.22), and (3.23).

Let us define the A-dimensional matrices

$$M = (\mu_a \delta_{ab}), \quad Z^\pm = (Z_{ab}^\pm) \tag{3.32}$$

and the A-dimensional vectors

$$\boldsymbol{u}_a = (U_{a1}, \ldots, U_{aA})^{\mathrm{T}}, \quad \boldsymbol{v}_a = (V_{a1}, \ldots, V_{aA})^{\mathrm{T}}. \tag{3.33}$$

Then, the set of Eqs. (3.30) and (3.31) is written as the eigenvalue equation

$$\boldsymbol{\psi}_a^{\mathrm{T}}\mathcal{E} = \boldsymbol{\psi}_a^{\mathrm{T}}\varepsilon_a, \tag{3.34}$$

where

$$\mathcal{E} := \begin{pmatrix} M + Z^{+} & Z^{-*} \\ -Z^{-} & -M - Z^{+*} \end{pmatrix} \tag{3.35}$$

is a $2A$-dimensional matrix and $\boldsymbol{\psi}_a := (\boldsymbol{u}_a^{\mathrm{T}}, \boldsymbol{v}_a^{\mathrm{T}})^{\mathrm{T}}$ is a $2A$-dimensional vector. Equation (3.34) shows that ε_a are eigenvalues of $\mathcal{E}$ and $\boldsymbol{\psi}_a^{\mathrm{T}}$ are the corresponding left eigenvectors.

We can show that $\varepsilon_a \in \mathbb{R}$ holds if $|\boldsymbol{u}_a|^2 \neq |\boldsymbol{v}_a|^2$. In the following, we assume that all of the eigenvalues of $\mathcal{E}$ are real numbers. Notice that the eigenvalue equation (3.34) yields another eigenvalue equation

$$\boldsymbol{\psi}_{-a}^{\mathrm{T}}\mathcal{E} = \boldsymbol{\psi}_{-a}^{\mathrm{T}}\varepsilon_{-a}, \tag{3.36}$$

where

$$\boldsymbol{\psi}_{-a} := (\boldsymbol{u}_{-a}^{\mathrm{T}}, \boldsymbol{v}_{-a}^{\mathrm{T}})^{\mathrm{T}} := (\boldsymbol{v}_a^{\dagger}, \boldsymbol{u}_a^{\dagger})^{\mathrm{T}}, \quad \varepsilon_{-a} := -\varepsilon_a. \tag{3.37}$$

This means that the $2A$-dimensional matrix $\mathcal{E}$ has $2A$ eigenvalues $\varepsilon_{\pm 1}, \ldots, \varepsilon_{\pm A}$. Let $\varepsilon_1, \ldots, \varepsilon_A$ be non-negative eigenvalues of $\mathcal{E}$, which become the frequencies of the quasi-particles created by $\hat{b}_a'^{\dagger}$.

The commutation relations (3.24) are equivalent to the following constraints on $\boldsymbol{u}_a$ and $\boldsymbol{v}_a$:

$$\boldsymbol{u}_a^{\mathrm{T}}\boldsymbol{u}_b^{*} - \boldsymbol{v}_a^{\mathrm{T}}\boldsymbol{v}_b^{*} = \delta_{ab}, \quad \boldsymbol{u}_a^{\mathrm{T}}\boldsymbol{v}_b - \boldsymbol{v}_a^{\mathrm{T}}\boldsymbol{u}_b = 0 \quad (a, b = 1, \ldots, A). \tag{3.38}$$

These constraints are rewritten as the pseudo orthonormality of $\boldsymbol{\psi}_a$,

$$\boldsymbol{u}_a^{\mathrm{T}}\boldsymbol{u}_b^{*} - \boldsymbol{v}_a^{\mathrm{T}}\boldsymbol{v}_b^{*} = \mathrm{sgn}(a)\delta_{ab} \quad (a, b = \pm 1, \ldots, \pm A). \tag{3.39}$$

We can show that Eq. (3.34) automatically yields Eq. (3.39) if $\varepsilon_a \neq \varepsilon_b$. For each degenerate eigenvalue, we impose the constraint (3.39) on the corresponding eigenvectors. The constraint for $a = b$, $|\boldsymbol{u}_a|^2 - |\boldsymbol{v}_a|^2 = \mathrm{sgn}(a)$, gives the normalization condition of the eigenvectors $\boldsymbol{\psi}_a$.

When ε_a are real numbers for all a and the pseudo orthonormality (3.39) holds, the energy gaps between the ground state and the low-energy excited states of the original Hamiltonian $\hat{H}$ are given by

$$\Delta_{\{n_a\}} := \sum_a \Delta_a n_a \tag{3.40}$$

with $n_a \in \{0, 1, 2, \ldots\}$. Here,

$$\Delta_a := \frac{N}{S}\varepsilon_a = 2A\varepsilon_a \tag{3.41}$$

are the energy gaps created by the quasi-particle excitations $\hat{b}_a'^{\dagger}$. We can assume that

$$\Delta_1 < \cdots < \Delta_A \iff \varepsilon_1 < \cdots < \varepsilon_A \tag{3.42}$$

without loss of generality. Then, the energy gap between the ground and first excited states is

$$\Delta = \Delta_1. \tag{3.43}$$

Notice that our method of calculating the energy gap is not applicable to a first-order transition point because the quasi-particle excitation $\hat{b}_1'^{\dagger}$ is a fluctuation around the single global minimum of the classical potential $h(\{\boldsymbol{m}_a\})$. Typically, the classical potential $h(\{\boldsymbol{m}_a\})$ is a double-well potential at a first-order transition and the ground and first excited states are superpositions of the states localized at the two minima. To calculate the gap between these states analytically, the discrete WKB (Wentzel–Kramers–Brillouin) method or the instanton method would be needed [83, 87–89].

3.2 Results for the mean-field weak-strong cluster model

We apply the semi-classical method explained in the previous section to a quantum annealing Hamiltonian for the mean-field weak-strong cluster problem, which was proposed in Ref. [42]. The model has two subsystems (clusters) and the problem Hamiltonian is defined as

$$\hat{H}_{\rm p} = -\sum_{r=1}^{N/2}(h_1\hat{Z}_{1r} + h_2\hat{Z}_{2r}) - \frac{1}{N}\sum_{r,r'=1}^{N/2}(\hat{Z}_{1r}\hat{Z}_{1r'} + \hat{Z}_{2r}\hat{Z}_{2r'} + \hat{Z}_{1r}\hat{Z}_{2r'}), \tag{3.44}$$

where N is the total number of spins (qubits) in the system and $\hat{\boldsymbol{\sigma}}_{ar} = (\hat{X}_{ar}, \hat{Y}_{ar}, \hat{Z}_{ar})^{\rm T}$ is the Pauli operator at (a, r), with $a = 1, 2$ representing the cluster index and $r = 1, \ldots, N/2$ the site index within each cluster. We set the strengths of longitudinal magnetic fields to $h_1 = 1$ and $h_2 = -0.49$. We refer to the first subsystem $a = 1$ as the strong cluster and the second subsystem $a = 2$ as the weak cluster. Notice that the strong longitudinal field h_1 and the weak one h_2 point in the opposite directions. The structure of the problem is schematically depicted in Fig. 3.1.

The ground state of $\hat{H}_{\rm p}$ is the eigenstate of $\hat{Z}_{1r}$ and $\hat{Z}_{2r}$ with eigenvalues $Z_{1r} = Z_{2r} = +1$ (all spins pointing up, to be called 'state A'), while a metastable state exists with eigenvalues $Z_{1r} = +1$ and $Z_{2r} = -1$ (spins in the strong cluster pointing up and those in the weak cluster pointing down, to be called 'state B'). The conventional quantum annealing with a uniform transverse field, in which the Hamiltonian is stoquastic, has a first-order phase transition when state A and state B exchange their (meta)stability, meaning a large-scale spin flip in the weak cluster [27].

Let us construct a quantum annealing Hamiltonian for the mean-field weak-strong cluster problem. Using the magnetization operators $\hat{\boldsymbol{m}}_a = (2/N)\sum_r \hat{\boldsymbol{\sigma}}_{ar}$, we define the

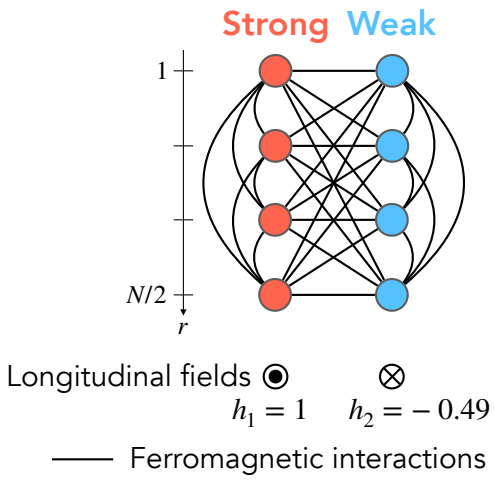

Figure 3.1: Mean-field weak-strong cluster problem. The circles in the left (right) side denote the spins in the strong (weak) cluster.

Hamiltonian $\hat{H}(s)$ of the mean-field weak-strong cluster model as

$$\begin{aligned}\frac{\hat{H}(s)}{N} = &-\frac{s}{2}\left(h_1\hat{m}_1^z + h_2\hat{m}_2^z\right) - \frac{s}{4}\left((\hat{m}_1^z)^2 + (\hat{m}_2^z)^2 + \hat{m}_1^z\hat{m}_2^z\right) \\ &- \frac{1-\gamma_1(s)}{2}\hat{m}_1^x - \frac{1-\gamma_2(s)}{2}\hat{m}_2^x - \frac{s(1-s)}{4}\left(\xi_{11}(\hat{m}_1^x)^2 + \xi_{22}(\hat{m}_2^x)^2 + \xi_{12}\hat{m}_1^x\hat{m}_2^x\right),\end{aligned} \tag{3.45}$$

where $s \in [0,1]$ denotes the dimensionless time. Suppose that $\gamma_1(s)$ and $\gamma_2(s)$ are monotonically increasing functions which satisfy $\gamma_1(0) = \gamma_2(0) = 0$ and $\gamma_1(1) = \gamma_2(1) = 1$, and ξ_{11}, ξ_{22}, and ξ_{12} are constants.

The Hamiltonian $\hat{H}(s)$ consists of the problem Hamiltonian (the first line of Eq. (3.45)) and the driver Hamiltonian (the second line). The strength of the problem Hamiltonian increases in proportion to s. The driver Hamiltonian is the sum of time-dependent transverse fields and XX interactions. The strength of the transverse field in each cluster decreases with time. We can achieve inhomogeneous driving of the transverse field by choosing different functions for $\gamma_1(s)$ and $\gamma_2(s)$. As for the XX interactions, non-zero ξ_{ab} makes the corresponding term non-vanishing except at the beginning and the end of annealing. When $0 < s < 1$, the Hamiltonian $\hat{H}(s)$ is non-stoquastic for $\xi_{11} < 0$, $\xi_{22} < 0$, or $\xi_{12} < 0$ and stoquastic for $\xi_{11}, \xi_{22}, \xi_{12} \geq 0$.

For the moment, we assume $\gamma_1(s) = \gamma_2(s) = s$ (homogeneous driving of the transverse field) and focus on effects of the XX interactions. First consider the case of the XX interaction between the clusters. Using the method explained in Section 3.1.1, we can calculate the magnetization $\boldsymbol{m}_a$ for each cluster in the ground state of the system in the thermodynamic limit $N \to \infty$. We show the magnetizations m_1^z and m_2^z as functions of s and $\xi = \xi_{12}$ for $\xi_{11} = \xi_{22} = 0$ in Fig. 3.2. A first-order transition occurs in the

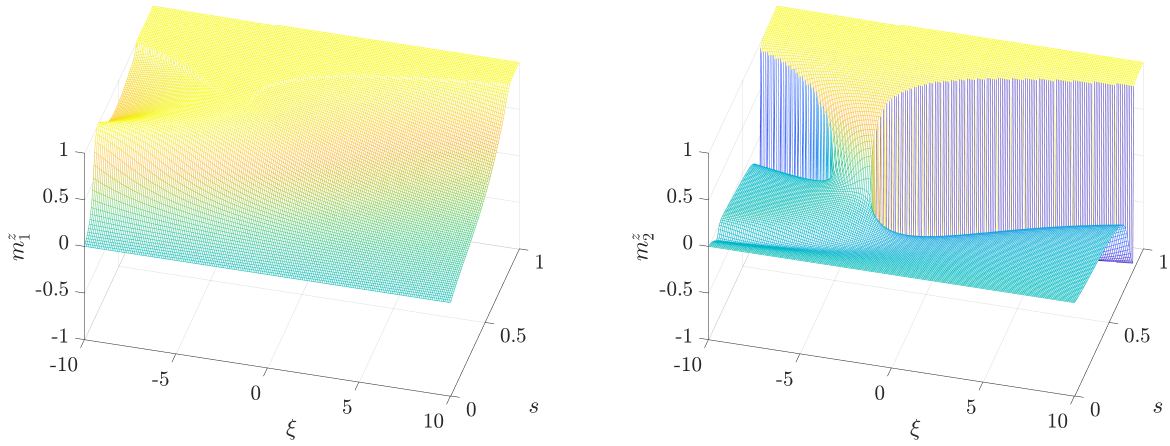

Figure 3.2: Magnetizations m_1^z and m_2^z of the mean-field weak-strong cluster model for $\gamma_1(s) = \gamma_2(s) = s$ and $(\xi_{11}, \xi_{22}, \xi_{12}) = (0, 0, \xi)$.

stoquastic case $\xi \geq 0$ including the case without the XX interactions ($\xi = 0$), where the magnetization in the strong cluster m_1^z slightly jumps and that in the weak cluster m_2^z jumps from a negative value to a positive value (a large-scale spin flip). On the other hand, there is no transition for $-5 \lesssim \xi \lesssim -3$. This means that the non-stoquastic XX interaction between the clusters with the appropriate strength removes the first-order transition, while too small or too large ones cannot. This result confirms the conclusion obtained by exact diagonalization of the finite-size systems [42].

We next calculate the energy gap between the ground state and the first excited state by use of the method in Section 3.1.2. We show the energy gaps Δ_a for $\xi_{11} = \xi_{22} = 0$ and $\xi_{12} = \xi = 0, -4, -10$ in Fig. 3.3. Here, Δ_a denote the energy gaps created by the quasi-particle excitations $\hat{b}_a^\dagger$ above the classical ground state. We calculated Δ_a by numerically diagonalizing the four-dimensional matrix $\mathcal{E}$ defined as Eq. (3.35) and multiplying the non-negative eigenvalues ε_a by four (see Eq. (3.41)). The smaller gap Δ_1 is equal to the energy gap between the ground and first excited states of the Hamiltonian $\hat{H}(s)$ except at the first-order transition point. The correct energy gap at a first-order transition is exponentially small as a function of the system size N [42], which cannot be evaluated by our method as explained in the previous section. In general, the energy gaps Δ_a calculated by our method are discontinuous at first-order transitions due to the discontinuity of the magnetizations $\boldsymbol{m}_a$, although we cannot clearly see a discontinuous jump in the lower of the two gaps Δ_1 for $\xi = 0$ at least in our precision whereas the other Δ_2 shows discontinuity. In the case of $\xi = -4$, the energy gaps Δ_a are continuous because there is no first-order transition.

Now we derive the minimum gap $\min_s \Delta_1$ for the range of ξ where there is no first-order transition. The result for $\xi_{11} = \xi_{22} = 0$ and $-5 \leq \xi_{12} = \xi \leq -3$ is shown in Fig. 3.4. We can see that $\min_s \Delta_1$ is maximized at $\xi \approx -4.0$, which is consistent with the result in Ref. [42] (notice that λ in Ref. [42] is equal to $-\xi/2$ in our definition).

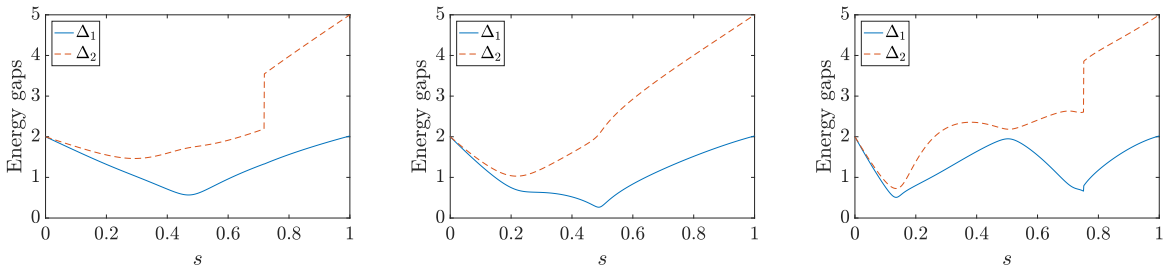

(a) $\xi = 0$. (b) $\xi = -4$. (c) $\xi = -10$.

Figure 3.3: Energy gaps Δ_a created by the quasi-particle excitations $\hat{b}_a'^{\dagger}$ for the mean-field weak-strong cluster model. We set $\gamma_1(s) = \gamma_2(s) = s$, $\xi_{11} = \xi_{22} = 0$, and $\xi_{12} = \xi = 0, -4, -10$.

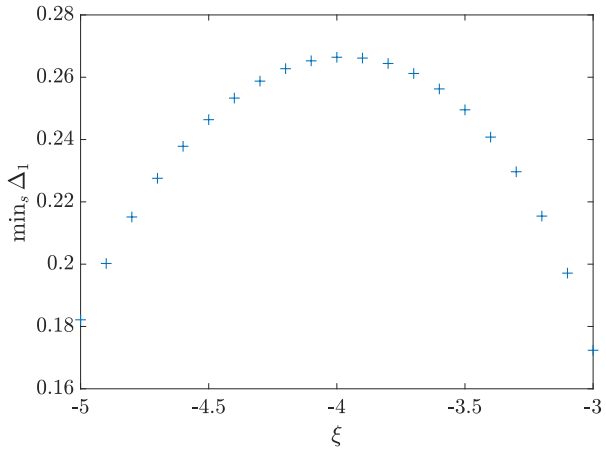

Figure 3.4: Minimum energy gap $\min_s \Delta_1$ of the mean-field weak-strong cluster model for $\gamma_1(s) = \gamma_2(s) = s$, $\xi_{11} = \xi_{22} = 0$, and $-5 \leq \xi_{12} = \xi \leq -3$. In this region of ξ, there is no first-order transition and Δ_1 is equal to the energy gap between the ground and first excited states of the Hamiltonian $\hat{H}(s)$ in the thermodynamic limit $N \to \infty$.

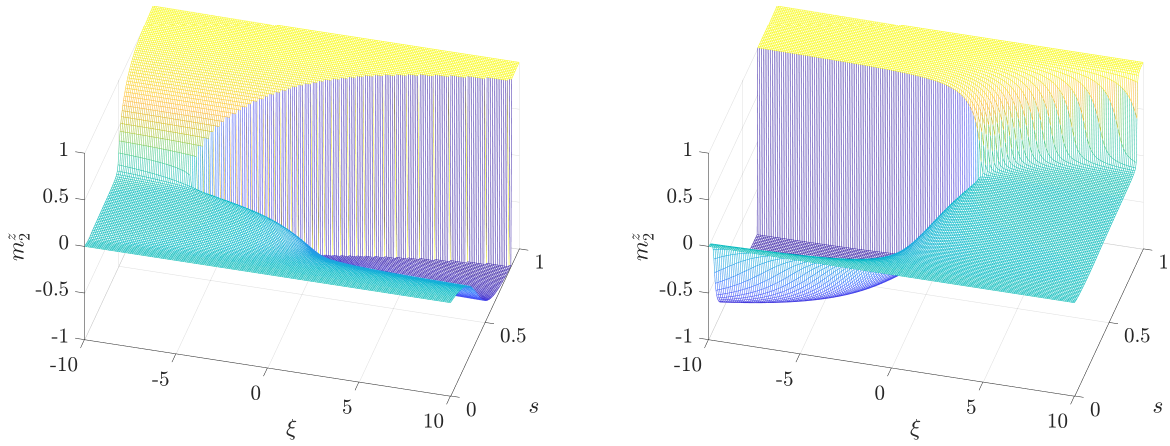

Figure 3.5: Magnetization in the weak cluster m_2^z of the mean-field weak-strong cluster model for $(\xi_{11}, \xi_{22}, \xi_{12}) = (\xi, 0, 0)$ (left) and for $(\xi_{11}, \xi_{22}, \xi_{12}) = (0, \xi, 0)$ (right). We set $\gamma_1(s) = \gamma_2(s) = s$ in both cases.

Let us move on to the case of the XX interaction in each cluster. We show the magnetization in the weak cluster m_2^z for $(\xi_{11}, \xi_{22}, \xi_{12}) = (\xi, 0, 0), (0, \xi, 0)$ as functions of s and ξ in Fig. 3.5. We find that the non-stoquastic XX interaction in the strong cluster or the stoquastic XX interaction in the weak cluster removes the first-order transition, while the other types of intracluster XX interaction do not.

We can interpret these results as follows: In the case of the non-stoquastic XX interaction in the strong cluster, $|m_1^x|$ becomes smaller and m_1^z larger, which makes m_2^z larger thanks to the ferromagnetic coupling between the clusters. In the case of the stoquastic XX interaction in the weak cluster, m_2^x becomes larger and $|m_2^z|$ smaller. Both of these types of XX interaction prevent m_2^z from being a large negative value due to the longitudinal field h_2, which reduces the possibility of a jump in m_2^z.

We also found that the first-order transition cannot be removed in the case where the XX interaction is proportional to $\frac{1}{2}(\hat{m}_1^x + \hat{m}_2^x)^2$ (i.e., $(\xi_{11}, \xi_{22}, \xi_{12}) = (\xi/2, \xi/2, \xi)$) regardless of the sign of the coefficient ξ, which is shown in Fig. 3.6. The result in the non-stoquastic case $\xi < 0$ is in agreement with the numerical consequence given in Appendix F of Ref. [42].

Finally we consider the model in which the transverse field is driven inhomogeneously and there is no XX interaction. Then, the Hamiltonian is stoquastic. We show the magnetization in the weak cluster m_2^z for $(\gamma_1(s), \gamma_2(s)) = (\gamma(s), s), (s, \gamma(s))$ in Fig. 3.7, where the increasing function $\gamma(s)$ can be chosen arbitrarily as long as $\gamma(0) = 0$ and $\gamma(1) = 1$. Notice that the value of m_2^z is indefinite at $s = 0$ and $\gamma_2 = 1$, where neither magnetic field nor interaction is applied to the weak cluster. We find that the weaker transverse field in the strong cluster and the stronger transverse field in the weak cluster can remove the first-order transition in the process of quantum annealing. The mechanism for removing the first-order transition is similar to the case of the non-stoquastic XX

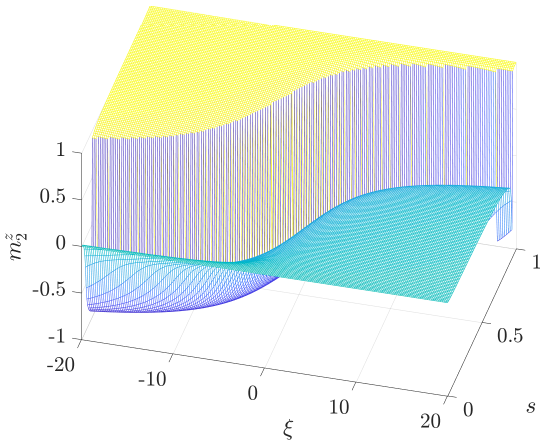

Figure 3.6: Magnetization in the weak cluster m_2^z of the mean-field weak-strong cluster model for $\gamma_1(s) = \gamma_2(s) = s$ and $(\xi_{11}, \xi_{22}, \xi_{12}) = (\xi/2, \xi/2, \xi)$.

interaction in the strong cluster or the stoquastic XX interaction in the weak cluster.

3.3 Summary

We have carried out the semi-classical analysis of the mean-field weak-strong cluster model. We showed that the first-order transition which appears in the case of the uniform transverse field and no XX interactions can be removed either by the non-stoquastic XX interaction between the clusters with the appropriate strength, the non-stoquastic XX interaction in the strong cluster, the stoquastic XX interaction in the weak cluster, or inhomogeneous field driving in which the transverse field in the weak cluster is stronger than that in the strong cluster. The result in the case of the non-stoquastic XX interaction between the clusters is consistent with the numerical consequence [42], including the analytically calculated value of the energy gap.

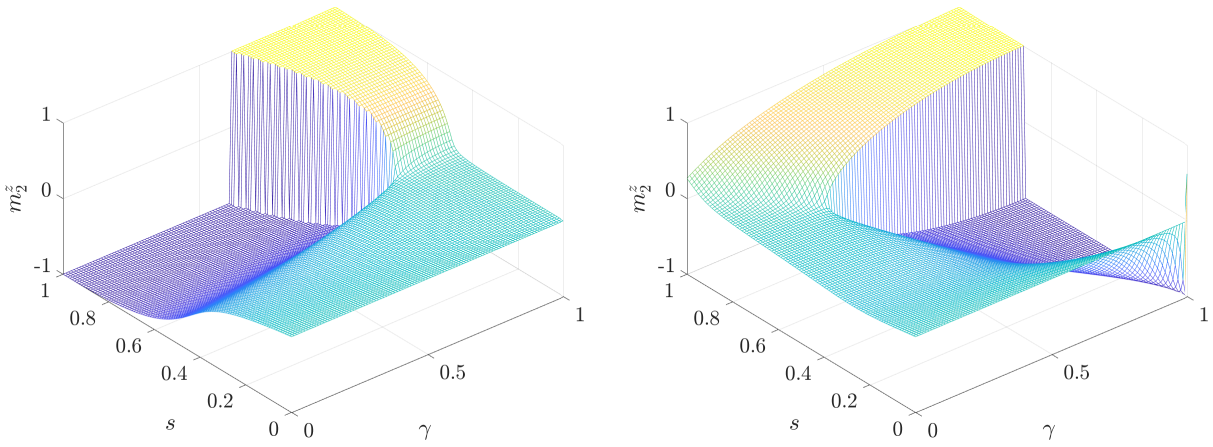

Figure 3.7: Magnetization in the weak cluster m_2^z of the mean-field weak-strong cluster model for $(\gamma_1, \gamma_2) = (\gamma, s)$ (left) and for $(\gamma_1, \gamma_2) = (s, \gamma)$ (right). We set $\xi_{11} = \xi_{22} = \xi_{12} = 0$ in both cases.

Chapter 4

Weak-strong cluster model with sparse intercluster interactions

In the previous chapter, we studied the mean-field weak-strong cluster model, which has all-to-all interactions. We now consider the weak-strong cluster model in which the interactions between clusters are sparse. This model has less connectivity than the mean-field model. In Section 4.1, we analyze a semi-infinite-range system which is formed by several subsystems and has sparse interactions between subsystems as well as mean-field-type interactions within subsystems. Section 4.2 shows results for the weak-strong cluster model with sparse interactions between clusters. Section 4.3 summarizes the chapter. This chapter is grounded on Ref. [71].

4.1 Analysis of a system with sparse interactions between subsystems

Let us analyze a semi-infinite-range spin system which consists of several subsystems and has sparse interactions between subsystems. We denote the number of spins by N, the number of subsystems by $A = \mathcal{O}(N^0)$, and the Pauli operator at site (a, r) $(a = 1, \dots, A;$ $r = 1, \dots, N/A)$ by $\hat{\boldsymbol{\sigma}}_{ar} = (\hat{\sigma}^{\alpha}_{ar})_{\alpha=x,y,z} = (\hat{X}_{ar}, \hat{Y}_{ar}, \hat{Z}_{ar})^{\mathrm{T}}$. Differently from the mean-field case analyzed in the previous chapter, we consider the Hamiltonian in the following form:

$$\hat{H} = N h_{\mathrm{m}}(\{\hat{\boldsymbol{m}}_a\}) - \frac{1}{2} \sum_{ab} \sum_{r} \hat{\boldsymbol{\sigma}}_{ar} \cdot K_{ab} \hat{\boldsymbol{\sigma}}_{br}, \tag{4.1}$$

where the first term $h_{\mathrm{m}}(\{\hat{\boldsymbol{m}}_a\})$ is the mean-field part written as a function of $\hat{\boldsymbol{m}}_a = \frac{A}{N} \sum_r \hat{\boldsymbol{\sigma}}_{ar}$ and the second term is the sum of sparse interactions between the subsystems which are determined by the matrices $K_{ab} = (K^{\alpha\beta}_{ab})_{\alpha,\beta=x,y,z}$. We assume that $h_{\mathrm{m}}(\{\hat{\boldsymbol{m}}_a\})$ is a polynomial of degree $P = \mathcal{O}(N^0)$ with coefficients of $\mathcal{O}(N^0)$. We can set $K^{\alpha\beta}_{aa} = 0$ and $K^{\alpha\beta}_{ab} = K^{\beta\alpha}_{ba} \in \mathbb{R}$ without loss of generality, because the term with the coefficient matrix K_{aa} can be included in the mean-field part and $[\hat{\sigma}^{\alpha}_{a}, \hat{\sigma}^{\beta}_{b}] = 0$ for $a \neq b$.

Now we introduce the path-integral representation of the partition function $Z = \mathrm{Tr}\, e^{-\beta \hat{H}}$ with inverse temperature β:

$$Z = \left(\prod_{ar} \int \mathcal{D}\boldsymbol{n}_{ar} \right) \exp\left[- \int_0^\beta d\tau \left(\sum_{ar} \langle \boldsymbol{n}_{ar}(\tau) | \frac{d}{d\tau} | \boldsymbol{n}_{ar}(\tau) \rangle \right.\right. \\ \left.\left. + \langle \{\boldsymbol{n}_{ar}(\tau)\} | \hat{H} | \{\boldsymbol{n}_{ar}(\tau)\} \rangle \right) \right]. \tag{4.2}$$

Here, $|\{\boldsymbol{n}_{ar}\}\rangle = \bigotimes_{ar} |\boldsymbol{n}_{ar}\rangle$ is the product state of the spin coherent states $|\boldsymbol{n}_{ar}\rangle$ determined by unit vectors $\boldsymbol{n}_{ar}$. The spin coherent state $|\boldsymbol{n}_{ar}\rangle$ at each site is the normalized eigenstate of $\hat{\boldsymbol{\sigma}}_{ar} \cdot \boldsymbol{n}_{ar}$ with the eigenvalue one. In addition, $\mathcal{D}\boldsymbol{n}_{ar}$ is the functional measure which is the product of the measures on the 2-sphere over imaginary time $\tau \in [0, \beta]$.

The energy expectation value in the spin coherent state is given by

$$\langle \{\boldsymbol{n}_{ar}\} | \hat{H} | \{\boldsymbol{n}_{ar}\} \rangle = N \langle \{\boldsymbol{n}_{ar}\} | h_{\mathrm{m}}(\{\hat{\boldsymbol{m}}_a\}) | \{\boldsymbol{n}_{ar}\} \rangle - \frac{1}{2} \sum_{ab} \sum_{r} \boldsymbol{n}_{ar} \cdot K_{ab} \boldsymbol{n}_{br}. \tag{4.3}$$

We use an approximation for the first term $\langle \{\boldsymbol{n}_{ar}\} | h_{\mathrm{m}}(\{\hat{\boldsymbol{m}}_a\}) | \{\boldsymbol{n}_{ar}\} \rangle$. The mean-field part of the Hamiltonian density $h_{\mathrm{m}}(\{\hat{\boldsymbol{m}}_a\})$ is a linear combination of $\hat{m}_{a_1}^{\alpha_1} \cdots \hat{m}_{a_p}^{\alpha_p}$ ($p = 1, \ldots, P$), which has the expectation value

$$\begin{aligned}
\langle \{\boldsymbol{n}_{ar}\} | \hat{m}_{a_1}^{\alpha_1} \cdots \hat{m}_{a_p}^{\alpha_p} | \{\boldsymbol{n}_{ar}\} \rangle &= \left(\frac{A}{N} \right)^p \sum_{r_1, \ldots, r_p} \langle \{\boldsymbol{n}_{ar}\} | \hat{\sigma}_{a_1 r_1}^{\alpha_1} \cdots \hat{\sigma}_{a_p r_p}^{\alpha_p} | \{\boldsymbol{n}_{ar}\} \rangle \\
&= \left(\frac{A}{N} \right)^p \sum_{\substack{r_1, \ldots, r_p \\ q \neq q' \Longrightarrow r_q \neq r_{q'}}} \langle \{\boldsymbol{n}_{ar}\} | \hat{\sigma}_{a_1 r_1}^{\alpha_1} \cdots \hat{\sigma}_{a_p r_p}^{\alpha_p} | \{\boldsymbol{n}_{ar}\} \rangle + \mathcal{O}(N^{-1}) \\
&= \left(\frac{A}{N} \right)^p \sum_{\substack{r_1, \ldots, r_p \\ q \neq q' \Longrightarrow r_q \neq r_{q'}}} n_{a_1 r_1}^{\alpha_1} \cdots n_{a_p r_p}^{\alpha_p} + \mathcal{O}(N^{-1}) \\
&= \left(\frac{A}{N} \right)^p \sum_{r_1, \ldots, r_p} n_{a_1 r_1}^{\alpha_1} \cdots n_{a_p r_p}^{\alpha_p} + \mathcal{O}(N^{-1}) \\
&= \left(\frac{A}{N} \sum_{r_1} n_{a_1 r_1}^{\alpha_1} \right) \cdots \left(\frac{A}{N} \sum_{r_p} n_{a_p r_p}^{\alpha_p} \right) + \mathcal{O}(N^{-1}).
\end{aligned} \tag{4.4}$$

In the second and fourth lines of this equation, we used the fact that the number of $(r_1, \ldots, r_p)$ including equal indices is of $\mathcal{O}(N^{p-1})$, while the number of $(r_1, \ldots, r_p)$ whose elements are different from each other is $\frac{N}{A}\left(\frac{N}{A} - 1\right) \cdots \left(\frac{N}{A} - p + 1\right) = \mathcal{O}(N^p)$. Therefore, we obtain the simplified expression

$$\langle \{\boldsymbol{n}_{ar}\} | h_{\mathrm{m}}(\{\hat{\boldsymbol{m}}_a\}) | \{\boldsymbol{n}_{ar}\} \rangle = h_{\mathrm{m}} \left(\left\{ \frac{A}{N} \sum_{r} \boldsymbol{n}_a \right\} \right) + \mathcal{O}(N^{-1}). \tag{4.5}$$

We ignore the term of $\mathcal{O}(N^{-1})$, which yields a non-extensive correction to the energy expectation value $\langle\{\boldsymbol{n}_{ar}\}|\hat{H}|\{\boldsymbol{n}_{ar}\}\rangle$.

Combining Eqs. (4.2), (4.3), and (4.5) yields

$$Z = \left(\prod_{ar}\int \mathcal{D}\boldsymbol{n}_{ar}\right)\exp\left[-\int_0^\beta d\tau\left(\sum_{ar}\langle\boldsymbol{n}_{ar}(\tau)|\frac{d}{d\tau}|\boldsymbol{n}_{ar}(\tau)\rangle + Nh_{\mathrm{m}}\left(\left\{\frac{A}{N}\sum_r \boldsymbol{n}_a(\tau)\right\}\right)\right.\right.$$
$$\left.\left. - \frac{1}{2}\sum_{ab}\sum_r \boldsymbol{n}_{ar}(\tau)\cdot K_{ab}\boldsymbol{n}_{br}(\tau)\right)\right]. \tag{4.6}$$

We insert the path integral of the delta functional

$$1 = \int \mathcal{D}\boldsymbol{m}_a\,\delta\left[\frac{N}{A}\boldsymbol{m}_a(\tau) - \sum_r \boldsymbol{n}_{ar}(\tau)\right]$$
$$= \int \mathcal{D}\boldsymbol{m}_a\int \mathcal{D}\widetilde{\boldsymbol{m}}_a\,\exp\left[-\int_0^\beta d\tau\,\widetilde{\boldsymbol{m}}_a(\tau)\cdot\left(\frac{N}{A}\boldsymbol{m}_a(\tau) - \sum_r \boldsymbol{n}_{ar}(\tau)\right)\right] \tag{4.7}$$

for each a into Eq. (4.6). Then, we obtain

$$Z = \left(\prod_a\int \mathcal{D}\boldsymbol{m}_a\int \mathcal{D}\widetilde{\boldsymbol{m}}_a\right)\exp\left[-N\int_0^\beta d\tau\left(\frac{1}{A}\sum_a \widetilde{\boldsymbol{m}}_a(\tau)\cdot\boldsymbol{m}_a(\tau) + h_{\mathrm{m}}(\{\boldsymbol{m}_a(\tau)\})\right)\right]$$
$$\times\prod_r\left\{\left(\prod_a\int \mathcal{D}\boldsymbol{n}_{ar}\right)\exp\left[-\int_0^\beta d\tau\left(\sum_a\langle\boldsymbol{n}_{ar}(\tau)|\frac{d}{d\tau}|\boldsymbol{n}_{ar}(\tau)\rangle - \sum_a \widetilde{\boldsymbol{m}}_a(\tau)\cdot\boldsymbol{n}_{ar}(\tau)\right.\right.\right.$$
$$\left.\left.\left. - \frac{1}{2}\sum_{ab}\boldsymbol{n}_{ar}(\tau)\cdot K_{ab}\boldsymbol{n}_{br}(\tau)\right)\right]\right\}$$
$$= \left(\prod_a\int \mathcal{D}\boldsymbol{m}_a\int \mathcal{D}\widetilde{\boldsymbol{m}}_a\right)\exp\left[-N\int_0^\beta d\tau\left(\frac{1}{A}\sum_a \widetilde{\boldsymbol{m}}_a(\tau)\cdot\boldsymbol{m}_a(\tau) + h_{\mathrm{m}}(\{\boldsymbol{m}_a(\tau)\})\right)\right]$$
$$\times\left\{\left(\prod_a\int \mathcal{D}\boldsymbol{n}_a\right)\exp\left[-\int_0^\beta d\tau\left(\sum_a\langle\boldsymbol{n}_a(\tau)|\frac{d}{d\tau}|\boldsymbol{n}_a(\tau)\rangle - \sum_a \widetilde{\boldsymbol{m}}_a(\tau)\cdot\boldsymbol{n}_a(\tau)\right.\right.\right.$$
$$\left.\left.\left. - \frac{1}{2}\sum_{ab}\boldsymbol{n}_a(\tau)\cdot K_{ab}\boldsymbol{n}_b(\tau)\right)\right]\right\}^{N/A}, \tag{4.8}$$

where we simplified the product over $r = 1, \ldots, N/A$ as the (N/A)th power, because the factor in the expression of Z depends on r only through $\boldsymbol{n}_{ar}$.

Let us evaluate the asymptotic form of the partition function in the thermodynamic limit $N \to \infty$ by the stationary-phase approximation. We assume that the stationary path (i.e., the set of the functions $\boldsymbol{m}_a(\tau)$ and $\widetilde{\boldsymbol{m}}_a(\tau)$ for which the functional derivatives of the integrand of Z vanish) satisfies the static ansatz

$$\boldsymbol{m}_a(\tau) = \boldsymbol{m}_a, \quad \widetilde{\boldsymbol{m}}_a(\tau) = \widetilde{\boldsymbol{m}}_a. \tag{4.9}$$

Then, we can write the partition function as an ordinary integral with respect to $\boldsymbol{m}_a$ and $\widetilde{\boldsymbol{m}}_a$:

$$Z = \left(\prod_a \int d^3\boldsymbol{m}_a \int d^3\widetilde{\boldsymbol{m}}_a\right) \exp\left[-N\beta\left(\frac{1}{A}\sum_a \widetilde{\boldsymbol{m}}_a\cdot\boldsymbol{m}_a + h_{\rm m}(\{\boldsymbol{m}_a\})\right)\right] \times\left\{\left(\prod_a\int \mathcal{D}\boldsymbol{n}_a\right)\exp\left[-\int_0^\beta d\tau\left(\sum_a\langle\boldsymbol{n}_a(\tau)|\frac{d}{d\tau}|\boldsymbol{n}_a(\tau)\rangle - \sum_a \widetilde{\boldsymbol{m}}_a\cdot\boldsymbol{n}_a(\tau) - \frac{1}{2}\sum_{ab}\boldsymbol{n}_a(\tau)\cdot K_{ab}\boldsymbol{n}_b(\tau)\right)\right]\right\}^{N/A}. \tag{4.10}$$

Replacing the path integral over $\boldsymbol{n}_a(\tau)$ with the trace of an exponentiated operator results in

$$Z = \left(\prod_a \int d^3\boldsymbol{m}_a \int d^3\widetilde{\boldsymbol{m}}_a\right)\exp\left[-N\beta\left(\frac{1}{A}\sum_a \widetilde{\boldsymbol{m}}_a\cdot\boldsymbol{m}_a + h_{\rm m}(\{\boldsymbol{m}_a\})\right) + \frac{N}{A}\ln{\rm Tr}\, e^{-\beta\hat{h}_{\rm eff}(\{\widetilde{\boldsymbol{m}}_a\})}\right]. \tag{4.11}$$

We defined the effective Hamiltonian of an A-spin system as

$$\hat{h}_{\rm eff}(\{\widetilde{\boldsymbol{m}}_a\}) = -\sum_a \widetilde{\boldsymbol{m}}_a\cdot\hat{\boldsymbol{\sigma}}_a - \frac{1}{2}\sum_{ab}\hat{\boldsymbol{\sigma}}_a\cdot K_{ab}\hat{\boldsymbol{\sigma}}_b, \tag{4.12}$$

where $\hat{\boldsymbol{\sigma}}_a$ $(a = 1,\ldots,A)$ are the Pauli operators.

Applying the saddle-point method (the stationary-phase approximation) to Eq. (4.11) in the thermodynamic limit $N\to\infty$, we derive the expression of the free-energy density $f = -\frac{1}{N\beta}\ln Z$ as follows:

$$f = \frac{1}{A}\sum_a \widetilde{\boldsymbol{m}}_a\cdot\boldsymbol{m}_a + h_{\rm m}(\{\boldsymbol{m}_a\}) - \frac{1}{A\beta}\ln{\rm Tr}\, e^{-\beta\hat{h}_{\rm eff}(\{\widetilde{\boldsymbol{m}}_a\})}. \tag{4.13}$$

We can calculate the order parameters $\boldsymbol{m}_a$, which are the magnetizations for the A subsystems, and their conjugate parameters $\widetilde{\boldsymbol{m}}_a$, by solving the saddle-point equations $\partial f/\partial\boldsymbol{m}_a = \partial f/\partial\widetilde{\boldsymbol{m}}_a = \boldsymbol{0}$, i.e.,

$$\boldsymbol{m}_a = \langle\hat{\boldsymbol{\sigma}}_a\rangle_{\{\widetilde{\boldsymbol{m}}_a\}}(\beta), \tag{4.14}$$

$$\widetilde{\boldsymbol{m}}_a = -A\frac{\partial h_{\rm m}}{\partial\boldsymbol{m}_a}. \tag{4.15}$$

Here,

$$\langle\cdots\rangle_{\{\widetilde{\boldsymbol{m}}_a\}}(\beta) := \frac{{\rm Tr}\, e^{-\beta\hat{h}_{\rm eff}(\{\widetilde{\boldsymbol{m}}_a\})}\cdots}{{\rm Tr}\, e^{-\beta\hat{h}_{\rm eff}(\{\widetilde{\boldsymbol{m}}_a\})}} \tag{4.16}$$

is the thermal expectation value for the effective A-spin system.

Let us denote the eigenvalues of $\hat{h}_{\rm eff}(\{\widetilde{\boldsymbol{m}}_a\})$ by $\lambda_n(\{\widetilde{\boldsymbol{m}}_a\})$ $(n = 0, 1, \ldots, 2^A - 1)$ and the corresponding eigenvectors by $|\lambda_n\rangle_{\{\widetilde{\boldsymbol{m}}_a\}}$. Suppose that the eigenvalues $\lambda_n(\{\widetilde{\boldsymbol{m}}_a\})$ are sorted in ascending order and the minimum eigenvalue is $g(\{\widetilde{\boldsymbol{m}}_a\})$-fold degenerate:

$$\lambda_0(\{\widetilde{\boldsymbol{m}}_a\}) = \cdots = \lambda_{g(\{\widetilde{\boldsymbol{m}}_a\})-1} < \lambda_{g(\{\widetilde{\boldsymbol{m}}_a\})} \leq \cdots \leq \lambda_{2^A-1}. \tag{4.17}$$

Defining the gaps from the minimum eigenvalue as $\delta_n(\{\widetilde{\boldsymbol{m}}_a\}) = \lambda_n(\{\widetilde{\boldsymbol{m}}_a\}) - \lambda_0(\{\widetilde{\boldsymbol{m}}_a\})$, we find that Eqs. (4.13) and (4.14) are rewritten as

$$f = \frac{1}{A}\sum_a \widetilde{\boldsymbol{m}}_a \cdot \boldsymbol{m}_a + h_{\rm m}(\{\boldsymbol{m}_a\}) + \frac{1}{A}\lambda_0(\{\widetilde{\boldsymbol{m}}_a\}) - \frac{1}{A\beta}\ln\sum_n e^{-\beta\delta_n(\{\widetilde{\boldsymbol{m}}_a\})} \tag{4.18}$$

and

$$\boldsymbol{m}_a = \frac{\sum_n e^{-\beta\delta_n(\{\widetilde{\boldsymbol{m}}_a\})}\,\langle\lambda_n|\hat{\boldsymbol{\sigma}}_a|\lambda_n\rangle_{\{\widetilde{\boldsymbol{m}}_a\}}}{\sum_n e^{-\beta\delta_n(\{\widetilde{\boldsymbol{m}}_a\})}}, \tag{4.19}$$

where $\langle\lambda_n|\hat{\boldsymbol{\sigma}}_a|\lambda_n\rangle_{\{\widetilde{\boldsymbol{m}}_a\}}$ is the expectation value of $\hat{\boldsymbol{\sigma}}_a$ in the state $|\lambda_n\rangle_{\{\widetilde{\boldsymbol{m}}_a\}}$.

Now we take the zero-temperature limit $\beta \to \infty$. Since the excited states of the effective Hamiltonian $\hat{h}_{\rm eff}(\{\widetilde{\boldsymbol{m}}_a\})$ do not contribute to the free-energy density (4.18) and the saddle-point equation (4.19) in the limit $\beta \to \infty$, the free-energy density f approaches the ground-state energy density

$$u = \frac{1}{A}\sum_a \widetilde{\boldsymbol{m}}_a \cdot \boldsymbol{m}_a + h_{\rm m}(\{\boldsymbol{m}_a\}) + \frac{1}{A}\lambda_0(\{\widetilde{\boldsymbol{m}}_a\}) \tag{4.20}$$

and the parameters $\boldsymbol{m}_a$ and $\widetilde{\boldsymbol{m}}_a$ satisfy

$$\boldsymbol{m}_a = \frac{1}{g(\{\widetilde{\boldsymbol{m}}_a\})}\sum_{n=0}^{g(\{\widetilde{\boldsymbol{m}}_a\})-1} \langle\lambda_n|\hat{\boldsymbol{\sigma}}_a|\lambda_n\rangle_{\{\widetilde{\boldsymbol{m}}_a\}}\,. \tag{4.21}$$

Notice that Eq. (4.15) still holds in the zero-temperature limit $\beta \to \infty$.

4.2 Results for the weak-strong cluster model with sparse intercluster interactions

We consider the weak-strong cluster model whose interactions between the clusters are sparse. The problem Hamiltonian is defined as

$$\hat{H}_{\rm p} = -\sum_{i=1}^{N/2}(h_1\hat{Z}_{1r} + h_2\hat{Z}_{2r}) - \frac{1}{N}\sum_{r,r'=1}^{N/2}(\hat{Z}_{1r}\hat{Z}_{1r'} + \hat{Z}_{2r}\hat{Z}_{2r'}) - \frac{1}{2}\sum_{r=1}^{N/2}\hat{Z}_{1r}\hat{Z}_{2r}, \tag{4.22}$$

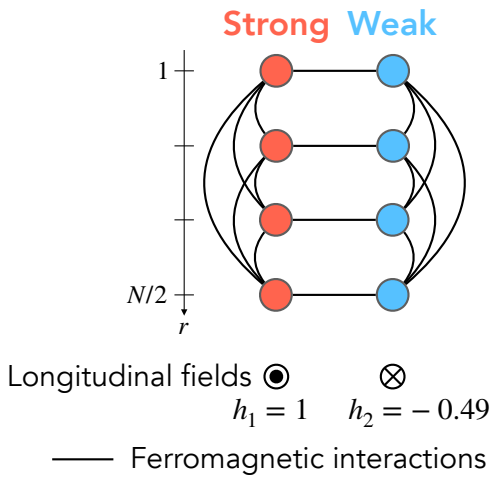

Figure 4.1: Weak-strong cluster problem with sparse intercluster interactions. The circles in the left (right) side denote the spins in the strong (weak) cluster.

where N is the total number of spins in the system and $\hat{\boldsymbol{\sigma}}_{ar} = (\hat{X}_{ar}, \hat{Y}_{ar}, \hat{Z}_{ar})^{\mathrm{T}}$ is the Pauli operator at (a, r) $(a = 1, 2;\ r = 1, \ldots, N/2)$. We set $h_1 = 1$ and $h_2 = -0.49$. The first subsystem $a = 1$ is the strong cluster and the second subsystem $a = 2$ is the weak cluster. Notice that the intercluster interactions exist only between the corresponding indices of the two clusters. We show the schematic diagram of the problem in Fig. 4.1.

The quantum annealing Hamiltonian for this problem is given by

$$\hat{H}(s) = s\hat{H}_{\mathrm{p}} - (1 - \gamma_1(s)) \sum_{r=1}^{N/2} \hat{X}_{1r} - (1 - \gamma_2(s)) \sum_{r=1}^{N/2} \hat{X}_{2r} \\ - s(1-s) \left(\frac{\xi_{11}}{N} \sum_{r,r'=1}^{N/2} \hat{X}_{1r}\hat{X}_{1r'} + \frac{\xi_{22}}{N} \sum_{r,r'=1}^{N/2} \hat{X}_{2r}\hat{X}_{2r'} + \frac{\xi_{12}}{2} \sum_{r=1}^{N/2} \hat{X}_{1r}\hat{X}_{2r} \right), \quad (4.23)$$

where $s \in [0, 1]$ is the dimensionless time. The functions $\gamma_1(s)$ and $\gamma_2(s)$ are monotonically increasing and are subject to $\gamma_1(0) = \gamma_2(0) = 0$ and $\gamma_1(1) = \gamma_2(1) = 1$. After taking the thermodynamic limit $N \to \infty$ and the zero-temperature limit $\beta \to \infty$, we calculate the magnetizations in the two clusters m_1^z and m_2^z using the imaginary-time path-integral formulation of the partition function and the saddle-point method with the static ansatz as detailed in the previous section.

We show the magnetizations m_1^z and m_2^z for $\gamma_1(s) = \gamma_2(s) = s$ and $(\xi_{11}, \xi_{22}, \xi_{12}) = (0, 0, \xi)$ in Fig. 4.2. We find that while the uniform transverse-field driver causes a first-order transition, both of the non-stoquastic XX interaction between the clusters and the stoquastic one can remove the transition. In contrast to the mean-field case analyzed in the previous chapter (see Fig. 3.2), there is no transition for large positive ξ and too large negative ξ.

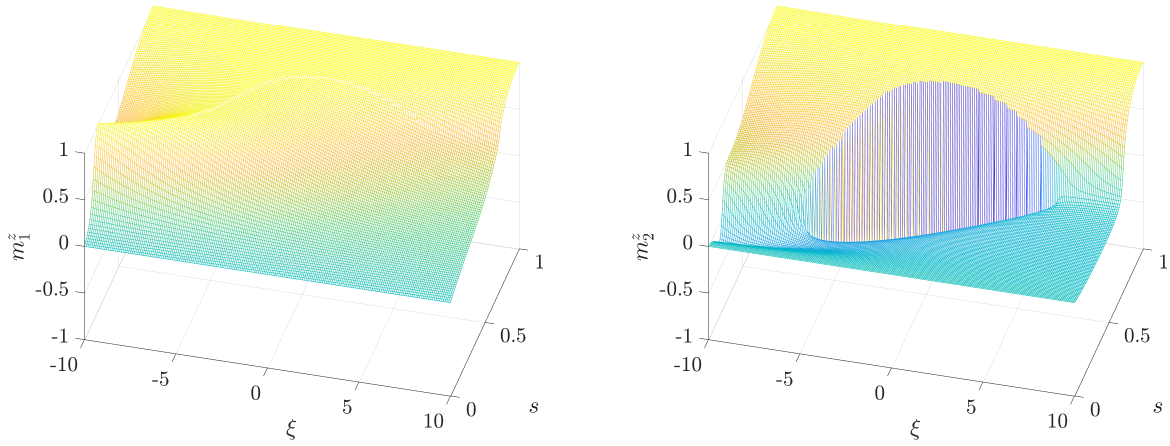

Figure 4.2: Magnetizations m_1^z and m_2^z of the weak-strong cluster model with sparse intercluster interactions for $\gamma_1(s) = \gamma_2(s) = s$ and $(\xi_{11}, \xi_{22}, \xi_{12}) = (0, 0, \xi)$.

On the other hand, Fig. 4.3 shows that the behavior of the magnetization m_2^z in the case of the XX interaction in each cluster, $\gamma_1(s) = \gamma_2(s) = s$ and $(\xi_{11}, \xi_{22}, \xi_{12}) = (\xi, 0, 0), (0, \xi, 0)$, is similar to that for the mean-field weak-strong cluster model (Fig. 3.5). Notice that the first-order transition is unavoidable in the case of the total XX interaction, $\gamma_1(s) = \gamma_2(s) = s$ and $(\xi_{11}, \xi_{22}, \xi_{12}) = (\xi/2, \xi/2, \xi)$, as shown in Fig. 4.4.

We next consider inhomogeneous driving of the transverse field. We set $\xi_{11} = \xi_{22} = \xi_{12} = 0$ and $(\gamma_1(s), \gamma_2(s)) = (\gamma(s), s), (s, \gamma(s))$, where $\gamma(s)$ is an arbitrary increasing function satisfying $\gamma(0) = 0$ and $\gamma(1) = 1$. Then, it turns out that the behavior of the magnetization m_2^z resembles that in the mean-field case (Fig. 3.7) as can be seen in Fig. 4.5.

4.3 Summary

We have analyzed the weak-strong cluster model with sparse interactions between the clusters by evaluating the partition function in the thermodynamic limit and the zero-temperature limit. The analysis was performed with the spin-coherent-state path-integral technique and the saddle-point method. We found several ways to avoid the first-order transition, which resemble those in the case with the mean-field-type all-to-all interactions analyzed in the previous chapter, except that not only the non-stoquastic intercluster XX interaction but also the stoquastic one can eliminate the first-order transition.

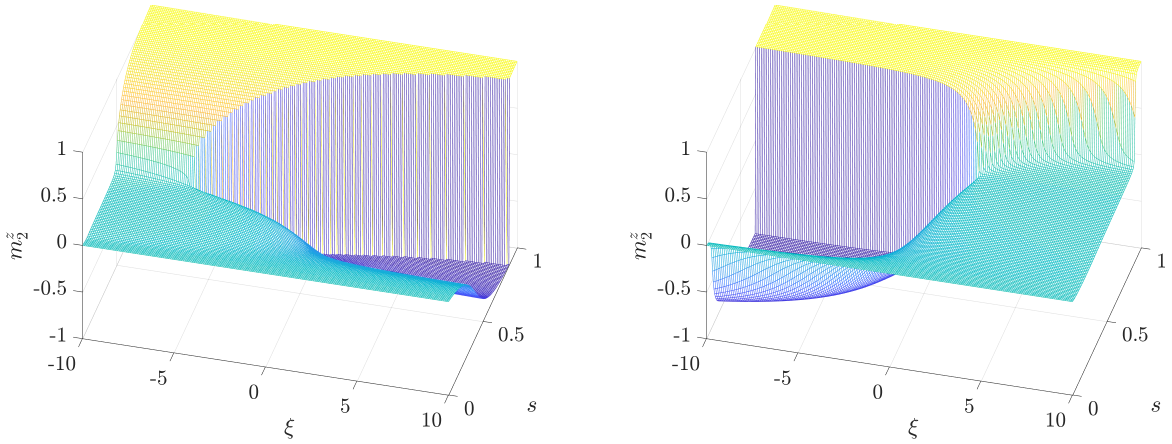

Figure 4.3: Magnetization in the weak cluster m_2^z of the weak-strong cluster model with sparse intercluster interactions for $(\xi_{11}, \xi_{22}, \xi_{12}) = (\xi, 0, 0)$ (left) and for $(\xi_{11}, \xi_{22}, \xi_{12}) = (0, \xi, 0)$ (right). We set $\gamma_1(s) = \gamma_2(s) = s$ in both cases.

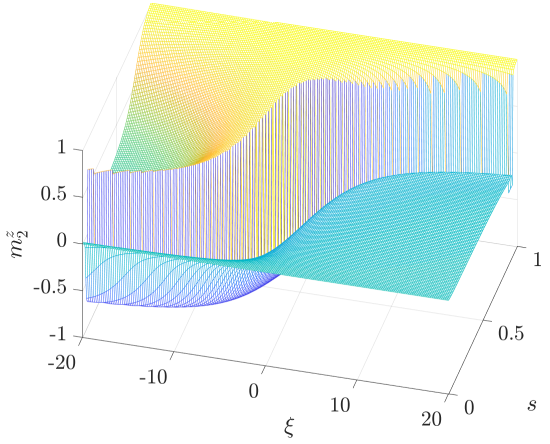

Figure 4.4: Magnetization in the weak cluster m_2^z of the weak-strong cluster model with sparse intercluster interactions for $\gamma_1(s) = \gamma_2(s) = s$ and $(\xi_{11}, \xi_{22}, \xi_{12}) = (\xi/2, \xi/2, \xi)$.

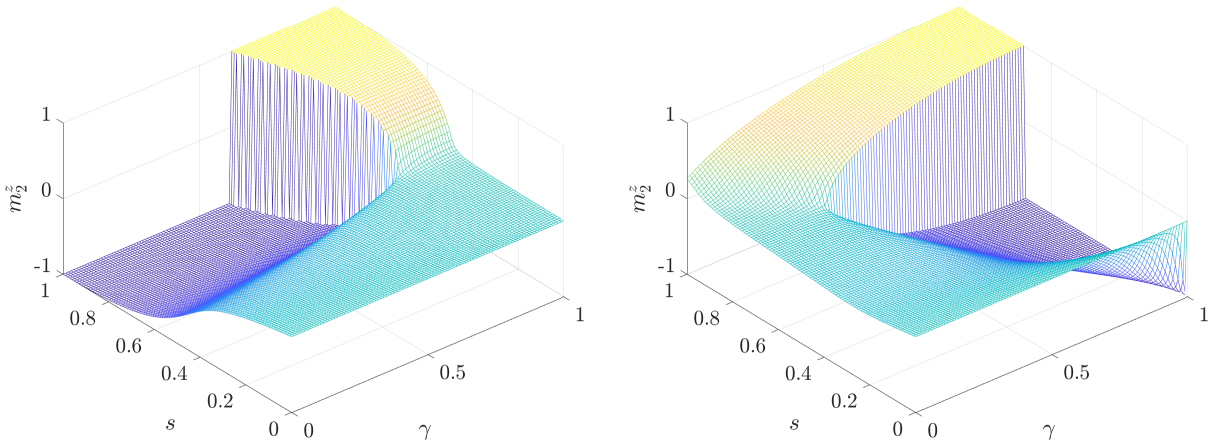

Figure 4.5: Magnetization in the weak cluster m_2^z of the weak-strong cluster model with sparse intercluster interactions for $(\gamma_1, \gamma_2) = (\gamma, s)$ (left) and for $(\gamma_1, \gamma_2) = (s, \gamma)$ (right). We set $\xi_{11} = \xi_{22} = \xi_{12} = 0$ in both cases.

Chapter 5

Frustrated Ising ladder

In this chapter, we analyze the frustrated Ising ladder as a problem which has only spatially local interactions, in contrast to the weak-strong cluster models studied in the previous chapters. This problem was proposed by Laumann *et al.* [68]. The frustrated Ising ladder is a quasi-one-dimensional Ising model defined on a two-leg ladder. One of the important features is that the model can be mapped onto the quantum dimer model on a two-leg ladder in the limit of infinite frustration. Laumann *et al.* showed by exact diagonalization of the small-size systems that the frustrated Ising ladder in a transverse field for large frustration has a first-order transition of essentially topological origin. The correspondence with the dimer model is the key to understanding the topological nature of the frustrated Ising ladder. The aim of this chapter lies in revealing non-stoquastic effects on such an interesting system.

Since the frustrated Ising ladder is a low-dimensional system, we cannot exactly analyze the model by the semi-classical method or the saddle-point method as in the previous chapters. We tackle the problem using the real-space renormalization group (RG) method. Although the real-space RG approach in general is not exact, we will see that our method extracts key features of the system as the RG transformation projects the Hilbert space onto a low-energy subspace.

We review physical pictures of the frustrated Ising ladder in Section 5.1 and the way of mapping onto the quantum dimer model in Section 5.2. In Section 5.3, we give the mathematical description of the low-energy states to prepare for the real-space RG analysis. Section 5.4 provides the detailed procedure of the real-space RG transformation. Section 5.5 demonstrates the results of the RG analysis, including the phase diagram and discussions on quantum annealing of this problem. The results are compared with the result of numerical diagonalization [68] and that of the density-matrix renormalization group calculation carried out by Sota and Yunoki [70]. This chapter is summarized in Section 5.6. Sections 5.4–5.6 are based on the author's original work.

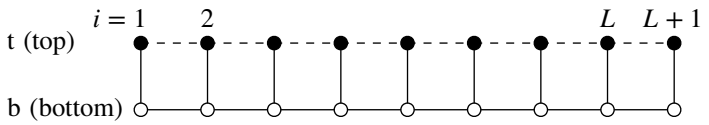

Figure 5.1: Frustrated Ising ladder with transverse fields and XX interactions. Spin-1/2 particles are located at the black and white points. The solid and dashed lines are ferromagnetic and antiferromagnetic interactions of the strength K, respectively. There are an upward longitudinal field K at each black point and a downward longitudinal field $U/2$ at each white point. A transverse field $\Gamma_{\rm t}$ is appended at every site on the top row and $\Gamma_{\rm b}$ on the bottom row. An XX interaction $\Xi_{\rm tt}$ is applied on each horizontal bond on the top row, $\Xi_{\rm bb}$ on each horizontal bond on the bottom row, and $\Xi_{\rm tb}$ on each vertical bond between the two rows. The sites at the horizontal position $i = L + 1$ are identified with those at $i = 1$ for the periodic boundary condition.

5.1 Introduction to the frustrated Ising ladder

We consider the frustrated Ising ladder with transverse fields and XX interactions. The version with the uniform transverse field and no XX interactions was proposed in Ref. [68]. The ladder has the top row (t) and the bottom row (b). The Hamiltonian is given by

$$\hat{H} = \sum_{i=1}^{L} \Bigg[K(\hat{Z}_{{\rm t},i}\hat{Z}_{{\rm t},i+1} - \hat{Z}_{{\rm b},i}\hat{Z}_{{\rm b},i+1} - \hat{Z}_{{\rm t},i}\hat{Z}_{{\rm b},i} - \hat{Z}_{{\rm t},i}) + \frac{U}{2}\hat{Z}_{{\rm b},i} \\ - (\Gamma_{\rm t}\hat{X}_{{\rm t},i} + \Gamma_{\rm b}\hat{X}_{{\rm b},i}) - (\Xi_{\rm tt}\hat{X}_{{\rm t},i}\hat{X}_{{\rm t},i+1} + \Xi_{\rm bb}\hat{X}_{{\rm b},i}\hat{X}_{{\rm b},i+1} + \Xi_{\rm tb}\hat{X}_{{\rm t},i}\hat{X}_{{\rm b},i}) \Bigg], \quad (5.1)$$

where $\hat{X}_{a,i}$, $\hat{Y}_{a,i}$, and $\hat{Z}_{a,i}$ are the Pauli operators at the position $i = 1, \dots, L$ on the row $a = {\rm t}, {\rm b}$. We assume the length L to be even and impose the periodic boundary condition

$$\hat{X}_{a,L+1} = \hat{X}_{a,1}, \quad \hat{Y}_{a,L+1} = \hat{Y}_{a,1}, \quad \hat{Z}_{a,L+1} = \hat{Z}_{a,1}. \quad (5.2)$$

Suppose that K, U, and Γ_a are positive. The terms proportional to K in the expression of the Hamiltonian $\hat{H}$ are interactions and a longitudinal field which cause frustration. In addition, $U/2$, Γ_a, and $\Xi_{aa'}$ are the strengths of a downward longitudinal field on the bottom row, transverse fields, and nearest-neighbor XX interactions, respectively. The Hamiltonian $\hat{H}$ is stoquastic for $\Xi_{\rm tt}, \Xi_{\rm bb}, \Xi_{\rm tb} \geq 0$ and non-stoquastic for $\Xi_{\rm tt} < 0$, $\Xi_{\rm bb} < 0$, or $\Xi_{\rm tb} < 0$. We show the schematic diagram of the model in Fig. 5.1.

Laumann *et al.* [68] revealed the phase diagram in the case of the uniform transverse field $\Gamma_{\rm t} = \Gamma_{\rm b} = \Gamma$ and no XX interactions $\Xi_{\rm tt} = \Xi_{\rm bb} = \Xi_{\rm tb} = 0$ using numerical diagonalization of the small-size systems, as displayed in Fig. 5.2. More precisely, they carried out exact diagonalization in the translationally invariant subspace for $L = 12$ and computed Γ/U which minimizes the energy gap between the ground state and the first excited state for each fixed K/U (notice that the translation operator is conserved and its value is unity in quantum annealing). The phase diagram shows that a first-order

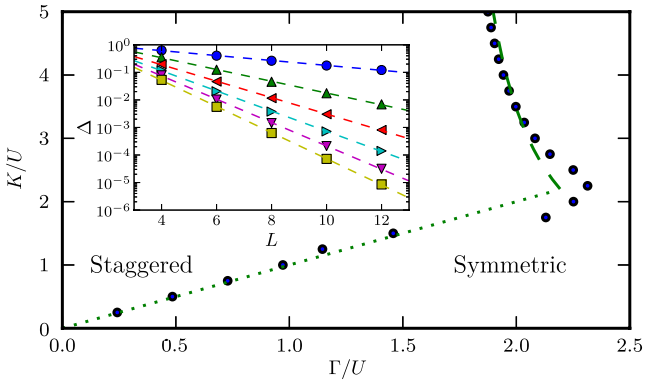

Figure 5.2: Phase diagram of the frustrated Ising ladder in a transverse field depicted by Laumann, Moessner, Scardicchio, and Sondhi (2012) [68]. The points indicate the values of Γ/U which minimize the energy gap in the translationally invariant subspace for $L = 12$ and fixed values of K/U. The dashed line is a first-order transition line predicted by the second-order perturbation theory in U/K combined with the result of numerical diagonalization of the quantum dimer model (see Section 5.2), $\Gamma/U = 1/b + U/(4Kb^3)$ with $b \approx 0.6$. The dotted line is a second-order transition line predicted to leading order in K/U, $\Gamma = K$. Inset: Exponential scaling of the energy gap in the translationally invariant subspace at the first-order transition points, where $K/U = 2.5, 3.0, 3.5, 4.0, 4.5, 5.0$ from top to bottom.

transition between the symmetric (columnar) phase and the staggered phase occurs when Γ/U is varied with K/U fixed to a large value. For small K/U, there is a second-order transition because the bottom spins are almost fixed to down and the top row is effectively regarded as an antiferromagnetic Ising chain in a transverse field. Laumann *et al.* also showed that the energy gap at the first-order transition which exists for large K/U decays exponentially as the length L grows, which can be seen in the inset of Fig. 5.2.

Let us focus on the case of large K/U, which is crucial for quantum annealing since there is a first-order transition. For $\Gamma_t = \Gamma_b = \Gamma$ and $\Xi_{tt} = \Xi_{bb} = \Xi_{tb} = 0$, the system is in the columnar phase for large Γ/U and in the staggered phase for small Γ/U. We can characterize the columnar and staggered phases using the perturbation theory in K^{-1}. Regard the sum of the terms proportional to K in the Hamiltonian (5.1) as a non-perturbative Hamiltonian and the sum of the other terms as a perturbation. Then, if the leading-order part of the state is a columnar (staggered) state, we can say that the system is in the columnar (staggered) phase. Columnar and staggered states are defined as follows:

- Columnar states are configurations in which all the bottom spins are up and there are no consecutive down spins on the top row, and their superpositions; and
- Staggered states are configurations in which all the bottom spins are down and the top spins are antiferromagnetically ordered, and their superpositions.

Here, we meant by a "configuration" a product state of local eigenstates of $\hat{Z}_{a,i}$. As shown in Section 5.3, both of the columnar states and the staggered states are the ground states of the non-perturbative Hamiltonian. These states are the low-energy states in the sense that the number of frustrated terms in the Hamiltonian is minimized. The perturbation lifts the degeneracy and causes the first-order transition. Accepting this picture, we can intuitively follow the reason why the system is in the columnar phase for large transverse field Γ: Some types of single spin flip are allowed in the columnar phase, while any single spin flip is not allowed in the staggered phase. On the other hand, small Γ or large U leads the system into the staggered phase.

Now we mention that there are only two independent staggered states, while the number of independent columnar states is $F_{L-1}+F_{L-3}$, the sum of two Fibonacci numbers. Here, F_L is defined by the recurrence relation $F_L = F_{L-1} + F_{L-2}$ and the initial values $F_1 = 2$ and $F_2 = 3$. Noticing that the Fibonacci number F_L is exponentially large as a function of the length L, we find that there are an exponentially large number of independent columnar states. We will derive the number of the low-energy states, namely columnar and staggered states, in Section 5.3.

When we consider the Hamiltonian (5.1) as a quantum annealing Hamiltonian, the problem Hamiltonian is given by the first line of Eq. (5.1), whose ground states are the two staggered states, and the driver Hamiltonian consists of the transverse fields and the XX interactions. The coefficients in the Hamiltonian $\hat{H}$ are varied with time such that the strength of the problem Hamiltonian increases from zero to a finite value while the transverse fields decrease and vanish at the end of annealing. If we apply the XX interactions $\Xi_{aa'}$, their absolute values $|\Xi_{aa'}|$ increase from zero to non-vanishing values and decrease to zero. For example, we can set $K, U \propto s$, $\Gamma_a \propto 1 - s$, and $\Xi_{aa'} \propto s(1-s)$ with $s \in [0, 1]$ being the dimensionless time. If a first-order transition exists, the energy gap at the transition becomes exponentially small, which requires exponentially long computation time.

5.2 Mapping onto the quantum dimer model

In this section, we review the way to map the frustrated Ising ladder onto the quantum dimer model following Ref. [68]. The quantum dimer model was first introduced by Rokhsar and Kivelson [90] for studying high-temperature superconductors. An instructive review of the quantum dimer model is found, e.g., in the lecture note [91]. Although the mapping between the frustrated quantum Ising model and the quantum dimer model is known for various lattices [92, 93], we focus on the quantum dimer model on a two-leg ladder and its correspondence with the frustrated Ising ladder.

The dimer model is formed by many dimers on a lattice. A dimer is a line segment between two nearest-neighbor sites. The model is subject to the constraint that each site is an end point of just one dimer, not zero or multiple dimers. A dimer configuration which satisfies this constraint is called a dimer covering. We show examples of dimer

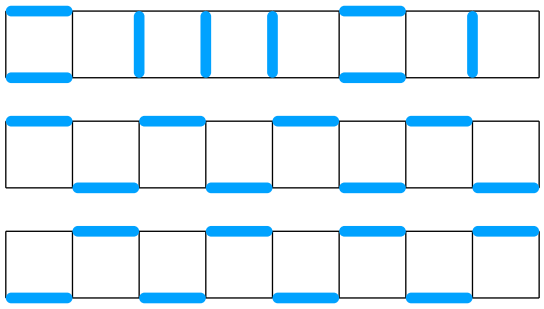

Figure 5.3: Examples of dimer coverings on a two-leg periodic ladder. The rightmost points are identified with the leftmost points for the periodic boundary condition. The blue thick line segments represent dimers. The topological number is $w = 0, +1, -1$ from top to bottom.

coverings on a two-leg periodic ladder in Fig. 5.3. For the quantum dimer model, the set of all dimer coverings constitutes the basis of the Hilbert space.

The dimer coverings on a two-leg ladder are classified into three topological sectors and characterized by the topological number $w = 0, \pm 1$. Here, the topological number w is the difference in the number of dimers between the top and bottom rows on a fixed plaquette (see Fig. 5.3). Notice that although a fixed plaquette is chosen arbitrarily, the definition of w depends on whether an even- or odd-numbered plaquette is chosen: $w = n_{\mathrm{t},i} - n_{\mathrm{b},i}$ for odd i and $w = n_{\mathrm{b},i} - n_{\mathrm{t},i}$ for even i, where $n_{\mathrm{t},i}$ ($n_{\mathrm{b},i}$) is the number of dimers on the top (bottom) row of the ith plaquette. We mean by "topological" that each dimer covering cannot be transformed into another dimer covering which has a different w by a series of local movements of dimers with the constraint of dimer coverings kept.

We refer to the topological sector $w = 0$ as the columnar sector and $w = \pm 1$ as the staggered sectors. Dimer coverings in the columnar sector consist of top and bottom horizontal dimers at corresponding positions and vertical dimers, while those in the staggered sectors are constituted by horizontal dimers alternately put on the top and bottom rows. We immediately find that the columnar sector $w = 0$ has many dimer coverings, while each of the staggered sectors $w = \pm 1$ has only one state. As shown below, the columnar and staggered states in the dimer model correspond to those in the frustrated Ising ladder in a one-to-one manner. This means that the number of dimer coverings in the columnar sector is $F_{L-1} + F_{L-3}$, the sum of two Fibonacci numbers, which diverges exponentially as the length of the ladder L becomes longer.

Let us explain how to map the columnar and staggered states in the frustrated Ising ladder (5.1) onto those in the dimer model on a two-leg ladder. Since the columnar and staggered states are the low-energy states (more precisely, the ground states of the non-perturbative Hamiltonian proportional to K, as shown in the next section), these states minimize the number of positive terms among the antiferromagnetic interactions on the top row $+K\hat{Z}_{\mathrm{t},i}\hat{Z}_{\mathrm{t},i+1}$, the ferromagnetic interactions between the top and bottom rows $-K\hat{Z}_{\mathrm{t},i}\hat{Z}_{\mathrm{b},i}$, and the upward fields on the top row $-K\hat{Z}_{\mathrm{t},i}$ (notice that the ferromagnetic

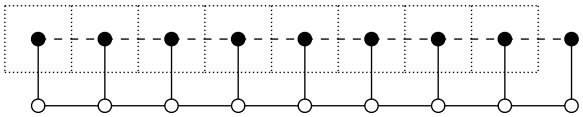

Figure 5.4: Frustrated Ising ladder and its dual lattice. The solid and dashed lines and the black and white points denote the same things as those in Fig. 5.1. The dotted lines constitute the dual lattice. The rightmost points are identified with the leftmost points for each lattice, which is subject to the periodic boundary condition.

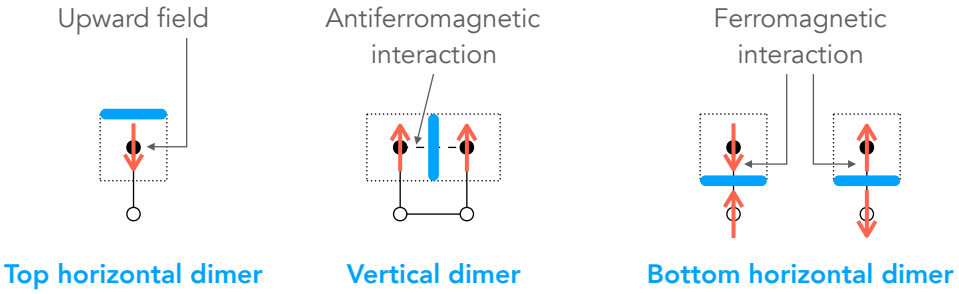

Figure 5.5: Frustrations on the Ising ladder and corresponding dimers on the dual lattice. Parts of the lattice for the Ising model and its dual lattice for the dimer model are depicted in the same manner as in Fig. 5.4. The red arrows represent directions of the spins and the blue thick line segments denote dimers. Notice that the upward field, the antiferromagnetic interaction, and the ferromagnetic interaction in this figure have the strength K.

interactions on the bottom row $-K\hat{Z}_{\mathrm{b},i}\hat{Z}_{\mathrm{b},i+1}$ are negative at all positions both in the columnar states and in the staggered states). Such positive terms proportional to K cannot entirely be removed, indicating the presence of frustrations. In order to map the low-energy states in the Ising ladder onto states in the dimer model, we consider the dual lattice whose position is shifted by half the unit length horizontally and vertically from the Ising ladder, as depicted in Fig. 5.4.

We put dimers on the dual lattice according to the types and positions of frustrations. See Fig. 5.5. Frustrations and corresponding dimers are classified into three types: First, a top horizontal dimer is put if there is a down spin on the top row. Second, a vertical dimer is put if there is a horizontally aligned ferromagnetic pair on the top row. Third, a bottom horizontal dimer is put if there is a vertically aligned antiferromagnetic pair.

Then, we find that the columnar and staggered states in the frustrated Ising ladder are mapped onto those in the dimer model on the dual lattice in a one-to-one manner. In other words, there is a bijection between the set of low-energy states in the frustrated Ising ladder and dimer coverings in the dimer model. Examples of the correspondence between states in the two models are shown in Fig. 5.6.

Notice that although there are high-energy states, which are neither columnar nor staggered states and are not mapped onto dimer coverings, in the frustrated Ising ladder

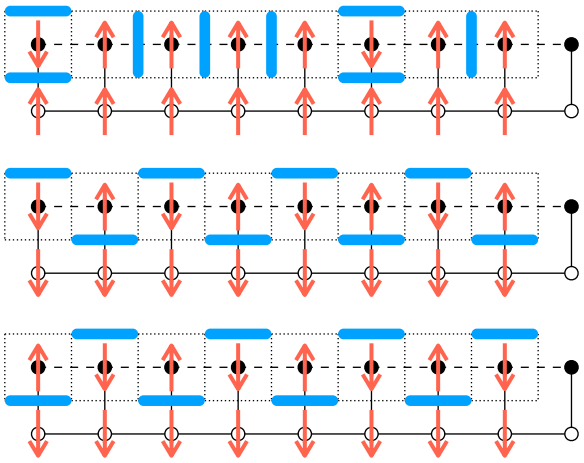

Figure 5.6: Examples of the correspondence between low-energy states in the frustrated Ising ladder and the dimer model on a two-leg ladder. The lattice for the Ising model and its dual lattice for the dimer model are depicted in the same manner as in Fig. 5.4. The red arrows are spins and the blue thick line segments are dimers. The topological number is $w = 0, +1, -1$ from top to bottom, the first being a columnar state for each model and the second and the third being staggered states.

with finite K, the existence of these states is strictly prohibited in the limit of infinite K. In this sense, we refer to the limit $K \to \infty$ as the dimer limit. Transition from the columnar phase to the staggered phase in the frustrated Ising ladder with infinite K requires flipping all the spins on the bottom row at the same time, which cannot be achieved by a series of local spin flips. Likewise, the change between the two staggered states demands simultaneously flipping every top spin when K is infinite. These facts indicate that the dimer limit $K \to \infty$ is the purely topological limit.

Now we map the perturbative terms in Eq. (5.1), which have the coefficients U, Γ_a, and $\Xi_{aa'}$, onto operators on the dimer model. Since the longitudinal field on the bottom row $+\frac{U}{2}\sum_i \hat{Z}_{\mathrm{b},i}$ makes energy difference U per unit length between the columnar and staggered states, we derive the mapping

$$+\frac{U}{2}\sum_{i=1}^{L}\hat{Z}_{\mathrm{b},i} \mapsto +U\left(\sum_{|}\Big|\,|\,\Big\rangle\Big\langle\,|\,\Big| + 2\sum_{\square}\Big|=\Big\rangle\Big\langle=\Big|\right) - \frac{U}{2}L. \tag{5.3}$$

Here, the first and second summations on the right-hand side are performed over vertical lines | and plaquettes □ on the dual lattice for the dimer model, respectively, and horizontal and vertical line segments in kets and bras denote states of dimers.

The transverse field on the top row $-\Gamma_{\mathrm{t}}\sum_i \hat{X}_{\mathrm{t},i} = -\Gamma_{\mathrm{t}}\sum_i(|{\uparrow}\rangle\langle{\downarrow}| + |{\downarrow}\rangle\langle{\uparrow}|)_{\mathrm{t},i}$ corresponds to the flip of pairs of dimers in the columnar sector:

$$-\Gamma_{\mathrm{t}}\sum_{i=1}^{L}\hat{X}_{\mathrm{t},i} \mapsto -\Gamma_{\mathrm{t}}\sum_{\square}\left(\Big|\,\|\,\Big\rangle\Big\langle=\Big| + \Big|=\Big\rangle\Big\langle\,\|\,\Big|\right). \tag{5.4}$$

Notice that this operator has no effect on the staggered states in the dimer model because any dimer is non-flippable in the staggered sectors. The transverse field on the bottom row $-\Gamma_{\rm b}\sum_i \hat{X}_{{\rm b},i}$ excites both of the columnar and staggered states into high-energy states paying energy penalties proportional to K and thus is irrelevant in the limit $K\to\infty$, or in the dimer model.

As for the XX interaction on the top row

$$-\Xi_{\rm tt}\sum_i \hat{X}_{{\rm t},i}\hat{X}_{{\rm t},i+1} = -\Xi_{\rm tt}\sum_i (|{\downarrow\uparrow}\rangle\langle{\uparrow\downarrow}| + |{\uparrow\downarrow}\rangle\langle{\downarrow\uparrow}| + |{\uparrow\uparrow}\rangle\langle{\downarrow\downarrow}| + |{\downarrow\downarrow}\rangle\langle{\uparrow\uparrow}|)_{{\rm t},(i,i+1)}, \quad (5.5)$$

the last two terms are meaningless in the dimer limit $K\to\infty$ (recall that the presence of consecutive down spins on the top row is not allowed) and the sum of the first two terms yields the following type of flip of dimers:

$$-\Xi_{\rm tt}\sum_i \hat{X}_{{\rm t},i}\hat{X}_{{\rm t},i+1} \mapsto -\Xi_{\rm tt}\sum_{\square\!\square}\left(\left|\ =|\ \right\rangle\left\langle\ |=\ \right| + \left|\ |=\ \right\rangle\left\langle\ =|\ \right|\right), \quad (5.6)$$

where the summation on the right-hand side is taken over double plaquettes $\square\!\square$ and the symbol $=|$ as well as $|=$ denotes a pair of horizontal dimers with a neighboring vertical dimer. The XX interactions on other pairs of spins, namely $-\Xi_{\rm bb}\sum_i \hat{X}_{{\rm b},i}\hat{X}_{{\rm b},i+1}$ and $-\Xi_{\rm tb}\sum_i \hat{X}_{{\rm t},i}\hat{X}_{{\rm b},i}$, are irrelevant in the dimer limit $K\to\infty$. It should be noticed that the same operator on the dimer model as in Eq. (5.6) can be derived from the YY interactions on the top row, because they are decomposed as $\hat{Y}_{{\rm t},i}\hat{Y}_{{\rm t},i+1} = (|{\downarrow\uparrow}\rangle\langle{\uparrow\downarrow}| + |{\uparrow\downarrow}\rangle\langle{\downarrow\uparrow}| - |{\uparrow\uparrow}\rangle\langle{\downarrow\downarrow}| - |{\downarrow\downarrow}\rangle\langle{\uparrow\uparrow}|)_{{\rm t},(i,i+1)}$, whose first two terms are identical with those of $\hat{X}_{{\rm t},i}\hat{X}_{{\rm t},i+1}$ and the others are irrelevant.

Consequently, the Hamiltonian of the frustrated Ising ladder (5.1) is mapped onto the following Hamiltonian in the dimer limit $K\to\infty$:

$$\begin{aligned}\hat{H}_{\rm dimer} = U\left(\sum_{|}\left|\ |\ \right\rangle\left\langle\ |\ \right| + 2\sum_{\square}\left|=\right\rangle\left\langle=\right|\right) - \Gamma_{\rm t}\sum_{\square}\left(\left|\ \|\ \right\rangle\left\langle\ =\right| + \left|=\right\rangle\left\langle\ \|\ \right|\right) \\ -\Xi_{\rm tt}\sum_{\square\!\square}\left(\left|\ =|\ \right\rangle\left\langle\ |=\ \right| + \left|\ |=\ \right\rangle\left\langle\ =|\ \right|\right), \end{aligned} \quad (5.7)$$

where a constant energy difference was ignored. It turns out that the only non-vanishing matrix elements of $\hat{H}_{\rm dimer}$ are those between states in the columnar sector. This indicates that the quantum dimer model with the Hamiltonian $\hat{H}_{\rm dimer}$ has a strict energy-level crossing between the columnar and staggered sectors, because the energy levels in the columnar sector vary with a change in the parameters while those in the staggered sectors remain unchanged.

In the case of no XX interaction on the top row $\Xi_{\rm tt}=0$, the corresponding quantum dimer model has a strict level crossing at $\Gamma_{\rm t}/U \approx 1/0.6 = 1.66\cdots$ according to numerical diagonalization of the quantum dimer model of small sizes [68]. For the frustrated Ising

ladder with large but finite K, the level crossing turns into an avoided crossing thanks to non-vanishing transition probabilities to high-energy states, but the energy gap at the first-order transition decays exponentially as the length L increases, reflecting the topological nature which relates to the quantum dimer model [68].

5.3 Preliminary analysis

We will analyze the zero-temperature transition of the frustrated Ising ladder (5.1) in the dimer limit $K \gg U, \Gamma_a, \Xi_{aa'}$ by the real-space RG method. This section demonstrates why the columnar and staggered states are the low-energy states and derives the number of the low-energy states, before the real-space RG analysis.

Since the overall energy scale does not change the statistical properties in the zero-temperature limit, we consider the dimensionless Hamiltonian $\hat{h} = \hat{H}/K$:

$$\hat{h} = \sum_{i=1}^{L} \Big(\hat{Z}_{\mathrm{t},i}\hat{Z}_{\mathrm{t},i+1} - \hat{Z}_{\mathrm{b},i}\hat{Z}_{\mathrm{b},i+1} - \hat{Z}_{\mathrm{t},i}\hat{Z}_{\mathrm{b},i} - \hat{Z}_{\mathrm{t},i} + \frac{u}{2}\hat{Z}_{\mathrm{b},i} \\ - (\gamma_{\mathrm{t}}\hat{X}_{\mathrm{t},i} + \gamma_{\mathrm{b}}\hat{X}_{\mathrm{b},i}) - (\xi_{\mathrm{tt}}\hat{X}_{\mathrm{t},i}\hat{X}_{\mathrm{t},i+1} + \xi_{\mathrm{bb}}\hat{X}_{\mathrm{b},i}\hat{X}_{\mathrm{b},i+1} + \xi_{\mathrm{tb}}\hat{X}_{\mathrm{t},i}\hat{X}_{\mathrm{b},i}) \Big), \tag{5.8}$$

where $u = U/K$, $\gamma_a = \Gamma_a/K$, and $\xi_{aa'} = \Xi_{aa'}/K$ are sufficiently small dimensionless parameters. We assume that u, γ_a, and $\xi_{aa'}$ are of the same order $\delta \ll 1$. We separate the Hamiltonian $\hat{h}$ into $\hat{h}^{(0)} = \mathcal{O}(\delta^0)$ and $\hat{h}^{(1)} = \mathcal{O}(\delta^1)$:

$$\hat{h} = \hat{h}^{(0)} + \hat{h}^{(1)}, \tag{5.9}$$

$$\hat{h}^{(0)} = \sum_{i=1}^{L} (\hat{Z}_{\mathrm{t},i}\hat{Z}_{\mathrm{t},i+1} - \hat{Z}_{\mathrm{b},i}\hat{Z}_{\mathrm{b},i+1} - \hat{Z}_{\mathrm{t},i}\hat{Z}_{\mathrm{b},i} - \hat{Z}_{\mathrm{t},i}) \\ = \sum_{i=1}^{L} \left(\hat{Z}_{\mathrm{t},i}\hat{Z}_{\mathrm{t},i+1} - \hat{Z}_{\mathrm{b},i}\hat{Z}_{\mathrm{b},i+1} - \hat{Z}_{\mathrm{t},i}\frac{1+\hat{Z}_{\mathrm{b},i}}{2} - \hat{Z}_{\mathrm{t},i+1}\frac{1+\hat{Z}_{\mathrm{b},i+1}}{2} \right), \tag{5.10}$$

$$\hat{h}^{(1)} = \sum_{i=1}^{L} \left(\frac{u}{2}\hat{Z}_{\mathrm{b},i} - (\gamma_{\mathrm{t}}\hat{X}_{\mathrm{t},i} + \gamma_{\mathrm{b}}\hat{X}_{\mathrm{b},i}) - (\xi_{\mathrm{tt}}\hat{X}_{\mathrm{t},i}\hat{X}_{\mathrm{t},i+1} + \xi_{\mathrm{bb}}\hat{X}_{\mathrm{b},i}\hat{X}_{\mathrm{b},i+1} + \xi_{\mathrm{tb}}\hat{X}_{\mathrm{t},i}\hat{X}_{\mathrm{b},i}) \right). \tag{5.11}$$

Let us write the zeroth-order Hamiltonian $\hat{h}^{(0)}$ as a linear combination of projectors:

$$\begin{aligned}\hat{h}^{(0)} = \sum_{i=1}^{L}\Bigg(&-2\left|\begin{matrix}\uparrow\uparrow\\ \uparrow\uparrow\end{matrix}\right\rangle\left\langle\begin{matrix}\uparrow\uparrow\\ \uparrow\uparrow\end{matrix}\right| - 2\left|\begin{matrix}\downarrow\uparrow\\ \uparrow\uparrow\end{matrix}\right\rangle\left\langle\begin{matrix}\downarrow\uparrow\\ \uparrow\uparrow\end{matrix}\right| - 2\left|\begin{matrix}\uparrow\downarrow\\ \uparrow\uparrow\end{matrix}\right\rangle\left\langle\begin{matrix}\uparrow\downarrow\\ \uparrow\uparrow\end{matrix}\right| + 2\left|\begin{matrix}\downarrow\downarrow\\ \uparrow\uparrow\end{matrix}\right\rangle\left\langle\begin{matrix}\downarrow\downarrow\\ \uparrow\uparrow\end{matrix}\right| \\ &+0\left|\begin{matrix}\uparrow\uparrow\\ \downarrow\downarrow\end{matrix}\right\rangle\left\langle\begin{matrix}\uparrow\uparrow\\ \downarrow\downarrow\end{matrix}\right| - 2\left|\begin{matrix}\downarrow\uparrow\\ \downarrow\downarrow\end{matrix}\right\rangle\left\langle\begin{matrix}\downarrow\uparrow\\ \downarrow\downarrow\end{matrix}\right| - 2\left|\begin{matrix}\uparrow\downarrow\\ \downarrow\downarrow\end{matrix}\right\rangle\left\langle\begin{matrix}\uparrow\downarrow\\ \downarrow\downarrow\end{matrix}\right| + 0\left|\begin{matrix}\downarrow\downarrow\\ \downarrow\downarrow\end{matrix}\right\rangle\left\langle\begin{matrix}\downarrow\downarrow\\ \downarrow\downarrow\end{matrix}\right| \\ &+1\left|\begin{matrix}\uparrow\uparrow\\ \downarrow\uparrow\end{matrix}\right\rangle\left\langle\begin{matrix}\uparrow\uparrow\\ \downarrow\uparrow\end{matrix}\right| - 1\left|\begin{matrix}\downarrow\uparrow\\ \downarrow\uparrow\end{matrix}\right\rangle\left\langle\begin{matrix}\downarrow\uparrow\\ \downarrow\uparrow\end{matrix}\right| + 1\left|\begin{matrix}\uparrow\downarrow\\ \downarrow\uparrow\end{matrix}\right\rangle\left\langle\begin{matrix}\uparrow\downarrow\\ \downarrow\uparrow\end{matrix}\right| + 3\left|\begin{matrix}\downarrow\downarrow\\ \downarrow\uparrow\end{matrix}\right\rangle\left\langle\begin{matrix}\downarrow\downarrow\\ \downarrow\uparrow\end{matrix}\right| \\ &+1\left|\begin{matrix}\uparrow\uparrow\\ \uparrow\downarrow\end{matrix}\right\rangle\left\langle\begin{matrix}\uparrow\uparrow\\ \uparrow\downarrow\end{matrix}\right| + 1\left|\begin{matrix}\downarrow\uparrow\\ \uparrow\downarrow\end{matrix}\right\rangle\left\langle\begin{matrix}\downarrow\uparrow\\ \uparrow\downarrow\end{matrix}\right| - 1\left|\begin{matrix}\uparrow\downarrow\\ \uparrow\downarrow\end{matrix}\right\rangle\left\langle\begin{matrix}\uparrow\downarrow\\ \uparrow\downarrow\end{matrix}\right| + 3\left|\begin{matrix}\downarrow\downarrow\\ \uparrow\downarrow\end{matrix}\right\rangle\left\langle\begin{matrix}\downarrow\downarrow\\ \uparrow\downarrow\end{matrix}\right|\Bigg)_{i,i+1}. \end{aligned} \tag{5.12}$$

Here, $|\uparrow\rangle_{a,i}$ and $|\downarrow\rangle_{a,i}$ are the normalized eigenstates of $\hat{Z}_{a,i}$ with the eigenvalues $+1$ and -1, respectively. Each state vector containing an array of arrows means a product state and the positions in the array correspond to those in the ladder:

$$\left|\begin{matrix}\sigma_{\mathrm{t},i}\ \sigma_{\mathrm{t},i+1}\\ \sigma_{\mathrm{b},i}\,\sigma_{\mathrm{b},i+1}\end{matrix}\right\rangle_{i,i+1} := |\sigma_{\mathrm{t},i}\rangle_{\mathrm{t},i}\,|\sigma_{\mathrm{b},i}\rangle_{\mathrm{b},i}\,|\sigma_{\mathrm{t},i+1}\rangle_{\mathrm{t},i+1}\,|\sigma_{\mathrm{b},i+1}\rangle_{\mathrm{b},i+1} \quad (\sigma_{a,j} = \uparrow, \downarrow). \tag{5.13}$$

Since a constant energy difference is unimportant, we redefine $\hat{h}^{(0)} + 2$ as $\hat{h}^{(0)}$:

$$\begin{aligned}\hat{h}^{(0)} = \sum_{i=1}^{L}\Bigg(&+4\left|\begin{matrix}\downarrow\downarrow\\ \uparrow\uparrow\end{matrix}\right\rangle\left\langle\begin{matrix}\downarrow\downarrow\\ \uparrow\uparrow\end{matrix}\right| + 2\left|\begin{matrix}\uparrow\uparrow\\ \downarrow\downarrow\end{matrix}\right\rangle\left\langle\begin{matrix}\uparrow\uparrow\\ \downarrow\downarrow\end{matrix}\right| + 2\left|\begin{matrix}\downarrow\downarrow\\ \downarrow\downarrow\end{matrix}\right\rangle\left\langle\begin{matrix}\downarrow\downarrow\\ \downarrow\downarrow\end{matrix}\right| \\ &+3\left|\begin{matrix}\uparrow\uparrow\\ \downarrow\uparrow\end{matrix}\right\rangle\left\langle\begin{matrix}\uparrow\uparrow\\ \downarrow\uparrow\end{matrix}\right| + 1\left|\begin{matrix}\downarrow\uparrow\\ \downarrow\uparrow\end{matrix}\right\rangle\left\langle\begin{matrix}\downarrow\uparrow\\ \downarrow\uparrow\end{matrix}\right| + 3\left|\begin{matrix}\uparrow\downarrow\\ \downarrow\uparrow\end{matrix}\right\rangle\left\langle\begin{matrix}\uparrow\downarrow\\ \downarrow\uparrow\end{matrix}\right| + 5\left|\begin{matrix}\downarrow\downarrow\\ \downarrow\uparrow\end{matrix}\right\rangle\left\langle\begin{matrix}\downarrow\downarrow\\ \downarrow\uparrow\end{matrix}\right| \\ &+3\left|\begin{matrix}\uparrow\uparrow\\ \uparrow\downarrow\end{matrix}\right\rangle\left\langle\begin{matrix}\uparrow\uparrow\\ \uparrow\downarrow\end{matrix}\right| + 3\left|\begin{matrix}\downarrow\uparrow\\ \uparrow\downarrow\end{matrix}\right\rangle\left\langle\begin{matrix}\downarrow\uparrow\\ \uparrow\downarrow\end{matrix}\right| + 1\left|\begin{matrix}\uparrow\downarrow\\ \uparrow\downarrow\end{matrix}\right\rangle\left\langle\begin{matrix}\uparrow\downarrow\\ \uparrow\downarrow\end{matrix}\right| + 5\left|\begin{matrix}\downarrow\downarrow\\ \uparrow\downarrow\end{matrix}\right\rangle\left\langle\begin{matrix}\downarrow\downarrow\\ \uparrow\downarrow\end{matrix}\right|\Bigg)_{i,i+1}. \end{aligned} \tag{5.14}$$

These terms can be regarded as energy penalties for the 11 configurations of each pair $(i, i+1)$. A state which does not pay a penalty for any pair $(i, i+1)$ is a ground state of $\hat{h}^{(0)}$ if such a state exists. We find that the ground states of $\hat{h}^{(0)}$ are the columnar and staggered states defined in Section 5.1 and their superpositions, on which no energy penalties are imposed. In other words, the ground space of $\hat{h}^{(0)}$ is given by $\mathcal{D}_L = \mathrm{span}\{\,|\sigma\rangle\,\}_{\sigma\in D_L}$, where

$$\begin{aligned} D_L := &\left\{ \begin{pmatrix}\sigma_{\mathrm{t},1}\cdots\sigma_{\mathrm{t},L}\\ \uparrow\ \cdots\ \uparrow\end{pmatrix};\ \begin{array}{l}\sigma_{\mathrm{t},1},\ldots,\sigma_{\mathrm{t},L}\in\{\uparrow,\downarrow\}\text{ and}\\ (\sigma_{\mathrm{t},1},\sigma_{\mathrm{t},2}),(\sigma_{\mathrm{t},2},\sigma_{\mathrm{t},3}),\ldots,(\sigma_{\mathrm{t},L-1},\sigma_{\mathrm{t},L}),(\sigma_{\mathrm{t},L},\sigma_{\mathrm{t},1})\neq(\downarrow,\downarrow)\end{array}\right\} \\ &\cup\left\{\begin{pmatrix}\downarrow\uparrow\cdots\downarrow\uparrow\\ \downarrow\downarrow\cdots\downarrow\downarrow\end{pmatrix},\begin{pmatrix}\uparrow\downarrow\cdots\uparrow\downarrow\\ \downarrow\downarrow\cdots\downarrow\downarrow\end{pmatrix}\right\}. \end{aligned} \tag{5.15}$$

Although the full Hilbert space is $\mathcal{H}_L = \mathrm{span}\{\,|\sigma\rangle\,\}_{\sigma\in H_L}$ with

$$H_L := \left\{ \begin{pmatrix} \sigma_{\mathrm{t},1}\cdots\sigma_{\mathrm{t},L} \\ \sigma_{\mathrm{b},1}\cdots\sigma_{\mathrm{b},1} \end{pmatrix};\ \sigma_{\mathrm{t},1},\ldots,\sigma_{\mathrm{t},L},\sigma_{\mathrm{b},1},\ldots,\sigma_{\mathrm{b},L}\in\{\uparrow,\downarrow\} \right\}, \tag{5.16}$$

$\hat{h}^{(0)}$ imposes a penalty on every state in $\mathcal{H}_L \setminus \mathcal{D}_L$. As shown in the previous section, we can assign the elements of D_L to dimer coverings on a two-leg ladder.

What is the dimension of the non-penalized subspace, $\dim \mathcal{D}_L = |D_L|$? First consider the open-ladder counterpart of D_L:

$$\begin{aligned} D'_L := &\left\{ \begin{pmatrix} \sigma_{\mathrm{t},1}\cdots\sigma_{\mathrm{t},L} \\ \uparrow\ \cdots\ \uparrow \end{pmatrix};\ \begin{array}{l} \sigma_{\mathrm{t},1},\ldots,\sigma_{\mathrm{t},L}\in\{\uparrow,\downarrow\} \text{ and} \\ (\sigma_{\mathrm{t},1},\sigma_{\mathrm{t},2}),(\sigma_{\mathrm{t},2},\sigma_{\mathrm{t},3}),\ldots,(\sigma_{\mathrm{t},L-1},\sigma_{\mathrm{t},L})\neq(\downarrow,\downarrow) \end{array} \right\} \\ &\cup \left\{ \begin{pmatrix} \downarrow\uparrow\cdots \\ \downarrow\downarrow\cdots \end{pmatrix}, \begin{pmatrix} \uparrow\downarrow\cdots \\ \downarrow\downarrow\cdots \end{pmatrix} \right\}. \end{aligned} \tag{5.17}$$

In particular, we focus on the columnar states:

$$D'^{\mathrm{columnar}}_L := \left\{ \begin{pmatrix} \sigma_{\mathrm{t},1}\cdots\sigma_{\mathrm{t},L} \\ \uparrow\ \cdots\ \uparrow \end{pmatrix};\ \begin{array}{l} \sigma_{\mathrm{t},1},\ldots,\sigma_{\mathrm{t},L}\in\{\uparrow,\downarrow\} \text{ and} \\ (\sigma_{\mathrm{t},1},\sigma_{\mathrm{t},2}),(\sigma_{\mathrm{t},2},\sigma_{\mathrm{t},3}),\ldots,(\sigma_{\mathrm{t},L-1},\sigma_{\mathrm{t},L})\neq(\downarrow,\downarrow) \end{array} \right\}. \tag{5.18}$$

The number of the elements of this set $F_L := |D'^{\mathrm{columnar}}_L|$ satisfies

$$F_1 = 2, \quad F_2 = 3, \quad F_L = F_{L-1} + F_{L-2}, \tag{5.19}$$

which means that F_L are the Fibonacci numbers (notice the values of F_1 and F_2). We can obtain the recurrence relation for the following reason: If $\sigma_{\mathrm{t},L}$ is up, $(\sigma_{\mathrm{t},1},\ldots,\sigma_{\mathrm{t},L-1})$ can be regarded as an open chain of length $L-1$. On the other hand, if $\sigma_{\mathrm{t},L}$ is down, $\sigma_{\mathrm{t},L-1}$ should be up and $(\sigma_{\mathrm{t},1},\ldots,\sigma_{\mathrm{t},L-2})$ is an open chain of length $L-2$.

We can express the dimension of the non-penalized subspace for the original periodic ladder $|D_L|$ using the Fibonacci numbers. If the bottom spins are up, setting $\sigma_{\mathrm{t},L} =\uparrow$ yields an open chain of length $L-1$ while setting $\sigma_{\mathrm{t},L} =\downarrow$ fixes $\sigma_{\mathrm{t},L-1}$ and $\sigma_{\mathrm{t},1}$ to up and yields an open chain of length $L-3$. If the bottom spins are down, the top spins can take the two antiferromagnetic states. Then, we derive

$$|D_L| = F_{L-1} + F_{L-3} + 2. \tag{5.20}$$

Since the Fibonacci sequence asymptotically behaves as

$$F_L \sim \varphi^L \quad (L\to\infty) \tag{5.21}$$

with $\varphi = (1+\sqrt{5})/2$ being the golden ratio, $|D_L|$ is exponentially large as a function of L. Thus, the lowest energy of $\hat{h}^{(0)}$ is exponentially degenerate.

5.4 Renormalization group transformation

In this section, we construct a real-space RG transformation for the frustrated Ising ladder in the dimer limit. We use the notations defined in Section 5.3 (specifically, the sets H_L, D_L, and D'_L and the spaces $\mathcal{H}_L$ and $\mathcal{D}_L$).

5.4.1 Hamiltonian

The original dimensionless Hamiltonian (the bare Hamiltonian) is given by Eqs. (5.9), (5.14), and (5.11). Now we define a more general Hamiltonian, because an RG transformation will produce interactions not included in the original Hamiltonian:

$$\hat{h} = \hat{h}^{(0)} + \hat{h}^{(1)}, \tag{5.22}$$

$$\hat{h}^{(0)} = \sum_{i=1}^{L} \sum_{(\sigma_i,\sigma_{i+1})\in H_2\setminus D'_2} k(\sigma_i,\sigma_{i+1})(|\sigma_i\sigma_{i+1}\rangle\langle\sigma_i\sigma_{i+1}|)_{i,i+1}, \tag{5.23}$$

$$\begin{aligned}\hat{h}^{(1)} = \sum_{i=1}^{L} \Bigg[&\frac{u}{2}\hat{Z}_{\mathrm{b},i} - \gamma\hat{X}_{\mathrm{t},i}\frac{1+\hat{Z}_{\mathrm{b},i}}{2} + v\hat{Z}_{\mathrm{t},i}\frac{1+\hat{Z}_{\mathrm{b},i}}{2} - \xi\left(\left|\begin{matrix}\uparrow\downarrow\\ \uparrow\uparrow\end{matrix}\right\rangle\left\langle\begin{matrix}\downarrow\uparrow\\ \uparrow\uparrow\end{matrix}\right| + \left|\begin{matrix}\downarrow\uparrow\\ \uparrow\uparrow\end{matrix}\right\rangle\left\langle\begin{matrix}\uparrow\downarrow\\ \uparrow\uparrow\end{matrix}\right|\right)_{i,i+1}\Bigg] \\ &+ \hat{o}\hat{P}(\mathcal{D}_L^{\perp}) + \hat{P}(\mathcal{D}_L^{\perp})\hat{o}^{\dagger},\end{aligned} \tag{5.24}$$

where $0 < k(\sigma_i,\sigma_{i+1}) = \mathcal{O}(\delta^0)$ for all $(\sigma_i,\sigma_{i+1}) \in H_2\setminus D'_2$ and $u,\gamma,v,\xi = \mathcal{O}(\delta^1)$. The length L is even and the position $L+1$ is identified as 1 for the periodic boundary condition. We denoted an arbitrary operator of $\mathcal{O}(\delta^1)$ by $\hat{o}$ and the projection operator onto $\mathcal{D}_L^{\perp}$ by $\hat{P}(\mathcal{D}_L^{\perp})$, where $\mathcal{D}_L^{\perp}$ is the orthogonal complement of $\mathcal{D}_L$. The operator $\hat{o}\hat{P}(\mathcal{D}_L^{\perp}) + \hat{P}(\mathcal{D}_L^{\perp})\hat{o}^{\dagger}$ in $\hat{h}^{(1)}$ will disappear after an RG transformation and is irrelevant in the sense of the RG theory. The bare Hamiltonian can be obtained by setting $\gamma = \gamma_{\mathrm{t}}$, $v = 0$, and $\xi = \xi_{\mathrm{tt}}$.

In Eq. (5.23), we denoted configurations of two spins at each position i by

$$\sigma_i \in H_1 = \left\{\begin{pmatrix}\uparrow\\ \uparrow\end{pmatrix}, \begin{pmatrix}\downarrow\\ \uparrow\end{pmatrix}, \begin{pmatrix}\uparrow\\ \downarrow\end{pmatrix}, \begin{pmatrix}\downarrow\\ \downarrow\end{pmatrix}\right\}, \tag{5.25}$$

where H_1 is defined by Eq. (5.16). Every configuration $(\sigma_i,\sigma_{i+1}) \in H_2 \setminus D'_2$ costs energy of $\mathcal{O}(\delta^0)$ for each pair $(i,i+1)$. Let us write down D'_2 and $H_2 \setminus D'_2$ defined by Eq. (5.16) and (5.17):

$$D'_2 = \left\{\begin{pmatrix}\uparrow\uparrow\\ \uparrow\uparrow\end{pmatrix}, \begin{pmatrix}\downarrow\uparrow\\ \uparrow\uparrow\end{pmatrix}, \begin{pmatrix}\uparrow\downarrow\\ \uparrow\uparrow\end{pmatrix}, \begin{pmatrix}\downarrow\uparrow\\ \downarrow\downarrow\end{pmatrix}, \begin{pmatrix}\uparrow\downarrow\\ \downarrow\downarrow\end{pmatrix}\right\}, \tag{5.26}$$

$$\begin{aligned}H_2 \setminus D'_2 = \Bigg\{&\begin{pmatrix}\downarrow\downarrow\\ \uparrow\uparrow\end{pmatrix}, \begin{pmatrix}\uparrow\uparrow\\ \downarrow\downarrow\end{pmatrix}, \begin{pmatrix}\downarrow\downarrow\\ \downarrow\downarrow\end{pmatrix}, \\ &\begin{pmatrix}\uparrow\uparrow\\ \downarrow\uparrow\end{pmatrix}, \begin{pmatrix}\downarrow\uparrow\\ \downarrow\uparrow\end{pmatrix}, \begin{pmatrix}\uparrow\downarrow\\ \downarrow\uparrow\end{pmatrix}, \begin{pmatrix}\downarrow\downarrow\\ \downarrow\uparrow\end{pmatrix}, \begin{pmatrix}\uparrow\uparrow\\ \uparrow\downarrow\end{pmatrix}, \begin{pmatrix}\downarrow\uparrow\\ \uparrow\downarrow\end{pmatrix}, \begin{pmatrix}\uparrow\downarrow\\ \uparrow\downarrow\end{pmatrix}, \begin{pmatrix}\downarrow\downarrow\\ \uparrow\downarrow\end{pmatrix}\Bigg\}.\end{aligned} \tag{5.27}$$

The zeroth-order Hamiltonian $\hat{h}^{(0)}$ imposes an energy penalty on every state in $\mathcal{H}_L \setminus \mathcal{D}_L$. The zeroth-order energy expectation value in a normalized state $|\psi\rangle \in \mathcal{H}_L$ is

$$\langle\psi|\hat{h}^{(0)}|\psi\rangle = \sum_{\sigma\in H_L\setminus D_L} \langle\sigma|\hat{h}^{(0)}|\sigma\rangle\,|\langle\sigma|\psi\rangle|^2, \tag{5.28}$$

where $\langle\sigma|\hat{h}^{(0)}|\sigma\rangle > 0$ for all $\sigma \in H_L \setminus D_L$ because $\sigma = (\sigma_1, \ldots, \sigma_L)$ satisfies

$$\sigma \in D_L \iff (\sigma_i, \sigma_{i+1}) \in D_2' \quad (\forall i = 1, \ldots, L), \tag{5.29}$$

or its contrapositive

$$\sigma \in H_L \setminus D_L \iff (\sigma_i, \sigma_{i+1}) \in H_2 \setminus D_2' \quad (\exists i = 1, \ldots, L). \tag{5.30}$$

If and only if $|\psi\rangle \notin \mathcal{D}_L$, there is $\sigma \in H_L \setminus D_L$ such that $\langle\sigma|\psi\rangle \neq 0$ and thus $\langle\psi|\hat{h}^{(0)}|\psi\rangle > 0$.

5.4.2 Block partition and introduction of a projector

We partition the ladder into blocks of spins as a first step of an RG transformation. A block should contain an odd number of steps to keep the antiferromagnetic order in the staggered phase because partition every even number of steps would change antiferromagnetic order into ferromagnetic order. Now we partition the ladder into $\widetilde{L} = L/3$ blocks and project the Hilbert space onto a four-dimensional space for each block. We write the projector as

$$\hat{Q} = \bigotimes_{I=1}^{\widetilde{L}} \hat{Q}_I = \sum_{\sigma\in H_{\widetilde{L}}} \widetilde{|\sigma\rangle}\widetilde{\langle\sigma|}, \tag{5.31}$$

$$\hat{Q}_I = \left(\widetilde{\left|\begin{smallmatrix}\uparrow\\\uparrow\end{smallmatrix}\right\rangle}\widetilde{\left\langle\begin{smallmatrix}\uparrow\\\uparrow\end{smallmatrix}\right|} + \widetilde{\left|\begin{smallmatrix}\downarrow\\\uparrow\end{smallmatrix}\right\rangle}\widetilde{\left\langle\begin{smallmatrix}\downarrow\\\uparrow\end{smallmatrix}\right|} + \widetilde{\left|\begin{smallmatrix}\uparrow\\\downarrow\end{smallmatrix}\right\rangle}\widetilde{\left\langle\begin{smallmatrix}\uparrow\\\downarrow\end{smallmatrix}\right|} + \widetilde{\left|\begin{smallmatrix}\downarrow\\\downarrow\end{smallmatrix}\right\rangle}\widetilde{\left\langle\begin{smallmatrix}\downarrow\\\downarrow\end{smallmatrix}\right|} \right)_I, \tag{5.32}$$

where $\widetilde{|\sigma\rangle} = \bigotimes_{I=1}^{\widetilde{L}} \widetilde{|\sigma_I\rangle}_I$ for $\sigma = (\sigma_1, \ldots, \sigma_{\widetilde{L}})$ and $\{\,\widetilde{|\sigma_I\rangle}_I\,\}_{\sigma_I\in H_1}$ is a set of four orthonormal states in the Ith block constituted by six sites (a, i) ($a = \mathrm{t}, \mathrm{b}$; $i = 3I-2, 3I-1, 3I$). Each $\widetilde{|\sigma_I\rangle}_I$ is a superposition of

$$|\tau_{3I-2}\tau_{3I-1}\tau_{3I}\rangle_I := |\tau_{3I-2}\rangle_{3I-2}\,|\tau_{3I-1}\rangle_{3I-1}\,|\tau_{3I}\rangle_{3I} \quad ((\tau_{3I-2}, \tau_{3I-1}, \tau_{3I}) \in H_3). \tag{5.33}$$

We suppose that for each $\sigma_1 \in H_1$, $\widetilde{|\sigma_1\rangle}_I$ take the same form except for the difference of the block. In other words, when we express $\widetilde{|\sigma_1\rangle}_I$ as a linear combination of $|\tau_1\tau_2\tau_3\rangle_I$, the coefficients are independent of I.

We expand the states $\widetilde{|\sigma_I\rangle}_I$ ($\sigma_I \in H_1$) up to first order in powers of δ:

$$\widetilde{|\sigma_I\rangle}_I = \widetilde{|\sigma_I\rangle}_I^{(0)} + \widetilde{|\sigma_I\rangle}_I^{(1)} + \mathcal{O}(\delta^2). \tag{5.34}$$

The normalization conditions of $\widetilde{|\sigma_I\rangle}_I$ are written as

$$1 = {}_I\widetilde{\langle\sigma_I|}\widetilde{|\sigma_I\rangle}_I = {}^{(0)}_I\widetilde{\langle\sigma_I|}\widetilde{|\sigma_I\rangle}^{(0)}_I + 2\,\mathrm{Re}\,{}^{(0)}_I\widetilde{\langle\sigma_I|}\widetilde{|\sigma_I\rangle}^{(1)}_I + \mathcal{O}(\delta^2). \tag{5.35}$$

Comparing each order of this equation results in

$${}^{(0)}_I\widetilde{\langle\sigma_I|}\widetilde{|\sigma_I\rangle}^{(0)}_I = 1, \quad \mathrm{Re}\,{}^{(0)}_I\widetilde{\langle\sigma_I|}\widetilde{|\sigma_I\rangle}^{(1)}_I = 0. \tag{5.36}$$

In addition, the orthogonality of $\{\,\widetilde{|\sigma_I\rangle}_I\,\}_{\sigma_I\in H_1}$ leads to

$$\sigma_I \neq \tau_I \Longrightarrow 0 = {}_I\widetilde{\langle\tau_I|}\widetilde{|\sigma_I\rangle}_I = {}^{(0)}_I\widetilde{\langle\tau_I|}\widetilde{|\sigma_I\rangle}^{(0)}_I + {}^{(0)}_I\widetilde{\langle\tau_I|}\widetilde{|\sigma_I\rangle}^{(1)}_I + {}^{(1)}_I\widetilde{\langle\tau_I|}\widetilde{|\sigma_I\rangle}^{(0)}_I + \mathcal{O}(\delta^2) \tag{5.37}$$

and we obtain the zeroth- and first-order equations:

$$\sigma_I \neq \tau_I \Longrightarrow {}^{(0)}_I\widetilde{\langle\tau_I|}\widetilde{|\sigma_I\rangle}^{(0)}_I = 0, \quad {}^{(0)}_I\widetilde{\langle\tau_I|}\widetilde{|\sigma_I\rangle}^{(1)}_I + {}^{(1)}_I\widetilde{\langle\tau_I|}\widetilde{|\sigma_I\rangle}^{(0)}_I = 0. \tag{5.38}$$

Expanding the product state

$$\widetilde{|\sigma\rangle} = \bigotimes_{I=1}^{\widetilde{L}} \widetilde{|\sigma_I\rangle}_I = \bigotimes_{I=1}^{\widetilde{L}} \left(\widetilde{|\sigma_I\rangle}^{(0)}_I + \widetilde{|\sigma_I\rangle}^{(1)}_I + \mathcal{O}(\delta^2) \right), \tag{5.39}$$

we find that the zeroth- and first-order parts of $\widetilde{|\sigma\rangle}$ are given by

$$\widetilde{|\sigma\rangle}^{(0)} = \widetilde{|\sigma_1\rangle}^{(0)}_1 \cdots \widetilde{|\sigma_{\widetilde{L}}\rangle}^{(0)}_{\widetilde{L}}, \tag{5.40}$$

$$\widetilde{|\sigma\rangle}^{(1)} = \sum_{I=1}^{\widetilde{L}} \widetilde{|\sigma_1\rangle}^{(0)}_1 \cdots \widetilde{|\sigma_{I-1}\rangle}^{(0)}_{I-1} \widetilde{|\sigma_I\rangle}^{(1)}_I \widetilde{|\sigma_{I+1}\rangle}^{(0)}_{I+1} \cdots \widetilde{|\sigma_{\widetilde{L}}\rangle}^{(0)}_{\widetilde{L}}. \tag{5.41}$$

The renormalized Hamiltonian is given by $\hat{\tilde{h}} = \hat{Q}\hat{h}\hat{Q}$. In the standard real-space RG method, the Hilbert space would be projected onto a low-energy space of the intrablock Hamiltonian after separating the Hamiltonian into intrablock and interblock Hamiltonians [69]. However, we do not adopt this method, because the interblock interactions are strong and diagonalization of the intrablock Hamiltonian will not yield a low-energy space correctly (recall that the interblock operators are of $\mathcal{O}(\delta^0)$). In the next section, we will propose a new RG procedure in which interblock operators as well as intrablock ones are taken into account to find a low-energy space.

5.4.3 Construction of the projector

How should we project the Hilbert space in an RG transformation? We construct the projector $\hat{Q}$ according to the following basic principles:

- An RG transformation projects the Hilbert space onto a low-energy space for the Hamiltonian $\hat{h}$; and
- The Hamiltonian goes toward a fixed point by RG transformations at the critical point.

Since we will study the zero-temperature transition, the first principle is clear. The second principle holds for the general RG theory. We should find the fixed point dominating the phase transition and examine behavior of the system near the fixed point.

Let us construct the zeroth-order projector $\hat{Q}^{(0)} = \sum_{\sigma \in H_{\tilde{L}}} \widetilde{|\sigma\rangle}^{(0)} \, {}^{(0)}\widetilde{\langle\sigma|}$, where $\widetilde{|\sigma\rangle}^{(0)}$ are given by Eq. (5.40). Now we need to consider only the penalty Hamiltonian $\hat{h}^{(0)}$. On the basis of the two principles, we determine the forms of $\widetilde{|\sigma_I\rangle}_I^{(0)}$ as follows:

1. Each $\widetilde{|\sigma_I\rangle}_I^{(0)}$ is a superposition of $|\tau_{3I-2}\tau_{3I-1}\tau_{3I}\rangle_I$ for $(\tau_{3I-2}, \tau_{3I-1}, \tau_{3I}) \in D_3'$ because the states for $(\tau_{3I-2}, \tau_{3I-1}, \tau_{3I}) \in H_3 \setminus D_3'$ pay energy penalties.
2. Each $\widetilde{|\sigma_I\rangle}_I^{(0)}$ does not include both components of $\left|\begin{matrix}\cdots\\ \uparrow\uparrow\uparrow\end{matrix}\right\rangle_I$ and $\left|\begin{matrix}\cdots\\ \downarrow\downarrow\downarrow\end{matrix}\right\rangle_I$. If $\widetilde{|\sigma_I\rangle}_I^{(0)}$ has both components of $\left|\begin{matrix}\cdots\\ \uparrow\uparrow\uparrow\end{matrix}\right\rangle_I$ and $\left|\begin{matrix}\cdots\\ \downarrow\downarrow\downarrow\end{matrix}\right\rangle_I$ for at least one of $\sigma_I \in H_1$, any state of length L in which the state in the Ith block is $\widetilde{|\sigma_I\rangle}_I^{(0)}$ has a component including $\downarrow\uparrow$ or $\uparrow\downarrow$ on the bottom row whether the $(3I+1)$th spin on the bottom row is up or down. This state pays a penalty.
3. We assume that $\widetilde{\left|\begin{matrix}\uparrow\\ \uparrow\end{matrix}\right\rangle}_I^{(0)}$ and $\widetilde{\left|\begin{matrix}\downarrow\\ \uparrow\end{matrix}\right\rangle}_I^{(0)}$ are superpositions of $\left|\begin{matrix}\uparrow\downarrow\uparrow\\ \uparrow\uparrow\uparrow\end{matrix}\right\rangle_I$, $\left|\begin{matrix}\uparrow\uparrow\uparrow\\ \uparrow\uparrow\uparrow\end{matrix}\right\rangle_I$, $\left|\begin{matrix}\downarrow\uparrow\downarrow\\ \uparrow\uparrow\uparrow\end{matrix}\right\rangle_I$, $\left|\begin{matrix}\uparrow\uparrow\downarrow\\ \uparrow\uparrow\uparrow\end{matrix}\right\rangle_I$, and $\left|\begin{matrix}\downarrow\uparrow\uparrow\\ \uparrow\uparrow\uparrow\end{matrix}\right\rangle_I$, while

$$\widetilde{\left|\begin{matrix}\uparrow\\ \downarrow\end{matrix}\right\rangle}_I^{(0)} = \left|\begin{matrix}\uparrow\downarrow\uparrow\\ \downarrow\downarrow\downarrow\end{matrix}\right\rangle_I, \quad \widetilde{\left|\begin{matrix}\downarrow\\ \downarrow\end{matrix}\right\rangle}_I^{(0)} = \left|\begin{matrix}\downarrow\uparrow\downarrow\\ \downarrow\downarrow\downarrow\end{matrix}\right\rangle_I. \tag{5.42}$$

The reason for this assumption is that we wish to study the phase transition between the columnar and staggered phases and we should keep states in the two phases. Notice that we do not need to take superpositions of $\left|\begin{matrix}\uparrow\downarrow\uparrow\\ \downarrow\downarrow\downarrow\end{matrix}\right\rangle_I$ and $\left|\begin{matrix}\downarrow\uparrow\downarrow\\ \downarrow\downarrow\downarrow\end{matrix}\right\rangle_I$ because the projector $\hat{Q}^{(0)}$ is independent of what superpositions of these states are taken.

4. We require that $\widetilde{\left|\begin{smallmatrix}\uparrow\\\uparrow\end{smallmatrix}\right\rangle}^{(0)}_{I}$ is a superposition only of $\left|\begin{smallmatrix}\uparrow\downarrow\uparrow\\\uparrow\uparrow\uparrow\end{smallmatrix}\right\rangle_{I}$ and $\left|\begin{smallmatrix}\uparrow\uparrow\uparrow\\\uparrow\uparrow\uparrow\end{smallmatrix}\right\rangle_{I}$, while $\widetilde{\left|\begin{smallmatrix}\downarrow\\\uparrow\end{smallmatrix}\right\rangle}^{(0)}_{I}$ can be a superposition of $\left|\begin{smallmatrix}\uparrow\downarrow\uparrow\\\uparrow\uparrow\uparrow\end{smallmatrix}\right\rangle_{I}$, $\left|\begin{smallmatrix}\uparrow\uparrow\uparrow\\\uparrow\uparrow\uparrow\end{smallmatrix}\right\rangle_{I}$, $\left|\begin{smallmatrix}\downarrow\uparrow\downarrow\\\uparrow\uparrow\uparrow\end{smallmatrix}\right\rangle_{I}$, $\left|\begin{smallmatrix}\uparrow\uparrow\downarrow\\\uparrow\uparrow\uparrow\end{smallmatrix}\right\rangle_{I}$, and $\left|\begin{smallmatrix}\downarrow\uparrow\uparrow\\\uparrow\uparrow\uparrow\end{smallmatrix}\right\rangle_{I}$. Let us explain the reason. The second principle implies that it is appropriate to keep the structure of the system related to the dimer model. We can achieve this by constructing a renormalized Hamiltonian $\widetilde{\hat{h}}$ which includes an $\mathcal{O}(\delta^0)$ term imposing a penalty on $\widetilde{|\sigma_I\sigma_{I+1}\rangle}^{(0)}_{I,I+1} := \widetilde{|\sigma_I\rangle}^{(0)}_{I}\widetilde{|\sigma_{I+1}\rangle}^{(0)}_{I+1}$ for any $I = 1, \ldots, \widetilde{L}$ and $(\sigma_I, \sigma_{I+1}) \in H_2 \setminus D_2'$. To prevent $\widetilde{\left|\begin{smallmatrix}\uparrow\uparrow\\\uparrow\uparrow\end{smallmatrix}\right\rangle}^{(0)}_{I,I+1}$ from paying a penalty, $\widetilde{\left|\begin{smallmatrix}\uparrow\\\uparrow\end{smallmatrix}\right\rangle}^{(0)}_{I}$ does not include $\left|\begin{smallmatrix}\downarrow\uparrow\downarrow\\\uparrow\uparrow\uparrow\end{smallmatrix}\right\rangle_{I}$ or both of $\left|\begin{smallmatrix}\uparrow\uparrow\downarrow\\\uparrow\uparrow\uparrow\end{smallmatrix}\right\rangle_{I}$ and $\left|\begin{smallmatrix}\downarrow\uparrow\uparrow\\\uparrow\uparrow\uparrow\end{smallmatrix}\right\rangle_{I}$. If $\widetilde{\left|\begin{smallmatrix}\uparrow\\\uparrow\end{smallmatrix}\right\rangle}^{(0)}_{I}$ includes $\left|\begin{smallmatrix}\uparrow\uparrow\downarrow\\\uparrow\uparrow\uparrow\end{smallmatrix}\right\rangle_{I}$ $\left(\text{but neither } \left|\begin{smallmatrix}\downarrow\uparrow\downarrow\\\uparrow\uparrow\uparrow\end{smallmatrix}\right\rangle_{I} \text{ nor } \left|\begin{smallmatrix}\downarrow\uparrow\uparrow\\\uparrow\uparrow\uparrow\end{smallmatrix}\right\rangle_{I}\right)$, then $\widetilde{\left|\begin{smallmatrix}\downarrow\\\uparrow\end{smallmatrix}\right\rangle}^{(0)}_{I}$ is also a superposition of $\left|\begin{smallmatrix}\uparrow\downarrow\uparrow\\\uparrow\uparrow\uparrow\end{smallmatrix}\right\rangle_{I}$, $\left|\begin{smallmatrix}\uparrow\uparrow\uparrow\\\uparrow\uparrow\uparrow\end{smallmatrix}\right\rangle_{I}$, and $\left|\begin{smallmatrix}\uparrow\uparrow\downarrow\\\uparrow\uparrow\uparrow\end{smallmatrix}\right\rangle_{I}$ to prevent $\widetilde{\left|\begin{smallmatrix}\uparrow\downarrow\\\uparrow\uparrow\end{smallmatrix}\right\rangle}^{(0)}_{I,I+1}$ from paying a penalty. In this case, however, $\widetilde{\left|\begin{smallmatrix}\downarrow\downarrow\\\uparrow\uparrow\end{smallmatrix}\right\rangle}^{(0)}_{I,I+1}$ does not cost energy of $\mathcal{O}(\delta^0)$ and we cannot keep the dimer structure. In addition, there is no reason why the $(3I-2)$th spin on the top row is up for any I. It is thus reasonable to suppose that $\widetilde{\left|\begin{smallmatrix}\uparrow\\\uparrow\end{smallmatrix}\right\rangle}^{(0)}_{I}$ does not include $\left|\begin{smallmatrix}\uparrow\uparrow\downarrow\\\uparrow\uparrow\uparrow\end{smallmatrix}\right\rangle_{I}$. Likewise, $\widetilde{\left|\begin{smallmatrix}\uparrow\\\uparrow\end{smallmatrix}\right\rangle}^{(0)}_{I}$ will not include $\left|\begin{smallmatrix}\downarrow\uparrow\uparrow\\\uparrow\uparrow\uparrow\end{smallmatrix}\right\rangle_{I}$. Therefore, $\widetilde{\left|\begin{smallmatrix}\uparrow\\\uparrow\end{smallmatrix}\right\rangle}^{(0)}_{I}$ is a superposition of $\left|\begin{smallmatrix}\uparrow\downarrow\uparrow\\\uparrow\uparrow\uparrow\end{smallmatrix}\right\rangle_{I}$ and $\left|\begin{smallmatrix}\uparrow\uparrow\uparrow\\\uparrow\uparrow\uparrow\end{smallmatrix}\right\rangle_{I}$, and $\widetilde{\left|\begin{smallmatrix}\downarrow\\\uparrow\end{smallmatrix}\right\rangle}^{(0)}_{I}$ is a superposition of $\left|\begin{smallmatrix}\uparrow\downarrow\uparrow\\\uparrow\uparrow\uparrow\end{smallmatrix}\right\rangle_{I}$, $\left|\begin{smallmatrix}\uparrow\uparrow\uparrow\\\uparrow\uparrow\uparrow\end{smallmatrix}\right\rangle_{I}$, $\left|\begin{smallmatrix}\downarrow\uparrow\downarrow\\\uparrow\uparrow\uparrow\end{smallmatrix}\right\rangle_{I}$, $\left|\begin{smallmatrix}\uparrow\uparrow\downarrow\\\uparrow\uparrow\uparrow\end{smallmatrix}\right\rangle_{I}$, and $\left|\begin{smallmatrix}\downarrow\uparrow\uparrow\\\uparrow\uparrow\uparrow\end{smallmatrix}\right\rangle_{I}$. Then, $\widetilde{\left|\begin{smallmatrix}\downarrow\downarrow\\\uparrow\uparrow\end{smallmatrix}\right\rangle}^{(0)}_{I,I+1}$ pays a penalty, while $\widetilde{\left|\begin{smallmatrix}\uparrow\uparrow\\\uparrow\uparrow\end{smallmatrix}\right\rangle}^{(0)}_{I,I+1}$, $\widetilde{\left|\begin{smallmatrix}\downarrow\uparrow\\\uparrow\uparrow\end{smallmatrix}\right\rangle}^{(0)}_{I,I+1}$, and $\widetilde{\left|\begin{smallmatrix}\uparrow\downarrow\\\uparrow\uparrow\end{smallmatrix}\right\rangle}^{(0)}_{I,I+1}$ do not. This means that we reproduce the dimer structure after projecting the Hilbert space.

5. Since $\widetilde{|\sigma_I\rangle}_I^{(0)}$ are orthonormal, we obtain

$$\widetilde{\left|\begin{matrix}\uparrow\\\uparrow\end{matrix}\right\rangle}_I^{(0)} = \alpha_1 \left|\begin{matrix}\uparrow\downarrow\uparrow\\\uparrow\uparrow\uparrow\end{matrix}\right\rangle_I + \alpha_2 \left|\begin{matrix}\uparrow\uparrow\uparrow\\\uparrow\uparrow\uparrow\end{matrix}\right\rangle_I, \tag{5.43}$$

$$\widetilde{\left|\begin{matrix}\downarrow\\\uparrow\end{matrix}\right\rangle}_I^{(0)} = -z^*\alpha_2^* \left|\begin{matrix}\uparrow\downarrow\uparrow\\\uparrow\uparrow\uparrow\end{matrix}\right\rangle_I + z^*\alpha_1^* \left|\begin{matrix}\uparrow\uparrow\uparrow\\\uparrow\uparrow\uparrow\end{matrix}\right\rangle_I + \beta_1^* \left|\begin{matrix}\downarrow\uparrow\downarrow\\\uparrow\uparrow\uparrow\end{matrix}\right\rangle_I + \beta_2^* \left|\begin{matrix}\uparrow\uparrow\downarrow\\\uparrow\uparrow\uparrow\end{matrix}\right\rangle_I + \beta_3^* \left|\begin{matrix}\downarrow\uparrow\uparrow\\\uparrow\uparrow\uparrow\end{matrix}\right\rangle_I, \tag{5.44}$$

$$\widetilde{\left|\begin{matrix}\uparrow\\\downarrow\end{matrix}\right\rangle}_I^{(0)} = \left|\begin{matrix}\uparrow\downarrow\uparrow\\\downarrow\downarrow\downarrow\end{matrix}\right\rangle_I, \tag{5.45}$$

$$\widetilde{\left|\begin{matrix}\downarrow\\\downarrow\end{matrix}\right\rangle}_I^{(0)} = \left|\begin{matrix}\downarrow\uparrow\downarrow\\\downarrow\downarrow\downarrow\end{matrix}\right\rangle_I, \tag{5.46}$$

where the parameters $\alpha_1, \alpha_2, z, \beta_1, \beta_2, \beta_3 \in \mathbb{C}$ satisfy the normalization conditions:

$$\begin{aligned}{}_I^{(0)}\widetilde{\langle\sigma_I|}\widetilde{|\sigma_I\rangle}_I^{(0)} = 1 \quad (\forall\sigma_I \in H_1) &\iff \begin{cases}|\alpha_1|^2 + |\alpha_2|^2 = 1,\\ |z|^2(|\alpha_1|^2 + |\alpha_2|^2) + |\beta_1|^2 + |\beta_2|^2 + |\beta_3|^2 = 1\end{cases}\\ &\iff \begin{cases}|\alpha_1|^2 + |\alpha_2|^2 = 1,\\ |z|^2 + |\beta_1|^2 + |\beta_2|^2 + |\beta_3|^2 = 1.\end{cases}\end{aligned} \tag{5.47}$$

The set of Eqs. (5.43)–(5.46) can be regarded as a variational ansatz for the projector $\hat{Q}^{(0)}$. We will determine the variational parameters α_1, α_2, z, β_1, β_2, and β_3 in Section 5.4.6.

5.4.4 Projection of the Hamiltonian

Let us calculate the renormalized Hamiltonian $\hat{\tilde{h}} = \hat{Q}\hat{h}\hat{Q}$ up to first order. First, the zeroth-order Hamiltonian $\hat{h}^{(0)}$ is projected onto

$$\begin{aligned}\hat{Q}\hat{h}^{(0)}\hat{Q} &= \sum_{\sigma,\tau\in H_{\tilde{L}}} \widetilde{|\tau\rangle}\widetilde{\langle\tau|}\hat{h}^{(0)}\widetilde{|\sigma\rangle}\widetilde{\langle\sigma|}\\ &= \sum_{\sigma,\tau\in H_{\tilde{L}}} \left[\widetilde{|\tau\rangle}\left({}^{(0)}\widetilde{\langle\tau|}\hat{h}^{(0)}\widetilde{|\sigma\rangle}^{(0)} + {}^{(0)}\widetilde{\langle\tau|}\hat{h}^{(0)}\widetilde{|\sigma\rangle}^{(1)} + {}^{(1)}\widetilde{\langle\tau|}\hat{h}^{(0)}\widetilde{|\sigma\rangle}^{(0)}\right)\widetilde{\langle\sigma|}\right] + \mathcal{O}(\delta^2).\end{aligned} \tag{5.48}$$

Focus on the matrix elements ${}^{(0)}\widetilde{\langle\tau|}\hat{h}^{(0)}\widetilde{|\sigma\rangle}^{(0)}$. It is convenient to write the zeroth-order

Hamiltonian as a summation over the block index I:

$$\hat{h}^{(0)} = \sum_{I=1}^{\widetilde{L}} \hat{h}^{(0)}_{I,I+1}, \tag{5.49}$$

$$\begin{aligned}\hat{h}^{(0)}_{I,I+1} = \sum_{(\sigma_1,\sigma_2)\in H_2\setminus D_2'} k(\sigma_1,\sigma_2)\Big[&\frac{1}{2}(|\sigma_1\sigma_2\rangle\langle\sigma_1\sigma_2|)_{3I-2,3I-1} + \frac{1}{2}(|\sigma_1\sigma_2\rangle\langle\sigma_1\sigma_2|)_{3I-1,3I} \\ &+ (|\sigma_1\sigma_2\rangle\langle\sigma_1\sigma_2|)_{3I,3I+1} \\ &+ \frac{1}{2}(|\sigma_1\sigma_2\rangle\langle\sigma_1\sigma_2|)_{3I+1,3I+2} + \frac{1}{2}(|\sigma_1\sigma_2\rangle\langle\sigma_1\sigma_2|)_{3I+2,3I+3}\Big].\end{aligned} \tag{5.50}$$

Since $(\tau_1,\tau_2)\in H_2\setminus D_2'$ and $\sigma_I\in H_1$ satisfy

$$(|\tau_1\tau_2\rangle\langle\tau_1\tau_2|)_{3I-2,3I-1}\widetilde{|\sigma_I\rangle}^{(0)}_I = (|\tau_1\tau_2\rangle\langle\tau_1\tau_2|)_{3I-1,3I}\widetilde{|\sigma_I\rangle}^{(0)}_I = 0, \tag{5.51}$$

we obtain

$$\hat{h}^{(0)}_{I,I+1}\widetilde{|\sigma_I\sigma_{I+1}\rangle}^{(0)}_{I,I+1} = \sum_{(\tau_1,\tau_2)\in H_2\setminus D_2'} k(\tau_1,\tau_2)(|\tau_1\tau_2\rangle\langle\tau_1\tau_2|)_{3I,3I+1}\widetilde{|\sigma_I\sigma_{I+1}\rangle}^{(0)}_{I,I+1} \tag{5.52}$$

for $(\sigma_I,\sigma_{I+1})\in H_2$. Calculation for each (σ_I,σ_{I+1}) results in

$$(\sigma_I,\sigma_{I+1})\in D_2' \Longrightarrow \hat{h}^{(0)}_{I,I+1}\widetilde{|\sigma_I\sigma_{I+1}\rangle}^{(0)}_{I,I+1} = 0 \tag{5.53}$$

and

$$\hat{h}^{(0)}_{I,I+1}\widetilde{\left|\begin{matrix}\downarrow\downarrow\\ \uparrow\uparrow\end{matrix}\right\rangle}^{(0)}_{I,I+1} = k\begin{pmatrix}\downarrow\downarrow\\ \uparrow\uparrow\end{pmatrix}\left(\beta_1^*\left|\begin{matrix}\downarrow\uparrow\downarrow\\ \uparrow\uparrow\uparrow\end{matrix}\right\rangle + \beta_2^*\left|\begin{matrix}\uparrow\uparrow\downarrow\\ \uparrow\uparrow\uparrow\end{matrix}\right\rangle\right)_I\left(\beta_1^*\left|\begin{matrix}\downarrow\uparrow\downarrow\\ \uparrow\uparrow\uparrow\end{matrix}\right\rangle + \beta_3^*\left|\begin{matrix}\downarrow\uparrow\uparrow\\ \uparrow\uparrow\uparrow\end{matrix}\right\rangle\right)_{I+1}, \tag{5.54}$$

$$\hat{h}^{(0)}_{I,I+1}\widetilde{\left|\begin{matrix}\uparrow\uparrow\\ \downarrow\downarrow\end{matrix}\right\rangle}^{(0)}_{I,I+1} = k\begin{pmatrix}\uparrow\uparrow\\ \downarrow\downarrow\end{pmatrix}\widetilde{\left|\begin{matrix}\uparrow\uparrow\\ \downarrow\downarrow\end{matrix}\right\rangle}^{(0)}_{I,I+1}, \tag{5.55}$$

$$\hat{h}^{(0)}_{I,I+1}\widetilde{\left|\begin{matrix}\downarrow\downarrow\\ \downarrow\downarrow\end{matrix}\right\rangle}^{(0)}_{I,I+1} = k\begin{pmatrix}\downarrow\downarrow\\ \downarrow\downarrow\end{pmatrix}\widetilde{\left|\begin{matrix}\downarrow\downarrow\\ \downarrow\downarrow\end{matrix}\right\rangle}^{(0)}_{I,I+1}, \tag{5.56}$$

$$\hat{h}^{(0)}_{I,I+1}\widetilde{\left|\begin{matrix}\uparrow\uparrow\\ \uparrow\downarrow\end{matrix}\right\rangle}^{(0)}_{I,I+1} = k\begin{pmatrix}\uparrow\uparrow\\ \uparrow\downarrow\end{pmatrix}\widetilde{\left|\begin{matrix}\uparrow\uparrow\\ \uparrow\downarrow\end{matrix}\right\rangle}^{(0)}_{I,I+1}, \tag{5.57}$$

$$\hat{h}^{(0)}_{I,I+1}\widetilde{\left|\begin{matrix}\uparrow\uparrow\\ \downarrow\uparrow\end{matrix}\right\rangle}^{(0)}_{I,I+1} = k\begin{pmatrix}\uparrow\uparrow\\ \downarrow\uparrow\end{pmatrix}\widetilde{\left|\begin{matrix}\uparrow\uparrow\\ \downarrow\uparrow\end{matrix}\right\rangle}^{(0)}_{I,I+1}, \tag{5.58}$$

$$\hat{h}^{(0)}_{I,I+1}\widetilde{\left|\begin{matrix}\uparrow\downarrow\\ \uparrow\downarrow\end{matrix}\right\rangle}^{(0)}_{I,I+1} = k\begin{pmatrix}\uparrow\downarrow\\ \uparrow\downarrow\end{pmatrix}\widetilde{\left|\begin{matrix}\uparrow\downarrow\\ \uparrow\downarrow\end{matrix}\right\rangle}^{(0)}_{I,I+1}, \tag{5.59}$$

$$\hat{h}^{(0)}_{I,I+1}\widetilde{\left|\begin{matrix}\downarrow\uparrow\\ \downarrow\uparrow\end{matrix}\right\rangle}^{(0)}_{I,I+1} = k\begin{pmatrix}\downarrow\uparrow\\ \downarrow\uparrow\end{pmatrix}\widetilde{\left|\begin{matrix}\downarrow\uparrow\\ \downarrow\uparrow\end{matrix}\right\rangle}^{(0)}_{I,I+1}, \tag{5.60}$$

$$\begin{aligned}\hat{h}^{(0)}_{I,I+1}\widetilde{\left|\begin{matrix}\downarrow\uparrow\\ \uparrow\downarrow\end{matrix}\right\rangle}^{(0)}_{I,I+1} = &\left[k\begin{pmatrix}\uparrow\uparrow\\ \uparrow\downarrow\end{pmatrix}\left(-z^*\alpha_2^*\left|\begin{matrix}\uparrow\downarrow\uparrow\\ \uparrow\uparrow\uparrow\end{matrix}\right\rangle + z^*\alpha_1^*\left|\begin{matrix}\uparrow\uparrow\uparrow\\ \uparrow\uparrow\uparrow\end{matrix}\right\rangle + \beta_3^*\left|\begin{matrix}\downarrow\uparrow\uparrow\\ \uparrow\uparrow\uparrow\end{matrix}\right\rangle\right)\right.\\ &\left.+ k\begin{pmatrix}\downarrow\uparrow\\ \uparrow\downarrow\end{pmatrix}\left(\beta_1^*\left|\begin{matrix}\downarrow\uparrow\downarrow\\ \uparrow\uparrow\uparrow\end{matrix}\right\rangle + \beta_2^*\left|\begin{matrix}\uparrow\uparrow\downarrow\\ \uparrow\uparrow\uparrow\end{matrix}\right\rangle\right)\right]_I\widetilde{\left|\begin{matrix}\uparrow\\ \downarrow\end{matrix}\right\rangle}^{(0)}_{I+1},\end{aligned} \tag{5.61}$$

$$\begin{aligned}\hat{h}^{(0)}_{I,I+1}\widetilde{\left|\begin{matrix}\uparrow\downarrow\\ \downarrow\uparrow\end{matrix}\right\rangle}^{(0)}_{I,I+1} = &\widetilde{\left|\begin{matrix}\uparrow\\ \downarrow\end{matrix}\right\rangle}^{(0)}_{I}\left[k\begin{pmatrix}\uparrow\uparrow\\ \downarrow\uparrow\end{pmatrix}\left(-z^*\alpha_2^*\left|\begin{matrix}\uparrow\downarrow\uparrow\\ \uparrow\uparrow\uparrow\end{matrix}\right\rangle + z^*\alpha_1^*\left|\begin{matrix}\uparrow\uparrow\uparrow\\ \uparrow\uparrow\uparrow\end{matrix}\right\rangle + \beta_2^*\left|\begin{matrix}\uparrow\uparrow\downarrow\\ \uparrow\uparrow\uparrow\end{matrix}\right\rangle\right)\right.\\ &\left.+ k\begin{pmatrix}\uparrow\downarrow\\ \downarrow\uparrow\end{pmatrix}\left(\beta_1^*\left|\begin{matrix}\downarrow\uparrow\downarrow\\ \uparrow\uparrow\uparrow\end{matrix}\right\rangle + \beta_3^*\left|\begin{matrix}\downarrow\uparrow\uparrow\\ \uparrow\uparrow\uparrow\end{matrix}\right\rangle\right)\right]_{I+1},\end{aligned} \tag{5.62}$$

$$\begin{aligned}\hat{h}^{(0)}_{I,I+1}\widetilde{\left|\begin{matrix}\downarrow\downarrow\\ \uparrow\downarrow\end{matrix}\right\rangle}^{(0)}_{I,I+1} = &\left[k\begin{pmatrix}\uparrow\downarrow\\ \uparrow\downarrow\end{pmatrix}\left(-z^*\alpha_2^*\left|\begin{matrix}\uparrow\downarrow\uparrow\\ \uparrow\uparrow\uparrow\end{matrix}\right\rangle + z^*\alpha_1^*\left|\begin{matrix}\uparrow\uparrow\uparrow\\ \uparrow\uparrow\uparrow\end{matrix}\right\rangle + \beta_3^*\left|\begin{matrix}\downarrow\uparrow\uparrow\\ \uparrow\uparrow\uparrow\end{matrix}\right\rangle\right)\right.\\ &\left.+ k\begin{pmatrix}\downarrow\downarrow\\ \uparrow\downarrow\end{pmatrix}\left(\beta_1^*\left|\begin{matrix}\downarrow\uparrow\downarrow\\ \uparrow\uparrow\uparrow\end{matrix}\right\rangle + \beta_2^*\left|\begin{matrix}\uparrow\uparrow\downarrow\\ \uparrow\uparrow\uparrow\end{matrix}\right\rangle\right)\right]_I\widetilde{\left|\begin{matrix}\downarrow\\ \downarrow\end{matrix}\right\rangle}^{(0)}_{I+1},\end{aligned} \tag{5.63}$$

$$\begin{aligned}\hat{h}^{(0)}_{I,I+1}\widetilde{\left|\begin{matrix}\downarrow\downarrow\\ \downarrow\uparrow\end{matrix}\right\rangle}^{(0)}_{I,I+1} = &\widetilde{\left|\begin{matrix}\downarrow\\ \downarrow\end{matrix}\right\rangle}^{(0)}_{I}\left[k\begin{pmatrix}\downarrow\uparrow\\ \downarrow\uparrow\end{pmatrix}\left(-z^*\alpha_2^*\left|\begin{matrix}\uparrow\downarrow\uparrow\\ \uparrow\uparrow\uparrow\end{matrix}\right\rangle + z^*\alpha_1^*\left|\begin{matrix}\uparrow\uparrow\uparrow\\ \uparrow\uparrow\uparrow\end{matrix}\right\rangle + \beta_2^*\left|\begin{matrix}\uparrow\uparrow\downarrow\\ \uparrow\uparrow\uparrow\end{matrix}\right\rangle\right)\right.\\ &\left.+ k\begin{pmatrix}\downarrow\downarrow\\ \downarrow\uparrow\end{pmatrix}\left(\beta_1^*\left|\begin{matrix}\downarrow\uparrow\downarrow\\ \uparrow\uparrow\uparrow\end{matrix}\right\rangle + \beta_3^*\left|\begin{matrix}\downarrow\uparrow\uparrow\\ \uparrow\uparrow\uparrow\end{matrix}\right\rangle\right)\right]_{I+1}.\end{aligned} \tag{5.64}$$

It turns out that for $(\sigma_I, \sigma_{I+1}), (\tau_I, \tau_{I+1}) \in H_2$,

$$\overset{(0)}{{}_{I,I+1}}\widetilde{\langle\tau_I\tau_{I+1}|}\hat{h}^{(0)}_{I,I+1}\widetilde{|\sigma_I\sigma_{I+1}\rangle}^{(0)}_{I,I+1} = \delta_{(\tau_I,\tau_{I+1}),(\sigma_I,\sigma_{I+1})}\ \overset{(0)}{{}_{I,I+1}}\widetilde{\langle\sigma_I\sigma_{I+1}|}\hat{h}^{(0)}_{I,I+1}\widetilde{|\sigma_I\sigma_{I+1}\rangle}^{(0)}_{I,I+1}, \tag{5.65}$$

where the diagonal elements are

$$(\sigma_I, \sigma_{I+1}) \in D_2' \Longrightarrow {}^{(0)}_{I,I+1}\langle\widetilde{\sigma_I\sigma_{I+1}}|\hat{h}^{(0)}_{I,I+1}|\widetilde{\sigma_I\sigma_{I+1}}\rangle^{(0)}_{I,I+1} = 0 \tag{5.66}$$

and

$$\begin{aligned}
{}^{(0)}_{I,I+1}\left\langle \widetilde{\begin{matrix}\downarrow\downarrow\\ \uparrow\uparrow\end{matrix}}\right| \hat{h}^{(0)}_{I,I+1} \left|\widetilde{\begin{matrix}\downarrow\downarrow\\ \uparrow\uparrow\end{matrix}}\right\rangle^{(0)}_{I,I+1} &= k\begin{pmatrix}\downarrow\downarrow\\ \uparrow\uparrow\end{pmatrix}(|\beta_1|^2+|\beta_2|^2)(|\beta_1|^2+|\beta_3|^2), && (5.67)\\
{}^{(0)}_{I,I+1}\left\langle \widetilde{\begin{matrix}\uparrow\uparrow\\ \downarrow\downarrow\end{matrix}}\right| \hat{h}^{(0)}_{I,I+1} \left|\widetilde{\begin{matrix}\uparrow\uparrow\\ \downarrow\downarrow\end{matrix}}\right\rangle^{(0)}_{I,I+1} &= k\begin{pmatrix}\uparrow\uparrow\\ \downarrow\downarrow\end{pmatrix}, && (5.68)\\
{}^{(0)}_{I,I+1}\left\langle \widetilde{\begin{matrix}\downarrow\downarrow\\ \downarrow\downarrow\end{matrix}}\right| \hat{h}^{(0)}_{I,I+1} \left|\widetilde{\begin{matrix}\downarrow\downarrow\\ \downarrow\downarrow\end{matrix}}\right\rangle^{(0)}_{I,I+1} &= k\begin{pmatrix}\downarrow\downarrow\\ \downarrow\downarrow\end{pmatrix}, && (5.69)\\
{}^{(0)}_{I,I+1}\left\langle \widetilde{\begin{matrix}\uparrow\uparrow\\ \uparrow\downarrow\end{matrix}}\right| \hat{h}^{(0)}_{I,I+1} \left|\widetilde{\begin{matrix}\uparrow\uparrow\\ \uparrow\downarrow\end{matrix}}\right\rangle^{(0)}_{I,I+1} &= k\begin{pmatrix}\uparrow\uparrow\\ \uparrow\downarrow\end{pmatrix}, && (5.70)\\
{}^{(0)}_{I,I+1}\left\langle \widetilde{\begin{matrix}\uparrow\uparrow\\ \downarrow\uparrow\end{matrix}}\right| \hat{h}^{(0)}_{I,I+1} \left|\widetilde{\begin{matrix}\uparrow\uparrow\\ \downarrow\uparrow\end{matrix}}\right\rangle^{(0)}_{I,I+1} &= k\begin{pmatrix}\uparrow\uparrow\\ \downarrow\uparrow\end{pmatrix}, && (5.71)\\
{}^{(0)}_{I,I+1}\left\langle \widetilde{\begin{matrix}\uparrow\downarrow\\ \uparrow\downarrow\end{matrix}}\right| \hat{h}^{(0)}_{I,I+1} \left|\widetilde{\begin{matrix}\uparrow\downarrow\\ \uparrow\downarrow\end{matrix}}\right\rangle^{(0)}_{I,I+1} &= k\begin{pmatrix}\uparrow\downarrow\\ \uparrow\downarrow\end{pmatrix}, && (5.72)\\
{}^{(0)}_{I,I+1}\left\langle \widetilde{\begin{matrix}\downarrow\uparrow\\ \downarrow\uparrow\end{matrix}}\right| \hat{h}^{(0)}_{I,I+1} \left|\widetilde{\begin{matrix}\downarrow\uparrow\\ \downarrow\uparrow\end{matrix}}\right\rangle^{(0)}_{I,I+1} &= k\begin{pmatrix}\downarrow\uparrow\\ \downarrow\uparrow\end{pmatrix}, && (5.73)\\
{}^{(0)}_{I,I+1}\left\langle \widetilde{\begin{matrix}\downarrow\uparrow\\ \uparrow\downarrow\end{matrix}}\right| \hat{h}^{(0)}_{I,I+1} \left|\widetilde{\begin{matrix}\downarrow\uparrow\\ \uparrow\downarrow\end{matrix}}\right\rangle^{(0)}_{I,I+1} &= k\begin{pmatrix}\uparrow\uparrow\\ \uparrow\downarrow\end{pmatrix}(|z|^2+|\beta_3|^2) + k\begin{pmatrix}\downarrow\uparrow\\ \uparrow\downarrow\end{pmatrix}(|\beta_1|^2+|\beta_2|^2), && (5.74)\\
{}^{(0)}_{I,I+1}\left\langle \widetilde{\begin{matrix}\uparrow\downarrow\\ \downarrow\uparrow\end{matrix}}\right| \hat{h}^{(0)}_{I,I+1} \left|\widetilde{\begin{matrix}\uparrow\downarrow\\ \downarrow\uparrow\end{matrix}}\right\rangle^{(0)}_{I,I+1} &= k\begin{pmatrix}\uparrow\uparrow\\ \downarrow\uparrow\end{pmatrix}(|z|^2+|\beta_2|^2) + k\begin{pmatrix}\uparrow\downarrow\\ \downarrow\uparrow\end{pmatrix}(|\beta_1|^2+|\beta_3|^2), && (5.75)\\
{}^{(0)}_{I,I+1}\left\langle \widetilde{\begin{matrix}\downarrow\downarrow\\ \uparrow\downarrow\end{matrix}}\right| \hat{h}^{(0)}_{I,I+1} \left|\widetilde{\begin{matrix}\downarrow\downarrow\\ \uparrow\downarrow\end{matrix}}\right\rangle^{(0)}_{I,I+1} &= k\begin{pmatrix}\uparrow\downarrow\\ \uparrow\downarrow\end{pmatrix}(|z|^2+|\beta_3|^2) + k\begin{pmatrix}\downarrow\downarrow\\ \uparrow\downarrow\end{pmatrix}(|\beta_1|^2+|\beta_2|^2), && (5.76)\\
{}^{(0)}_{I,I+1}\left\langle \widetilde{\begin{matrix}\downarrow\downarrow\\ \downarrow\uparrow\end{matrix}}\right| \hat{h}^{(0)}_{I,I+1} \left|\widetilde{\begin{matrix}\downarrow\downarrow\\ \downarrow\uparrow\end{matrix}}\right\rangle^{(0)}_{I,I+1} &= k\begin{pmatrix}\downarrow\uparrow\\ \downarrow\uparrow\end{pmatrix}(|z|^2+|\beta_2|^2) + k\begin{pmatrix}\downarrow\downarrow\\ \downarrow\uparrow\end{pmatrix}(|\beta_1|^2+|\beta_3|^2). && (5.77)
\end{aligned}$$

The matrix elements ${}^{(0)}\widetilde{\langle\tau|}\hat{h}^{(0)}\widetilde{|\sigma\rangle}^{(0)}$ ($\sigma=(\sigma_1,\dots,\sigma_{\widetilde{L}}),\tau=(\tau_1,\dots,\tau_{\widetilde{L}})\in H_{\widetilde{L}}$) are given by

$$ {}^{(0)}\widetilde{\langle\tau|}\hat{h}^{(0)}\widetilde{|\sigma\rangle}^{(0)}=\delta_{\tau\sigma}\sum_{I=1}^{\widetilde{L}}{}^{(0)}_{I,I+1}\widetilde{\langle\sigma_I\sigma_{I+1}|}\hat{h}^{(0)}_{I,I+1}\widetilde{|\sigma_I\sigma_{I+1}\rangle}^{(0)}_{I,I+1}. \tag{5.78}$$

Substituting Eq. (5.78) into Eq. (5.48), we obtain

$$\begin{aligned}\hat{Q}\hat{h}^{(0)}\hat{Q}=&\sum_{I=1}^{\widetilde{L}}\sum_{(\sigma_1,\dots,\sigma_{\widetilde{L}})\in H_{\widetilde{L}}}\widetilde{|\sigma_1\cdots\sigma_{\widetilde{L}}\rangle}\ {}^{(0)}_{I,I+1}\widetilde{\langle\sigma_I\sigma_{I+1}|}\hat{h}^{(0)}_{I,I+1}\widetilde{|\sigma_I\sigma_{I+1}\rangle}^{(0)}_{I,I+1}\ \widetilde{\langle\sigma_1\cdots\sigma_{\widetilde{L}}|}\\&+\left(\sum_{\sigma,\tau\in H_{\widetilde{L}}}\widetilde{|\tau\rangle}\ {}^{(1)}\widetilde{\langle\tau|}\hat{h}^{(0)}\widetilde{|\sigma\rangle}^{(0)}\ \widetilde{\langle\sigma|}+\text{h.c.}\right)+\mathcal{O}(\delta^2),\end{aligned} \tag{5.79}$$

where h.c. stands for the Hermitian conjugate. Equation (5.66) and

$$\sigma\in D_{\widetilde{L}}\Longrightarrow\hat{h}^{(0)}\widetilde{|\sigma\rangle}^{(0)}=0, \tag{5.80}$$

which follows from Eqs. (5.29) and (5.53), lead to

$$\begin{aligned}\hat{Q}\hat{h}^{(0)}\hat{Q}=&\sum_{I=1}^{\widetilde{L}}\sum_{\sigma_1,\dots,\sigma_{I-1},\sigma_{I+2},\dots,\sigma_{\widetilde{L}}\in H_1}\sum_{(\sigma_I,\sigma_{I+1})\in H_2\setminus D_2'}\widetilde{k}(\sigma_I,\sigma_{I+1})\widetilde{|\sigma_1\cdots\sigma_{\widetilde{L}}\rangle}\widetilde{\langle\sigma_1\cdots\sigma_{\widetilde{L}}|}\\&+\left(\sum_{\tau\in H_{\widetilde{L}}}\sum_{\sigma\in H_{\widetilde{L}}\setminus D_{\widetilde{L}}}\widetilde{|\tau\rangle}\ {}^{(1)}\widetilde{\langle\tau|}\hat{h}^{(0)}\widetilde{|\sigma\rangle}^{(0)}\ \widetilde{\langle\sigma|}+\text{h.c.}\right)+\mathcal{O}(\delta^2).\end{aligned} \tag{5.81}$$

Here, we defined

$$\widetilde{k}(\sigma_I,\sigma_{I+1}):={}^{(0)}_{I,I+1}\widetilde{\langle\sigma_I\sigma_{I+1}|}\hat{h}^{(0)}_{I,I+1}\widetilde{|\sigma_I\sigma_{I+1}\rangle}^{(0)}_{I,I+1}. \tag{5.82}$$

Since $0<k(\tau_1,\tau_2)=\mathcal{O}(\delta^0)$ for all $(\tau_1,\tau_2)\in H_2\setminus D_2'$, it follows from Eqs. (5.67)–(5.77) that if

$$\begin{aligned}|\beta_1|^2+|\beta_2|^2>0\wedge|\beta_1|^2+|\beta_3|^2>0&\iff(\beta_1\neq0\vee\beta_2\neq0)\wedge(\beta_1\neq0\vee\beta_3\neq0)\\&\iff\beta_1\neq0\vee(\beta_2\neq0\wedge\beta_3\neq0),\end{aligned} \tag{5.83}$$

then

$$\forall(\sigma_I,\sigma_{I+1})\in H_2\setminus D_2',\quad 0<\widetilde{k}(\sigma_I,\sigma_{I+1})=\mathcal{O}(\delta^0). \tag{5.84}$$

This means that $\widetilde{k}(\sigma_I,\sigma_{I+1})$ for $(\sigma_I,\sigma_{I+1})\in H_2\setminus D_2'$ will be renormalized penalties.

The projection of the first-order Hamiltonian $\hat{h}^{(1)}$ is given by

$$\hat{Q}\hat{h}^{(1)}\hat{Q}=\sum_{\sigma,\tau\in H_{\widetilde{L}}}\widetilde{|\tau\rangle}\widetilde{\langle\tau|}\hat{h}^{(1)}\widetilde{|\sigma\rangle}\widetilde{\langle\sigma|}=\sum_{\sigma,\tau\in H_{\widetilde{L}}}\widetilde{|\tau\rangle}\ {}^{(0)}\widetilde{\langle\tau|}\hat{h}^{(1)}\widetilde{|\sigma\rangle}^{(0)}\ \widetilde{\langle\sigma|}+\mathcal{O}(\delta^2), \tag{5.85}$$

where we used $\widetilde{|\sigma\rangle}=\widetilde{|\sigma\rangle}^{(0)}+\mathcal{O}(\delta^1)$. We relegate calculation of the specific form of $\hat{Q}\hat{h}^{(1)}\hat{Q}$ to the next section.

5.4.5 Hamiltonian operator on the coarse-grained space

We can regard $\hat{Q}\hat{h}^{(0)}\hat{Q}$ and $\hat{Q}\hat{h}^{(1)}\hat{Q}$ as operators on the coarse-grained Hilbert space $\mathcal{H}_{\widetilde{L}} = \mathrm{span}\{\,|\widetilde{\sigma}\rangle\,\}_{\sigma\in H_{\widetilde{L}}}$. Omitting $\mathcal{O}(\delta^2)$ terms in Eqs. (5.81) and (5.85), we derive the expression of the renormalized Hamiltonian $\hat{\widetilde{h}} = \hat{Q}\hat{h}\hat{Q}$ as an operator on $\mathcal{H}_{\widetilde{L}}$:

$$\hat{\widetilde{h}} = \hat{\widetilde{h}}^{(0)} + \hat{\widetilde{h}}^{(1)}, \tag{5.86}$$

$$\hat{\widetilde{h}}^{(0)} = \sum_{I=1}^{\widetilde{L}} \sum_{(\sigma_I,\sigma_{I+1})\in H_2\setminus D_2'} \widetilde{k}(\sigma_I,\sigma_{I+1}) \left(\widetilde{|\sigma_I\sigma_{I+1}\rangle}\widetilde{\langle\sigma_I\sigma_{I+1}|}\right)_{I,I+1}, \tag{5.87}$$

$$\hat{\widetilde{h}}^{(1)} = \sum_{\sigma,\tau\in H_{\widetilde{L}}} \widetilde{|\tau\rangle}^{(0)}\widetilde{\langle\tau|}\hat{h}^{(1)}\widetilde{|\sigma\rangle}^{(0)}\,\widetilde{\langle\sigma|} + \hat{\widetilde{o}}\hat{P}(\mathcal{D}_{\widetilde{L}}^{\perp}) + \hat{P}(\mathcal{D}_{\widetilde{L}}^{\perp})\hat{\widetilde{o}}^{\dagger}, \tag{5.88}$$

where $\hat{P}(\mathcal{D}_{\widetilde{L}}^{\perp})$ is the projector onto the orthogonal complement of $\mathcal{D}_{\widetilde{L}}$ and

$$\hat{\widetilde{o}} := \sum_{\tau\in H_{\widetilde{L}}} \sum_{\sigma\in H_{\widetilde{L}}\setminus D_{\widetilde{L}}} \widetilde{|\tau\rangle}^{(1)}\widetilde{\langle\tau|}\hat{h}^{(0)}\widetilde{|\sigma\rangle}^{(0)}\,\widetilde{\langle\sigma|} = \mathcal{O}(\delta^1). \tag{5.89}$$

Notice that $\hat{\widetilde{o}} = \hat{\widetilde{o}}\hat{P}(\mathcal{D}_{\widetilde{L}}^{\perp})$ because $\widetilde{|\sigma\rangle} \in \mathcal{D}_{\widetilde{L}}^{\perp}$ for $\sigma \in H_{\widetilde{L}} \setminus D_{\widetilde{L}}$.

The zeroth-order renormalized Hamiltonian $\hat{\widetilde{h}}^{(0)}$ imposes penalties $0 < \widetilde{k}(\sigma_I,\sigma_{I+1}) = \mathcal{O}(\delta^0)$ on $\widetilde{|\sigma_I\sigma_{I+1}\rangle}_{I,I+1}$ for $(\sigma_I,\sigma_{I+1}) \in H_2 \setminus D_2'$, which means that states in $\mathcal{H}_{\widetilde{L}} \setminus \mathcal{D}_{\widetilde{L}}$ pay energy penalties. In addition, the operator $\hat{\widetilde{o}}\hat{P}(\mathcal{D}_{\widetilde{L}}^{\perp}) + \hat{P}(\mathcal{D}_{\widetilde{L}}^{\perp})\hat{\widetilde{o}}^{\dagger}$ will be irrelevant.

Using Eqs. (5.24), (5.43)–(5.46), and (5.88), we obtain the specific form of the first-order renormalized Hamiltonian:

$$\begin{aligned}
\hat{\widetilde{h}}^{(1)} = \sum_{I=1}^{\widetilde{L}} \Bigg[& \frac{3}{2}u \left(\widetilde{\left|\begin{smallmatrix}\uparrow\\\uparrow\end{smallmatrix}\right\rangle}\widetilde{\left\langle\begin{smallmatrix}\uparrow\\\uparrow\end{smallmatrix}\right|} + \widetilde{\left|\begin{smallmatrix}\downarrow\\\uparrow\end{smallmatrix}\right\rangle}\widetilde{\left\langle\begin{smallmatrix}\downarrow\\\uparrow\end{smallmatrix}\right|} - \widetilde{\left|\begin{smallmatrix}\uparrow\\\downarrow\end{smallmatrix}\right\rangle}\widetilde{\left\langle\begin{smallmatrix}\uparrow\\\downarrow\end{smallmatrix}\right|} - \widetilde{\left|\begin{smallmatrix}\downarrow\\\downarrow\end{smallmatrix}\right\rangle}\widetilde{\left\langle\begin{smallmatrix}\downarrow\\\downarrow\end{smallmatrix}\right|} \right) \\
& - \gamma \Bigg(2\,\mathrm{Re}(\alpha_2^*\alpha_1) \widetilde{\left|\begin{smallmatrix}\uparrow\\\uparrow\end{smallmatrix}\right\rangle}\widetilde{\left\langle\begin{smallmatrix}\uparrow\\\uparrow\end{smallmatrix}\right|} + 2\,\mathrm{Re}[(\beta_2^*+\beta_3^*)(\beta_1+z\alpha_1) - |z|^2\alpha_2^*\alpha_1] \widetilde{\left|\begin{smallmatrix}\downarrow\\\uparrow\end{smallmatrix}\right\rangle}\widetilde{\left\langle\begin{smallmatrix}\downarrow\\\uparrow\end{smallmatrix}\right|} \\
& \quad + [(\beta_2+\beta_3)\alpha_2 + z(\alpha_1^2-\alpha_2^2)] \widetilde{\left|\begin{smallmatrix}\downarrow\\\uparrow\end{smallmatrix}\right\rangle}\widetilde{\left\langle\begin{smallmatrix}\uparrow\\\uparrow\end{smallmatrix}\right|} \\
& \quad + [(\beta_2+\beta_3)\alpha_2 + z(\alpha_1^2-\alpha_2^2)]^* \widetilde{\left|\begin{smallmatrix}\uparrow\\\uparrow\end{smallmatrix}\right\rangle}\widetilde{\left\langle\begin{smallmatrix}\downarrow\\\uparrow\end{smallmatrix}\right|} \Bigg)
\end{aligned}$$

$$
\begin{aligned}
&+ v \Bigg((|\alpha_1|^2 + 3|\alpha_2|^2) \widetilde{\left|\begin{matrix}\uparrow\\\uparrow\end{matrix}\right\rangle}\widetilde{\left\langle\begin{matrix}\uparrow\\\uparrow\end{matrix}\right|} \\
&\qquad + [|z|^2(3|\alpha_1|^2 + |\alpha_2|^2) - |\beta_1|^2 + |\beta_2|^2 + |\beta_3|^2] \widetilde{\left|\begin{matrix}\downarrow\\\uparrow\end{matrix}\right\rangle}\widetilde{\left\langle\begin{matrix}\downarrow\\\uparrow\end{matrix}\right|} \\
&\qquad + 2z\alpha_1\alpha_2 \widetilde{\left|\begin{matrix}\downarrow\\\uparrow\end{matrix}\right\rangle}\widetilde{\left\langle\begin{matrix}\uparrow\\\uparrow\end{matrix}\right|} + (2z\alpha_1\alpha_2)^* \widetilde{\left|\begin{matrix}\uparrow\\\uparrow\end{matrix}\right\rangle}\widetilde{\left\langle\begin{matrix}\downarrow\\\uparrow\end{matrix}\right|} \Bigg) \\
&- \xi \Bigg((\beta_2 + \beta_3)\alpha_1 \widetilde{\left|\begin{matrix}\downarrow\\\uparrow\end{matrix}\right\rangle}\widetilde{\left\langle\begin{matrix}\uparrow\\\uparrow\end{matrix}\right|} + (\beta_2^* + \beta_3^*)\alpha_1^* \widetilde{\left|\begin{matrix}\uparrow\\\uparrow\end{matrix}\right\rangle}\widetilde{\left\langle\begin{matrix}\downarrow\\\uparrow\end{matrix}\right|} \\
&\qquad - 2\,\mathrm{Re}[(\beta_2^* + \beta_3^*)z\alpha_2] \widetilde{\left|\begin{matrix}\downarrow\\\uparrow\end{matrix}\right\rangle}\widetilde{\left\langle\begin{matrix}\downarrow\\\uparrow\end{matrix}\right|} \Bigg) \Bigg]_I \\
&- \sum_{I=1}^{\widetilde{L}} \xi \left(|\alpha_2|^2\beta_2^*\beta_3 \widetilde{\left|\begin{matrix}\uparrow\downarrow\\\uparrow\uparrow\end{matrix}\right\rangle}\widetilde{\left\langle\begin{matrix}\downarrow\uparrow\\\uparrow\uparrow\end{matrix}\right|} + |\alpha_2|^2\beta_2\beta_3^* \widetilde{\left|\begin{matrix}\downarrow\uparrow\\\uparrow\uparrow\end{matrix}\right\rangle}\widetilde{\left\langle\begin{matrix}\uparrow\downarrow\\\uparrow\uparrow\end{matrix}\right|} \right)_{I,I+1} \\
&+ \hat{\tilde{o}}\hat{P}(\mathcal{D}_{\widetilde{L}}^{\perp}) + \hat{P}(\mathcal{D}_{\widetilde{L}}^{\perp})\hat{\tilde{o}}^{\dagger}. \qquad (5.90)
\end{aligned}
$$

5.4.6 Determination of the variational parameters

Now we determine the parameters $\alpha_1, \alpha_2, z, \beta_1, \beta_2, \beta_3 \in \mathbb{C}$. We should construct the projector $\hat{Q}$ such that the subspace $\mathcal{H}_{\widetilde{L}} = \mathrm{span}\{\, \widetilde{|\sigma\rangle} \,\}_{\sigma \in H_{\widetilde{L}}} \subset \mathcal{H}_L$ is a low-energy space. One may consider that we should minimize the sum of the eigenenergies of the renormalized Hamiltonian, i.e., the trace of $\hat{\tilde{h}}$. However, minimizing the ordinary trace $\mathrm{Tr}\,\hat{\tilde{h}}$ is inappropriate for our purpose. We wish to study the transition between the columnar and staggered states, both of which pay no energy penalty of $\mathcal{O}(\delta^0)$. This implies that we should ignore states which cost energies of $\mathcal{O}(\delta^0)$. Hence, we minimize the restricted trace $\mathrm{Tr}_{|\mathcal{D}_{\widetilde{L}}}\hat{\tilde{h}}$. We denoted the trace in the subspace $\mathcal{D}_{\widetilde{L}} = \mathrm{span}\{\, \widetilde{|\sigma\rangle} \,\}_{\sigma \in D_{\widetilde{L}}} \subset \mathcal{H}_{\widetilde{L}}$ by $\mathrm{Tr}_{|\mathcal{D}_{\widetilde{L}}}$:

$$
\mathrm{Tr}_{|\mathcal{D}_{\widetilde{L}}} \cdots := \mathrm{Tr}\, \hat{P}(\mathcal{D}_{\widetilde{L}}) \cdots \hat{P}(\mathcal{D}_{\widetilde{L}}) = \mathrm{Tr}\, \hat{P}(\mathcal{D}_{\widetilde{L}}) \cdots , \qquad (5.91)
$$

where $\hat{P}(\mathcal{D}_{\widetilde{L}})$ is the projector onto $\mathcal{D}_{\widetilde{L}}$ and we used the cyclic invariance of the trace and $\hat{P}(\mathcal{D}_{\widetilde{L}})^2 = \hat{P}(\mathcal{D}_{\widetilde{L}})$. The projector $\hat{P}(\mathcal{D}_{\widetilde{L}})$ has the spectral decomposition

$$
\hat{P}(\mathcal{D}_{\widetilde{L}}) = \sum_{\sigma \in D_{\widetilde{L}}} \widetilde{|\sigma\rangle}\widetilde{\langle\sigma|} \qquad (5.92)
$$

and the restricted trace can be written as

$$\mathrm{Tr}_{|\mathcal{D}_{\widetilde{L}}} \cdots = \sum_{\sigma \in D_{\widetilde{L}}} \widetilde{\langle \sigma |} \cdots \widetilde{| \sigma \rangle}. \tag{5.93}$$

Since any $\sigma = (\sigma_1, \ldots, \sigma_{\widetilde{L}}) \in D_{\widetilde{L}}$ satisfies $(\sigma_I, \sigma_{I+1}) \in D_2'$ $(\forall I = 1, \ldots, \widetilde{L})$ and thus $\widetilde{\langle \sigma |} \hat{\tilde{h}}^{(0)} \widetilde{| \sigma \rangle} = 0$, we have $\mathrm{Tr}_{|\mathcal{D}_{\widetilde{L}}} \hat{\tilde{h}} = \mathrm{Tr}_{|\mathcal{D}_{\widetilde{L}}} \hat{\tilde{h}}^{(1)}$. To calculate the restricted trace, we use the formulae

$$\mathrm{Tr}_{|\mathcal{D}_{\widetilde{L}}} \left(\widetilde{\left| \begin{matrix} \uparrow \\ \uparrow \end{matrix} \right\rangle} \widetilde{\left\langle \begin{matrix} \uparrow \\ \uparrow \end{matrix} \right|} \right)_I = F_{\widetilde{L}-1}, \quad \mathrm{Tr}_{|\mathcal{D}_{\widetilde{L}}} \left(\widetilde{\left| \begin{matrix} \downarrow \\ \uparrow \end{matrix} \right\rangle} \widetilde{\left\langle \begin{matrix} \downarrow \\ \uparrow \end{matrix} \right|} \right)_I = F_{\widetilde{L}-3}, \tag{5.94}$$

$$\mathrm{Tr}_{|\mathcal{D}_{\widetilde{L}}} \left(\widetilde{\left| \begin{matrix} \uparrow \\ \downarrow \end{matrix} \right\rangle} \widetilde{\left\langle \begin{matrix} \uparrow \\ \downarrow \end{matrix} \right|} \right)_I = \mathrm{Tr}_{|\mathcal{D}_{\widetilde{L}}} \left(\widetilde{\left| \begin{matrix} \downarrow \\ \downarrow \end{matrix} \right\rangle} \widetilde{\left\langle \begin{matrix} \downarrow \\ \downarrow \end{matrix} \right|} \right)_I = 1 \tag{5.95}$$

for $I = 1, \ldots, \widetilde{L}$, where $F_{\widetilde{L}-1}$ and $F_{\widetilde{L}-3}$ are the Fibonacci numbers defined by Eq. (5.19).

For the present first-order renormalized Hamiltonian (5.90), the restricted trace of the renormalized Hamiltonian is

$$\begin{aligned} \mathrm{Tr}_{|\mathcal{D}_{\widetilde{L}}} \hat{\tilde{h}} = \widetilde{L} \Big(& \frac{3}{2} u (F_{\widetilde{L}-1} + F_{\widetilde{L}-3} - 2) \\ & - \gamma \{ 2F_{\widetilde{L}-1} \,\mathrm{Re}(\alpha_2^* \alpha_1) + 2F_{\widetilde{L}-3} \,\mathrm{Re}[(\beta_2^* + \beta_3^*)(\beta_1 + z\alpha_1) - |z|^2 \alpha_2^* \alpha_1] \} \\ & + v \{ F_{\widetilde{L}-1} (|\alpha_1|^2 + 3|\alpha_2|^2) + F_{\widetilde{L}-3} [|z|^2 (3|\alpha_1|^2 + |\alpha_2|^2) - |\beta_1|^2 + |\beta_2|^2 + |\beta_3|^2] \} \\ & + 2\xi F_{\widetilde{L}-3} \,\mathrm{Re}[(\beta_2^* + \beta_3^*) z \alpha_2] \Big). \end{aligned} \tag{5.96}$$

The minimization of $\mathrm{Tr}_{|\mathcal{D}_{\widetilde{L}}} \hat{\tilde{h}}$ is equivalent to minimizing the function

$$\begin{aligned} f_{\gamma,v,\xi}(\alpha_1, \alpha_2, z, \beta_1, \beta_2, \beta_3) = -\frac{1}{2} \{ & \gamma [(\varphi_{\widetilde{L}}^2 - |z|^2) \alpha_2^* \alpha_1 + (\varphi_{\widetilde{L}}^2 - |z|^2) \alpha_2 \alpha_1^* \\ & \quad + (\beta_2^* + \beta_3^*)(\beta_1 + z\alpha_1) + (\beta_2 + \beta_3)(\beta_1^* + z^* \alpha_1^*)] \\ & + 2v [(\varphi_{\widetilde{L}}^2 - |z|^2) |\alpha_1|^2 + |\beta_1|^2] \\ & - \xi [(\beta_2^* + \beta_3^*) z \alpha_2 + (\beta_2 + \beta_3) z^* \alpha_2^*] \} \end{aligned} \tag{5.97}$$

on the constraints given by Eq. (5.47), where $\varphi_{\widetilde{L}}^2 := F_{\widetilde{L}-1}/F_{\widetilde{L}-3}$. Since the difference of $\varphi_{\widetilde{L}}^2$ from the golden ratio squared φ^2 becomes exponentially small for large system size L, we apply the approximation $\varphi_{\widetilde{L}}^2 \simeq \varphi^2$. The function $f_{\gamma,v,\xi}$ is rewritten as

$$\begin{aligned} f_{\gamma,v,\xi}(\alpha_1, \alpha_2, z, \beta_1, \beta_2, \beta_3) = -\frac{1}{2} \{ & \gamma [(\varphi^2 - |z|^2) \alpha_2^* \alpha_1 + (\varphi^2 - |z|^2) \alpha_2 \alpha_1^* \\ & \quad + (\beta_2^* + \beta_3^*)(\beta_1 + z\alpha_1) + (\beta_2 + \beta_3)(\beta_1^* + z^* \alpha_1^*)] \\ & + 2v [(\varphi^2 - |z|^2) |\alpha_1|^2 + |\beta_1|^2] \\ & - \xi [(\beta_2^* + \beta_3^*) z \alpha_2 + (\beta_2 + \beta_3) z^* \alpha_2^*] \}. \end{aligned} \tag{5.98}$$

Minimizing this function determines the variational parameters α_1, α_2, z, β_1, β_2, and β_3.

5.4.7 Renormalization group equations

We employ the ansatz in which the variational parameters are real: $\alpha_1, \alpha_2, z, \beta_1, \beta_2, \beta_3 \in \mathbb{R}$. We also suppose that $\beta_2 = \beta_3$ for the sake of symmetry. Denote the Pauli operators on $\mathrm{span}\{\, \widetilde{|\sigma_{a,I}\rangle}_{a,I} \,\}_{\sigma_{a,I}=\uparrow,\downarrow}$ by $\hat{\tilde{X}}_{a,I}$, $\hat{\tilde{Y}}_{a,I}$, and $\hat{\tilde{Z}}_{a,I}$ for $a = \mathrm{t}, \mathrm{b}$ and $I = 1, \ldots, \widetilde{L}$. It follows from Eq. (5.90) that

$$
\begin{aligned}
\hat{\tilde{h}}^{(1)} = \sum_{I=1}^{\widetilde{L}} \Bigg(& \frac{1}{2}\{3u - \gamma[(\beta_2+\beta_3)(\beta_1+z\alpha_1) + (1-z^2)\alpha_2\alpha_1] \\
& \quad + v[2 - (1-z^2)\alpha_1^2 - \beta_1^2] + \xi(\beta_2+\beta_3)z\alpha_2\}\hat{\tilde{Z}}_{\mathrm{b},I} \\
& + \{\gamma[(\beta_2+\beta_3)(\beta_1+z\alpha_1) - (1+z^2)\alpha_2\alpha_1] \\
& \quad + v[1 - (1+z^2)\alpha_1^2 + \beta_1^2] - \xi(\beta_2+\beta_3)z\alpha_2\}\hat{\tilde{Z}}_{\mathrm{t},I}\frac{1+\hat{\tilde{Z}}_{\mathrm{b},I}}{2} \\
& - \{\gamma[(\beta_2+\beta_3)\alpha_2 + z(\alpha_1^2 - \alpha_2^2)] - 2vz\alpha_1\alpha_2 + \xi(\beta_2+\beta_3)\alpha_1\}\hat{\tilde{X}}_{\mathrm{t},I}\frac{1+\hat{\tilde{Z}}_{\mathrm{b},I}}{2} \\
& - \xi\alpha_2^2\beta_2\beta_3 \left(\widetilde{\left|\begin{matrix}\uparrow\downarrow\\ \uparrow\uparrow\end{matrix}\right\rangle}\widetilde{\left\langle\begin{matrix}\downarrow\uparrow\\ \uparrow\uparrow\end{matrix}\right|} + \widetilde{\left|\begin{matrix}\downarrow\uparrow\\ \uparrow\uparrow\end{matrix}\right\rangle}\widetilde{\left\langle\begin{matrix}\uparrow\downarrow\\ \uparrow\uparrow\end{matrix}\right|} \right)_{I,I+1} \\
& + \frac{1}{2}\{-\gamma[(\beta_2+\beta_3)(\beta_1+z\alpha_1) + (1-z^2)\alpha_2\alpha_1] \\
& \quad + v[2 - (1-z^2)\alpha_1^2 - \beta_1^2] + \xi(\beta_2+\beta_3)z\alpha_2\} \Bigg) \\
& + \hat{\tilde{o}}\hat{P}(\mathcal{D}_{\widetilde{L}}^{\perp}) + \hat{P}(\mathcal{D}_{\widetilde{L}}^{\perp})\hat{\tilde{o}}^{\dagger}.
\end{aligned}
\tag{5.99}
$$

Omitting the term proportional to the identity in $\hat{\tilde{h}}^{(1)}$, we arrive at the expression of

the renormalized Hamiltonian:

$$\widetilde{\hat{h}} = \widetilde{\hat{h}}^{(0)} + \widetilde{\hat{h}}^{(1)}, \tag{5.100}$$

$$\widetilde{\hat{h}}^{(0)} = \sum_{I=1}^{\widetilde{L}} \sum_{(\sigma_I,\sigma_{I+1})\in H_2\setminus D_2'} \widetilde{k}(\sigma_I,\sigma_{I+1}) \left(\widetilde{|\sigma_I\sigma_{I+1}\rangle\langle\sigma_I\sigma_{I+1}|} \right)_{I,I+1}, \tag{5.101}$$

$$\begin{aligned}\widetilde{\hat{h}}^{(1)} = \sum_{I=1}^{\widetilde{L}} \Bigg[& \frac{\widetilde{u}}{2}\widetilde{\hat{Z}}_{\mathrm{b},I} - \widetilde{\gamma}\widetilde{\hat{X}}_{\mathrm{t},I}\frac{1+\widetilde{\hat{Z}}_{\mathrm{b},I}}{2} + \widetilde{v}\widetilde{\hat{Z}}_{\mathrm{t},I}\frac{1+\widetilde{\hat{Z}}_{\mathrm{b},I}}{2} \\ & -\widetilde{\xi}\left(\widetilde{\left|\begin{matrix}\uparrow\downarrow\\ \uparrow\uparrow\end{matrix}\right\rangle\left\langle\begin{matrix}\uparrow\downarrow\\ \uparrow\uparrow\end{matrix}\right|} + \widetilde{\left|\begin{matrix}\downarrow\uparrow\\ \uparrow\uparrow\end{matrix}\right\rangle\left\langle\begin{matrix}\uparrow\downarrow\\ \uparrow\uparrow\end{matrix}\right|} \right)_{I,I+1} \Bigg] + \widetilde{\hat{o}}\hat{P}(\mathcal{D}_{\widetilde{L}}^{\perp}) + \hat{P}(\mathcal{D}_{\widetilde{L}}^{\perp})\widetilde{\hat{o}}^{\dagger}.\end{aligned} \tag{5.102}$$

The renormalized coupling constants $\widetilde{u}$, $\widetilde{\gamma}$, $\widetilde{v}$, and $\widetilde{\xi}$ satisfy the following RG equations:

$$\begin{aligned}\widetilde{u} &= 3u - \gamma[(\beta_2+\beta_3)(\beta_1+z\alpha_1) + (1-z^2)\alpha_2\alpha_1] \\ &\quad + v[2-(1-z^2)\alpha_1^2 - \beta_1^2] + \xi(\beta_2+\beta_3)z\alpha_2, \qquad (5.103)\\ \widetilde{\gamma} &= \gamma[(\beta_2+\beta_3)\alpha_2 + z(\alpha_1^2-\alpha_2^2)] - 2vz\alpha_1\alpha_2 + \xi(\beta_2+\beta_3)\alpha_1, \qquad (5.104)\\ \widetilde{v} &= \gamma[(\beta_2+\beta_3)(\beta_1+z\alpha_1) - (1+z^2)\alpha_2\alpha_1] \\ &\quad + v[1-(1+z^2)\alpha_1^2 + \beta_1^2] - \xi(\beta_2+\beta_3)z\alpha_2, \qquad (5.105)\\ \widetilde{\xi} &= \xi\alpha_2^2\beta_2\beta_3, \qquad (5.106)\end{aligned}$$

where $\alpha_1, \alpha_2, z, \beta_1, \beta_2 = \beta_3 \in \mathbb{R}$ are the arguments minimizing the function $f_{\gamma,v,\xi}$ given by Eq. (5.98) on the constraints (5.47).

Of course, the penalty constants $k(\sigma_1,\sigma_2)$ are renormalized into $\widetilde{k}(\sigma_1,\sigma_2)$ for $(\sigma_1,\sigma_2) \in H_2 \setminus D_2'$. However, the specific values of the renormalized penalty constants are unimportant for our analysis of the zero-temperature phase transition in the dimer limit. The only essential thing is that all the penalty constants are positive and of zeroth order in δ. This means that any spin configuration which is not mapped onto a dimer covering does not contribute to the leading-order part of the ground state.

5.4.8 Repeat of the renormalization group transformation

We apply the RG transformation defined by Eqs. (5.100)–(5.106) repeatedly. Let us denote by l how many times the RG transformation has been performed. We regard the system size and the coupling constants as functions of the "time" l. Since the scaling factor is three, the length of the system scales as $L(l) = 3^{-l}L$. The coupling constants $u(l)$, $\gamma(l)$, $v(l)$, and $\xi(l)$ have the initial values

$$u(0) = u, \quad \gamma(0) = \gamma, \quad v(0) = v, \quad \xi(0) = \xi \tag{5.107}$$

and satisfy the recurrence relations

$$\begin{aligned}
u(l+1) &= 3u(l) - \gamma(l)[(\beta_2(l)+\beta_3(l))(\beta_1(l)+z(l)\alpha_1(l)) + (1-z(l)^2)\alpha_1(l)\alpha_2(l)] \\
&\quad + v(l)[2-(1-z(l)^2)\alpha_1(l)^2 - \beta_1(l)^2] + \xi(l)(\beta_2(l)+\beta_3(l))z(l)\alpha_2(l), \quad (5.108)\\
\gamma(l+1) &= \gamma(l)[(\beta_2(l)+\beta_3(l))\alpha_2(l) + z(l)(\alpha_1(l)^2 - \alpha_2(l)^2)] \\
&\quad - 2v(l)z(l)\alpha_1(l)\alpha_2(l) + \xi(l)(\beta_2(l)+\beta_3(l))\alpha_1(l), \quad (5.109)\\
v(l+1) &= \gamma(l)[(\beta_2(l)+\beta_3(l))(\beta_1(l)+z(l)\alpha_1(l)) - (1+z(l)^2)\alpha_1(l)\alpha_2(l)] \\
&\quad + v(l)[1-(1+z(l)^2)\alpha_1(l)^2 + \beta_1(l)^2] - \xi(l)(\beta_2(l)+\beta_3(l))z(l)\alpha_2(l), \quad (5.110)\\
\xi(l+1) &= \xi(l)\alpha_2(l)^2\beta_2(l)\beta_3(l), \quad (5.111)
\end{aligned}$$

where $\alpha_1(l), \alpha_2(l), z(l), \beta_1(l), \beta_2(l) = \beta_3(l) \in \mathbb{R}$ are the arguments minimizing the function $f_{\gamma(l),v(l),\xi(l)}$ defined by Eq. (5.98) on the constraints (5.47). Writing the coupling constant $u(l)$ as

$$u(l) = 3^l(u - \overline{u}(l)), \quad (5.112)$$

we find $\overline{u}(0) = 0$ and

$$\begin{aligned}
\overline{u}(l+1) = \overline{u}(l) + 3^{-l-1}\{&\gamma(l)[(\beta_2(l)+\beta_3(l))(\beta_1(l)+z(l)\alpha_1(l)) + (1-z(l)^2)\alpha_1(l)\alpha_2(l)] \\
&- v(l)[2-(1-z(l)^2)\alpha_1(l)^2 - \beta_1(l)^2] \\
&- \xi(l)(\beta_2(l)+\beta_3(l))z(l)\alpha_2(l)\}. \quad (5.113)
\end{aligned}$$

5.5 Results and their implications for quantum annealing

Let us apply the RG transformation described in the previous section to the frustrated Ising ladder (5.1) in the dimer limit $K \to \infty$ and the thermodynamic limit $L \to \infty$. The bare dimensionless Hamiltonian is defined by Eqs. (5.9), (5.14), and (5.11) with $\hat{h}^{(1)}$ regarded as a perturbation to $\hat{h}^{(0)}$. Comparing the bare Hamiltonian with the general form given by Eqs. (5.22)–(5.24), we see that the bare couplings are

$$u(0) = u, \quad \gamma(0) = \gamma = \gamma_{\rm t}, \quad v(0) = 0, \quad \xi(0) = \xi = \xi_{\rm tt}. \quad (5.114)$$

The other couplings $\gamma_{\rm b}$, $\xi_{\rm bb}$, and $\xi_{\rm tb}$ can be set to arbitrary values. We renormalize the coupling constants repeatedly according to the recurrence relations (5.108)–(5.111). In addition, the coupling constant $\overline{u}(l)$ defined as Eq. (5.112) obeys $\overline{u}(0) = 0$ and Eq. (5.113). It follows from mathematical induction that $\overline{u}(l)$, $\gamma(l)$, $v(l)$, and $\xi(l)$ are determined only by the "time" l and the initial values γ and ξ, because the function $f_{\gamma(l),v(l),\xi(l)}$ and Eqs. (5.109)–(5.111) and (5.113) are independent of u and $u(l)$.

We show the coupling constants $\overline{u}(l)$, $\gamma(l)$, $v(l)$, and $\xi(l)$ as well as the variational parameters $\alpha_1(l)$, $\alpha_2(l)$, $z(l)$, $\beta_1(l)$, and $\beta_2(l) = \beta_3(l)$ as functions of l for several sets of bare couplings γ and ξ in Figs. 5.7–5.9 (regarding $u(l)$ and its initial value u, see the

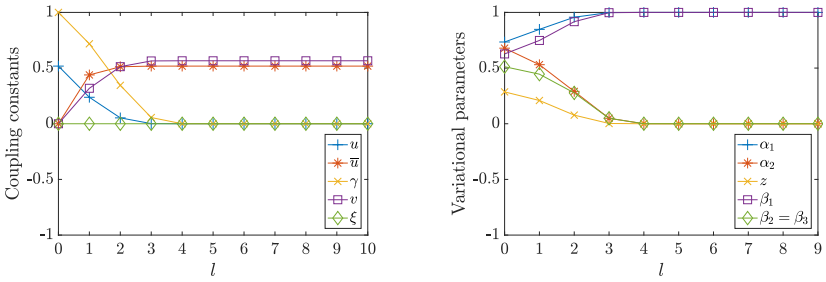

Figure 5.7: Coupling constants $u(l)$, $\overline{u}(l)$, $\gamma(l)$, $v(l)$, and $\xi(l)$ and variational parameters $\alpha_1(l)$, $\alpha_2(l)$, $z(l)$, $\beta_1(l)$, and $\beta_2(l) = \beta_3(l)$ as functions of l for the bare couplings $u = \overline{u}_{\gamma,\xi} = 0.51773501$, $\gamma = 1$, $v = 0$, and $\xi = 0$.

next paragraph). Here, Fig. 5.7 is for the case of no XX interactions $\xi = 0$, Fig. 5.8 for the case of the stoquastic XX interaction on the top row $\xi > 0$, and Fig. 5.9 for the case of the non-stoquastic one $\xi < 0$. Notice that multiplying all the bare couplings by a positive constant c makes every renormalized coupling multiplied by c, when the variational parameters at each l are invariant. This operation corresponds to the scale transformation of the vertical axis of each left graph in Figs. 5.7–5.9.

We find that $\overline{u}(l)$ and $v(l)$ converge to finite positive values and γ and ξ vanish in the limit $l \to \infty$. The coupling constant $u(l)$ asymptotically behaves as

$$u(l) \approx 3^l (u - \overline{u}_{\gamma,\xi}) \quad (l \to \infty), \tag{5.115}$$

where $\overline{u}_{\gamma,\xi} := \lim_{l\to\infty} \overline{u}(l)$ is the limiting value of $\overline{u}(l)$ determined by the bare couplings γ and ξ (recall that $v = 0$). This asymptotic behavior shows that $u(l)$ diverges and its sign coincides with the sign of $u - \overline{u}_{\gamma,\xi}$. When $u = \overline{u}_{\gamma,\xi}$, $u(l)$ converges to zero as shown in Figs. 5.7–5.9. Therefore, the limit of $u(l)$ is

$$u(l) \to \begin{cases} -\infty, & u < \overline{u}_{\gamma,\xi}, \\ 0, & u = \overline{u}_{\gamma,\xi}, \\ +\infty, & u > \overline{u}_{\gamma,\xi} \end{cases} \quad (l \to \infty). \tag{5.116}$$

This indicates that the fixed points of the present RG transformation are $(u, \gamma, v, \xi) = (0, 0, v, 0), (\pm\infty, 0, v, 0)$ with v being an arbitrary positive value. Indeed, we can confirm that these points are fixed points by noticing that $f_{\gamma=0,v,\xi=0}$ is minimized at $\alpha_1 = \beta_1 = 1$ and $\alpha_2 = z = \beta_2 = \beta_3 = 0$ on the constraints (5.47) and substituting these values into the RG equations (5.108)–(5.111).

The fixed points $(u, \gamma, v, \xi) = (\pm\infty, 0, v, 0)$ are stable (i.e., any coupling constant is irrelevant around these fixed points) and these correspond to the two phases: $(u, \gamma, v, \xi) = (-\infty, 0, v, 0)$ is for the columnar phase and $(u, \gamma, v, \xi) = (+\infty, 0, v, 0)$ for the staggered phase. On the other hand, the fixed point $(u, \gamma, v, \xi) = (0, 0, v, 0)$ for each $v > 0$ is unstable for the deviation of u. Around this fixed point, u is relevant and the other coupling constants are irrelevant.

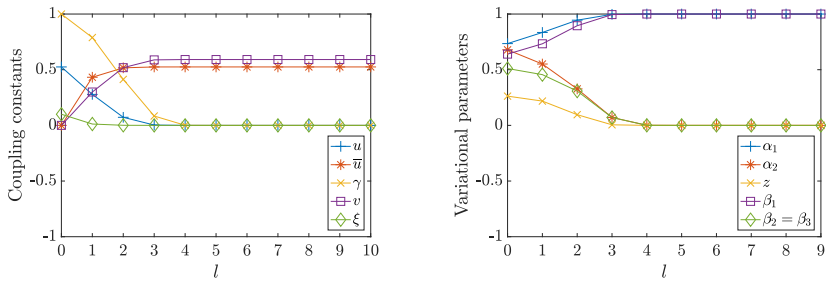

(a) $(u, \gamma, v, \xi) = (0.52489031, 1, 0, 0.1)$.

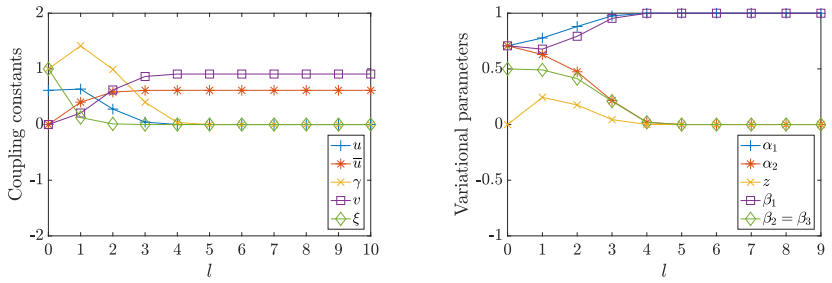

(b) $(u, \gamma, v, \xi) = (0.61474501, 1, 0, 1)$.

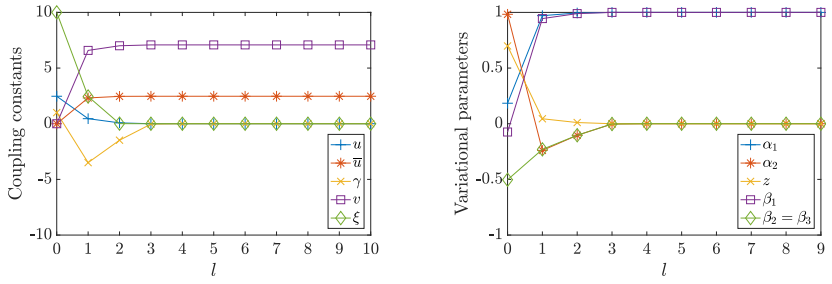

(c) $(u, \gamma, v, \xi) = (2.46771358, 1, 0, 10)$.

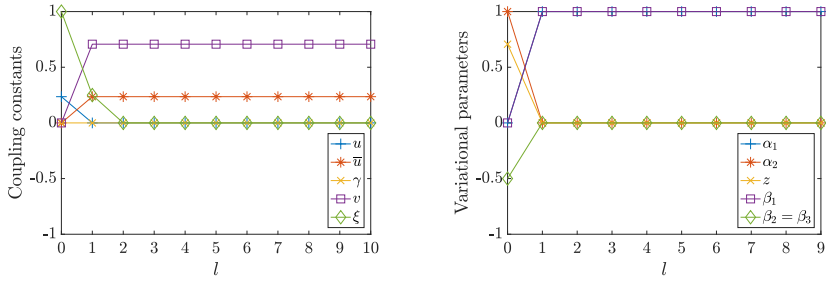

(d) $(u, \gamma, v, \xi) = (0.23570226, 0, 0, 1)$.

Figure 5.8: Coupling constants $u(l)$, $\overline{u}(l)$, $\gamma(l)$, $v(l)$, and $\xi(l)$ and variational parameters $\alpha_1(l)$, $\alpha_2(l)$, $z(l)$, $\beta_1(l)$, and $\beta_2(l) = \beta_3(l)$ as functions of l for several sets of the bare couplings $(u, \gamma, v, \xi) = (\overline{u}_{\gamma,\xi}, \gamma, 0, \xi)$ with $\xi > 0$.

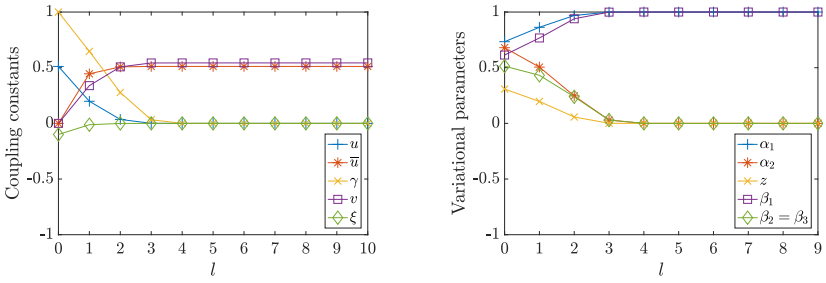

(a) $(u, \gamma, v, \xi) = (0.51144374, 1, 0, -0.1)$.

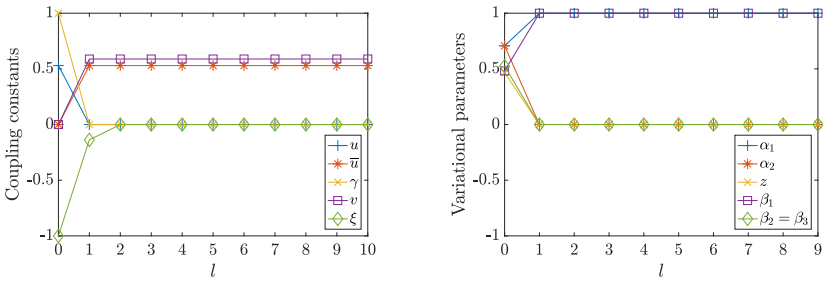

(b) $(u, \gamma, v, \xi) = (0.52956828, 1, 0, -1)$.

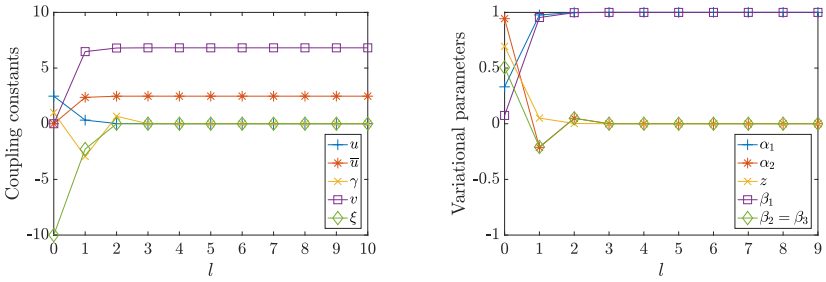

(c) $(u, \gamma, v, \xi) = (2.47583092, 1, 0, -10)$.

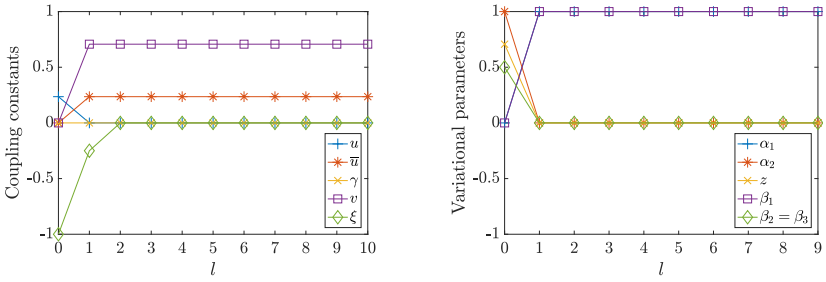

(d) $(u, \gamma, v, \xi) = (0.23570226, 0, 0, -1)$.

Figure 5.9: Coupling constants $u(l)$, $\overline{u}(l)$, $\gamma(l)$, $v(l)$, and $\xi(l)$ and variational parameters $\alpha_1(l)$, $\alpha_2(l)$, $z(l)$, $\beta_1(l)$, and $\beta_2(l) = \beta_3(l)$ as functions of l for several sets of the bare couplings $(u, \gamma, v, \xi) = (\overline{u}_{\gamma,\xi}, \gamma, 0, \xi)$ with $\xi < 0$.

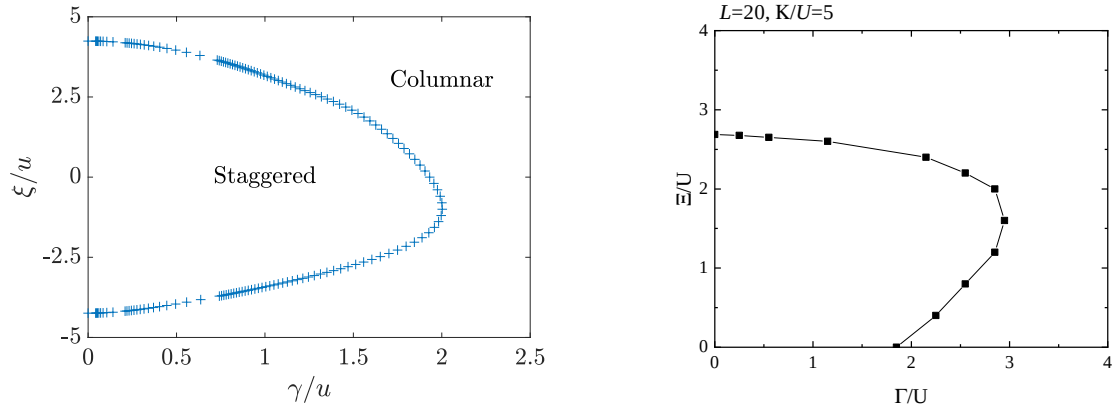

(a) (b)

Figure 5.10: (a) Phase diagram of the frustrated Ising ladder in the dimer limit $K \to \infty$ derived from the real-space RG method. The horizontal and vertical axes are $\gamma/u = \gamma_{\rm t}/u = \Gamma_{\rm t}/U$ and $\xi/u = \xi_{\rm tt}/u = \Xi_{\rm tt}/U$, respectively. The blue plus signs indicate first-order transition points. (b) Phase diagram of the frustrated Ising ladder of length $L = 20$ for $K/U = 5$, $\Gamma_{\rm t} = \Gamma_{\rm b}$, $\Xi_{\rm tt} < 0$, and $\Xi_{\rm bb} = \Xi_{\rm tb} = 0$, depicted by Sota and Yunoki (2019) [70]. They carried out the DMRG calculation and found the first-order transition points indicated by the black squares. The horizontal axis is $\gamma/u = \Gamma_{\rm t}/U$ and the vertical axis is $-\xi_{\rm tt}/u = -\Xi_{\rm tt}/U$ in our definition.

In addition, Eq. (5.116) shows the bare coupling $u = \overline{u}_{\gamma,\xi}$ to be the critical point for each γ and ξ, meaning that only the fine-tuned $u = \overline{u}_{\gamma,\xi}$ flows into the unstable fixed point $(u, \gamma, v, \xi) = (0, 0, v, 0)$ in the sense of the RG theory. Other values of the bare coupling u are absorbed into the stable fixed points (namely, $u < \overline{u}_{\gamma,\xi}$ into the columnar phase $(u, \gamma, v, \xi) = (-\infty, 0, v, 0)$ and $u > \overline{u}_{\gamma,\xi}$ into the staggered phase $(u, \gamma, v, \xi) = (+\infty, 0, v, 0)$) as the RG transformation is performed many times.

Let us depict the phase diagram of the frustrated Ising ladder in the dimer limit. Although we have the three couplings u, γ, and ξ, it is sufficient to plot the phase diagram on the ξ/u-γ/u plane because dividing these couplings by $u > 0$ does not change the phase (notice that $\overline{u}_{c\gamma,c\xi} = c\overline{u}_{\gamma,\xi}$ for any $c > 0$ and thus $\lim_{l\to\infty} u(l)$ is unchanged under the multiplication of every bare coupling by c). We can draw the phase diagram by marking the critical points $(\gamma/u, \xi/u) = (\gamma/\overline{u}_{\gamma,\xi}, \xi/\overline{u}_{\gamma,\xi})$ for a number of sets of γ and ξ. The resulting phase diagram is shown in Fig. 5.10(a).

We can deduce from the scaling theory [69], which is closely related to the RG thoery, that the phase boundary shown in Fig. 5.10(a) is of first order as explained in the following: Recalling that the scaling factor of our RG transformation is three and $u(l)$ is asymptotically proportional to 3^l as shown in Eq. (5.115), we find that the scaling dimension of u around the unstable fixed point $(u, \gamma, v, \xi) = (0, 0, v, 0)$ is $y_u = 1$. Here, the scaling dimension y_u around a fixed point $u = u^*$ is defined as $u(l+1) - u^* \approx b^{y_u}(u(l) - u^*)$ in the vicinity of $u(l) = u^*$ for any scaling factor b. The fact that the scaling dimension of

the longitudinal field on the bottom row y_u is equal to the spatial dimensionality of the system $d = 1$ indicates that the phase transition is of first order, because the correlation function on the bottom row at the critical point does not decay:

$$G_{\mathrm{b}i,\mathrm{b}j} := \langle \hat{Z}_{\mathrm{b},i} \hat{Z}_{\mathrm{b},j} \rangle_{u=\overline{u}_{\gamma,\xi}} \sim |i-j|^{-2(d-y_u)} = 1, \tag{5.117}$$

where $\langle \cdots \rangle_{u=\overline{u}_{\gamma,\xi}}$ denotes the expectation value at the critical point $u = \overline{u}_{\gamma,\xi}$ and the approximation is a consequence of the scaling theory [69]. This behavior of the correlation function leads to the value of the anomalous dimension η, one of the critical exponents defined by $G_{\mathrm{b}i,\mathrm{b}j} \sim |i-j|^{2-d-\eta}$:

$$\eta = 2 + d - 2y_u = 2 - d = 1. \tag{5.118}$$

One may point out that the scaling law for a quantum system in general is $G_{\mathrm{b}i,\mathrm{b}j} \sim |i-j|^{-2(d+z-y_u)}$ with z being the dynamic critical exponent [94] (which should not be confused with the variational parameter z) instead of Eq. (5.117). However, we find that $z = 0$ for the present system since a sufficient number of the RG transformations eliminate the transverse field γ and the XX interaction ξ and make the system almost classical.

Consequently, Fig. 5.10(a) demonstrates that there is a first-order phase boundary separating the staggered phase from the columnar phase on the ξ/u-γ/u plane. One of the important features of the phase diagram is that the phase boundary continues to the vertical axis $\gamma = 0$ in each of the upper half $\xi > 0$ and the lower half $\xi < 0$. Notice that the critical points on $\gamma = 0$, $\overline{u}_{\gamma=0,\xi}$, are invariant under the change of the sign of ξ, which reflects the fact that flipping the signs of Ξ_{tt} and Ξ_{bb} in the system without the transverse fields is equivalent to the gauge transformation $(\hat{X}_{a,i}, \hat{Y}_{a,i}, \hat{Z}_{a,i}) \to (-\hat{X}_{a,i}, -\hat{Y}_{a,i}, \hat{Z}_{a,i})$ for $a = \mathrm{t}, \mathrm{b}$ and every odd i.

Now we compare the phase boundary shown in Fig. 5.10(a) with results of two numerical methods. First, the transition point in the case of infinite K and no XX interactions obtained by exact diagonalization of the quantum dimer model of small sizes, whose Hamiltonian is given by Eq. (5.7) with $\Xi_{\mathrm{tt}} = 0$, is $\Gamma_{\mathrm{t}}/U \approx 1/0.6 = 1.66\cdots$ [68] (recall that the frustrated Ising ladder in the limit $K \to \infty$ is equivalent to the quantum dimer model). Remarkably, the value derived from our method $\Gamma_{\mathrm{t}}/U = \gamma/\overline{u}_{\gamma,\xi=0} = 1.9314900$ is not far from the result of numerical diagonalization in spite of the fact that the real-space RG analysis we carried out is not an exact method.

Second, Sota and Yunoki [70] revealed the phase diagram of the frustrated Ising ladder of length $L = 20$ with the uniform transverse field ($\Gamma_{\mathrm{t}} = \Gamma_{\mathrm{b}}$) and the non-stoquastic XX interaction on the top row ($\Xi_{\mathrm{tt}} < 0$ and $\Xi_{\mathrm{bb}} = \Xi_{\mathrm{tb}} = 0$) for $K/U = 5$, which is displayed in Fig. 5.10(b). They numerically computed the first-order transition points by the density-matrix renormalization group (DMRG) method [95]. It is noteworthy that the shapes of the phase boundaries obtained by our method and the DMRG method, namely the lower half of Fig. 5.10(a) vertically inverted and Fig. 5.10(b), resemble each other, though the former is for infinite K and the latter for finite K.

We finally discuss the implications of our result for quantum annealing. We showed that the first-order transition of the frustrated Ising ladder in the dimer limit persists as the XX interactions are implemented, unfortunately. Since our RG analysis with the perturbation theory predicts the behavior of the system at leading order in $1/K$, it is also expected that the first-order transition is unavoidable for large but finite K, which is partly shown by the DMRG result [70] (see Fig. 5.10(b)). This implies that the minimum energy gap in quantum annealing of the frustrated Ising ladder for large K is exponentially small as a function of the length L, which becomes strictly zero in the limit $K \to \infty$ as explained in Section 5.2.

Let us explore the possibility of opening the energy gap through the XX interactions, although it is exponentially small. More specifically, we make a rough prediction about whether the XX interactions reduce the decay rate of the minimum energy gap in quantum annealing as a function of the system size L. To do this, we assume the following annealing schedule for the time-dependent couplings:

$$K = Cs, \quad U = s, \quad \Gamma_{\rm t} = 1 - s, \quad \Xi_{\rm tt} = xs(1-s), \tag{5.119}$$

where C and x are constants and $s \in [0, 1]$ is the dimensionless time. The limit $C \to \infty$ corresponds to the dimer limit. The parametrization

$$s = \frac{U}{U + \Gamma_{\rm t}} = \frac{u}{u + \gamma}, \quad x = \frac{\Xi_{\rm tt}(U + \Gamma_{\rm t})}{U\Gamma_{\rm t}} = \frac{\xi(u + \gamma)}{u\gamma} \tag{5.120}$$

allows us to convert the phase diagram on the ξ/u-γ/u plane in the limit $K \to \infty$ depicted in Fig. 5.10(a) into that on the s-x plane in the limit $C \to \infty$, which is shown in Fig. 5.11(a). It turns out that for any $x \in \mathbb{R}$ there is a unique s at which the first-order transition occurs (to be denoted by $\overline{s}_x$). Since there are first-order transitions on $\gamma = 0$ with ξ finite (positive and negative), the limits of s in infinite $|x|$ are given by $\lim_{x \to \pm\infty} \overline{s}_x = 1$.

We regard Fig. 5.11(a) as the leading-order approximation in $1/C$ to the phase diagram of the frustrated Ising ladder with large but finite C. Then, causing the first-order transition at earlier time s lowers the strength of the frustration at the transition, $K = Cs$, and may be expected to soften the avoided crossing between the two lowest energy levels and to mitigate the decay of the energy gap at the transition as a function of L. Indeed, the inset of Fig. 5.2 depicted by Laumann *et al.* [68] indicates that lowering the strength of the frustration K decreases the decay rate of the energy gap in the case of the uniform transverse field and no XX interactions.

Let us focus on the vicinity of the minimum of the curve $\overline{s}_x$ as can be seen in Fig. 5.11(b). We find that $\overline{s}_x$ is minimized at $x \approx -1.5$, where $\overline{s}_x \approx 0.3330$ is slightly smaller than $\overline{s}_{x=0} = 0.3411$ in the case of no XX interactions. As a result, the non-stoquastic XX interaction on the top row with the appropriate strength x advances the time $\overline{s}_x$ when the first-order transition occurs, possibly reducing the decay rate of the energy gap at the transition as a function of the system size L.

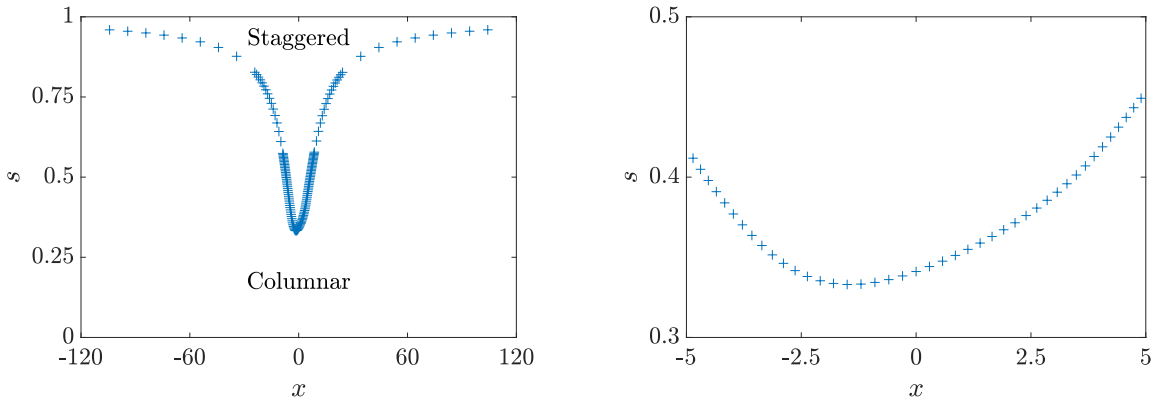

(a) (b)

Figure 5.11: (a) Phase diagram of the frustrated Ising ladder in the dimer limit $C \to \infty$ on the s-x plane. The blue plus signs indicate first-order transition points. The phase boundary extends to $(x, s) = (\pm\infty, 1)$. (b) Enlargement of (a) near the point at which the critical s is minimized as a function of x.

A similar discussion is found for a geometrically local Ising model on connected two rings which was studied by Albash [42]. The problem Hamiltonian of this model contains large couplings and a small coupling which separates the energy levels between the ground and first excited states. Albash showed by numerical diagonalization of the small-size systems that non-stoquastic XX interactions added to the driver Hamiltonian make the minimum energy gap in quantum annealing larger than that in the case without XX interactions and that in the case with stoquastic XX interactions. He argued that the softening of the avoided level crossing with the non-stoquastic driver may partly be explained by the perturbation theory, which predicts that the driver Hamiltonian with the non-stoquastic XX interactions causes the level crossing earlier than that with the stoquastic XX interactions.

Although for the frustrated Ising ladder the difference in $\overline{s}_x$ between the optimal non-stoquastic XX interaction $x \approx -1.5$, its stoquasticized interaction $x \approx 1.5$, and no XX interaction $x = 0$ is small, it is notable that we obtained the result which implies that the driver Hamiltonian including the non-stoquastic XX interaction on the top row with the appropriate strength might enjoy a slight computational advantage in quantum annealing over the stoquastic drivers.

5.6 Summary

We have analyzed the frustrated Ising ladder with transverse fields and XX interactions in the dimer limit by the real-space RG method with the variational ansatz. We obtained the phase diagram which indicates that we cannot avoid the first-order transition for large

frustration, with the help of the scaling theory. Our results are comparable with the two numerical results: First, the transition point in the case of no XX interactions is not far from the result of numerical diagonalization [68]. Second, the shape of the phase diagram in the case of the non-stoquastic XX interaction on the top row resembles that obtained by the DMRG calculation for a finite amplitude of the frustration [70]. We further predicted that the non-stoquastic XX interaction on the top row might have a slight computational advantage in quantum annealing, by focusing on the time of the transition.

Chapter 6

Conclusion

We have studied the phase transitions of the three quantum Ising models with the ultimate goal of revealing when non-stoquastic drivers gain increased performance of quantum annealing compared to stoquastic drivers which contain the stoquasticized drivers (namely, the operators with off-diagonal elements replaced by their absolute values times minus one) and homogeneous or inhomogeneous transverse-field drivers. The Hamiltonian of each model consists of longitudinal fields and ZZ interactions as well as transverse fields and XX interactions.

The first and second models are two types of the weak-strong cluster model. In these models, the ZZ interactions are ferromagnetically applied and the longitudinal fields in the weak and strong clusters have opposite directions and different strengths. This structure of the problem causes a first-order phase transition in the absence of the XX interactions or the inhomogeneity in the transverse field. The difference between the two models is the connectivity between the clusters: One has mean-field-type all-to-all interactions between the clusters and the other has sparse interactions.

We analyzed the weak-strong cluster model with all-to-all interactions between the clusters by a semi-classical method and found that non-stoquastic or stoquastic XX interactions can remove the first-order transition. More precisely, we first showed that the transition disappears if a non-stoquastic XX interaction is appended between the clusters with an appropriate strength while the transition persists if the XX interaction is stoquastic, which is consistent with the already known result of numerical diagonalization of the finite-size systems [42]. We also calculated the energy gap in the thermodynamic limit analytically and identified the optimal strength of the non-stoquastic intercluster XX interaction which maximizes the minimum energy gap. The result again confirms the consequence of the numerical study [42]. In addition to the non-stoquastic XX interaction between the clusters, we found other protocols to eliminate the first-order transition, namely, a non-stoquastic XX interaction in the strong cluster, a stoquastic XX interaction in the weak cluster, and inhomogeneous transverse-field driving in which the transverse field is weaker in the strong cluster or stronger in the weak cluster.

We next investigated the model with sparse interactions between the clusters by eval-

uating the partition function in the thermodynamic limit and the zero-temperature limit. Then, we found generally similar results as in the case with all-to-all interactions, except that a stoquastic XX interaction between the clusters as well as a non-stoquastic one can remove the first-order transition.

Significantly, the results for the weak-strong cluster models are rare examples of two-body interacting systems for which the removal of first-order transitions with XX interactions or an inhomogeneous transverse field has been shown analytically. From the viewpoint of comparison between non-stoquastic and stoquastic Hamiltonians, it is noteworthy that the non-stoquastic intercluster XX interaction with the appropriate strength outperforms the stoquastic one and the uniform transverse-field driver in quantum annealing of the mean-field model. For the model with sparse intercluster interactions, there is almost no difference in the efficiency of quantum annealing between the driver Hamiltonians with the non-stoquastic and stoquastic intercluster XX interactions.

A nice property of the XX interaction between the clusters is that it is symmetric under the interchange of the two clusters. Although we presented other types of driver (namely, the XX interaction within one of the clusters and the inhomogeneous transverse field whose value depends on the clusters), they are not symmetric under the interchange of the clusters, which means that more information about the problem is reflected. In this sense, the fact that the non-stoquastic XX interaction between the clusters eliminates the first-order transition in both of the two weak-strong cluster models is important.

The last model we analyzed is the frustrated Ising ladder with the transverse fields and the XX interactions. We carried out the real-space renormalization group analysis which applies to the limit of the large frustration. In this limit, the model is equivalent to the quantum dimer model. Obtaining the critical exponent which indicates a first-order transition, we showed that the first-order transition is unavoidable in quantum annealing with the XX interactions, whether they are non-stoquastic or stoquastic. Despite the fact that the real-space renormalization group method is not exact, the transition point in the case of no XX interactions is not far from that obtained by numerical diagonalization [68] and the phase diagram in the case of the non-stoquastic XX interaction on the top row has a similar shape to that derived from the density-matrix renormalization group calculation for a finite strength of the frustration [70]. We also pointed out that the non-stoquastic XX interaction on the top row might reduce the exponential decay rate of the energy gap at the transition as a function of the system size.

It is significant that the frustrated Ising ladder is an example of a model with sparse connectivity in which the non-stoquastic Hamiltonian possibly has an advantage over the stoquastic Hamiltonians, though the energy gap closes exponentially as a function of the length in any case considered. Although the first-order transition persists for the present model, our real-space renormalization group method, which is in agreement with the numerical methods at least qualitatively, may shed new light on the way to analyze spin systems with sparse couplings. Finding a low-dimensional model whose first-order transition is removed or reduced to a second-order transition by a non-stoquastic

interaction is one of the possible future directions toward realization of efficient quantum annealing with non-stoquasticity, in which the real-space renormalization group approach might be useful.

It is generally difficult to determine the optimal strength and position of a non-stoquastic interaction to enhance the performance of quantum annealing for a given real-world optimization problem. However, our results imply that introduction of XX interactions with adjustable signs and strengths as well as an inhomogeneous transverse field is likely to be useful in the design of hardware of quantum annealing. To better understand the effects of non-stoquastic interactions, analytical and numerical studies of many other problems are highly desired, especially in the cases of sparse connectivity to represent realistic situations.

List of publications

[A] K. Takada, Y. Yamashiro, and H. Nishimori, Mean-field solution of the weak-strong cluster problem for quantum annealing with stoquastic and non-stoquastic catalysts, arXiv:1912.09189, to be published in J. Phys. Soc. Jpn.

[B] H. Nishimori and K. Takada, Exponential enhancement of the efficiency of quantum annealing by non-stoquastic Hamiltonians, Frontiers in ICT **4**, 2 (2017).

[C] K. Takada and H. Nishimori, Critical properties of dissipative quantum spin systems in finite dimensions, J. Phys. A: Math. Theor. **49**, 435001 (2016).

References

[1] H. Nishimori, *Statistical Physics of Spin Glasses and Information Processing: An Introduction* (Oxford University Press, Oxford, United Kingdom, 2001).

[2] A. Perdomo-Ortiz, N. Dickson, M. Drew-Brook, G. Rose, and A. Aspuru-Guzik, Finding low-energy conformations of lattice protein models by quantum annealing, Sci. Rep. **2**, 571 (2012).

[3] T. Kadowaki and H. Nishimori, Quantum annealing in the transverse Ising model, Phys. Rev. E **58**, 5355 (1998).

[4] J. Brooke, D. Bitko, T. F. Rosenbaum, and G. Aeppli, Quantum annealing of a disordered magnet, Science **284**, 779 (1999).

[5] G. E. Santoro, R. Martoňák, E. Tosatti, and R. Car, Theory of quantum annealing of an Ising spin glass, Science **295**, 2427 (2002).

[6] G. E. Santoro and E. Tosatti, Optimization using quantum mechanics: quantum annealing through adiabatic evolution, J. Phys. A: Math. Gen. **39**, R393 (2006); *corrigendum*: J. Phys. A: Math. Theor. **41**, 209801 (2008).

[7] A. Das and B. K. Chakrabarti, *Colloquium*: Quantum annealing and analog quantum computation, Rev. Mod. Phys. **80**, 1061 (2008).

[8] S. Morita and H. Nishimori, Mathematical foundation of quantum annealing, J. Math. Phys. **49**, 125210 (2008).

[9] P. Hauke, H. G. Katzgraber, W. Lechner, H. Nishimori, and W. D. Oliver, Perspectives of quantum annealing: Methods and implementations, arXiv:1903.06559.

[10] M. W. Johnson, M. H. S. Amin, S. Gildert, T. Lanting, F. Hamze, N. Dickson, R. Harris, A. J. Berkley, J. Johansson, P. Bunyk, E. M. Chapple, C. Enderud, J. P. Hilton, K. Karimi, E. Ladizinsky, N. Ladizinsky, T. Oh, I. Perminov, C. Rich, M. C. Thom, E. Tolkacheva, C. J. S. Truncik, S. Uchaikin, J. Wang, B. Wilson, and G. Rose, Quantum annealing with manufactured spins, Nature **473**, 194 (2011).

[11] E. Farhi, J. Goldstone, S. Gutmann, J. Lapan, A. Lundgren, and D. Preda, A quantum adiabatic evolution algorithm applied to random instances of an NP-complete problem, Science **292**, 472 (2001).

[12] T. Albash and D. A. Lidar, Adiabatic quantum computation, Rev. Mod. Phys. **90**, 015002 (2018).

[13] S. Suzuki, J. Inoue, and B. K. Chakrabarti, *Quantum Ising Phases and Transitions in Transverse Ising Models* (Springer Berlin Heidelberg, 2013).

[14] T. F. Rønnow, Z. Wang, J. Job, S. Boixo, S. V. Isakov, D. Wecker, J. M. Martinis, D. A. Lidar, and M. Troyer, Defining and detecting quantum speedup, Science **345**, 420 (2014).

[15] S. Mandrà, Z. Zhu, W. Wang, A. Perdomo-Ortiz, and H. G. Katzgraber, Strengths and weaknesses of weak-strong cluster problems: A detailed overview of state-of-the-art classical heuristics versus quantum approaches, Phys. Rev. A **94**, 022337 (2016).

[16] L. K. Grover, Quantum mechanics helps in searching for a needle in a haystack, Phys. Rev. Lett. **79**, 325 (1997).

[17] P. W. Shor, Algorithms for quantum computation: discrete logarithms and factoring, in *Proceedings 35th Annual Symposium on Foundations of Computer Science*, p. 124 (IEEE, Santa Fe, NM, USA, 1994).

[18] P. W. Shor, Polynomial-time algorithms for prime factorization and discrete logarithms on a quantum computer, SIAM J. Comput. **26**, 1484 (1997).

[19] S. Kirkpatrick, C. D. Gelatt, and M. P. Vecchi, Optimization by simulated annealing, Science **220**, 671 (1983).

[20] R. Martoňák, G. E. Santoro, and E. Tosatti, Quantum annealing by the path-integral Monte Carlo method: The two-dimensional random Ising model, Phys. Rev. B **66**, 094203 (2002).

[21] S. Bravyi, D. P. Divincenzo, R. Oliveira, and B. M. Terhal, The complexity of stoquastic local Hamiltonian problems, Quantum Inf. Comput. **8**, 361 (2008).

[22] M. Suzuki, Relationship between d-dimensional quantal spin systems and $(d+1)$-dimensional Ising systems: Equivalence, critical exponents and systematic approximants of the partition function and spin correlations, Prog. Theor. Phys. **56**, 1454 (1976).

[23] S. Boixo, T. F. Rønnow, S. V. Isakov, Z. Wang, D. Wecker, D. A. Lidar, J. M. Martinis, and M. Troyer, Evidence for quantum annealing with more than one hundred qubits, Nature Phys. **10**, 218 (2014).

[24] E. Crosson and M. Deng, Tunneling through high energy barriers in simulated quantum annealing, arXiv:1410.8484.

[25] L. T. Brady and W. van Dam, Quantum Monte Carlo simulations of tunneling in quantum adiabatic optimization, Phys. Rev. A **93**, 032304 (2016).

[26] S. Muthukrishnan, T. Albash, and D. A. Lidar, Tunneling and speedup in quantum optimization for permutation-symmetric problems, Phys. Rev. X **6**, 031010 (2016).

[27] V. S. Denchev, S. Boixo, S. V. Isakov, N. Ding, R. Babbush, V. Smelyanskiy, J. Martinis, and H. Neven, What is the computational value of finite-range tunneling?, Phys. Rev. X **6**, 031015 (2016).

[28] E. Crosson and A. W. Harrow, Simulated quantum annealing can be exponentially faster than classical simulated annealing, in *2016 IEEE 57th Annual Symposium on Foundations of Computer Science (FOCS)*, p. 714 (IEEE, New Brunswick, NJ, USA, 2016).

[29] S. V. Isakov, G. Mazzola, V. N. Smelyanskiy, Z. Jiang, S. Boixo, H. Neven, and M. Troyer, Understanding quantum tunneling through quantum Monte Carlo simulations, Phys. Rev. Lett. **117**, 180402 (2016).

[30] M. B. Hastings and M. H. Freedman, Obstructions to classically simulating the quantum adiabatic algorithm, Quantum Inf. Comput. **13**, 1038 (2013).

[31] M. Jarret, S. P. Jordan, and B. Lackey, Adiabatic optimization versus diffusion Monte Carlo methods, Phys. Rev. A **94**, 042318 (2016).

[32] A. M. Childs, R. Cleve, E. Deotto, E. Farhi, S. Gutmann, and D. A. Spielman, Exponential algorithmic speedup by a quantum walk, in *Proceedings of the Thirty-Fifth Annual ACM Symposium on Theory of Computing*, p. 59, STOC '03 (Association for Computing Machinery, New York, NY, USA, 2003).

[33] R. D. Somma, D. Nagaj, and M. Kieferová, Quantum speedup by quantum annealing, Phys. Rev. Lett. **109**, 050501 (2012).

[34] L. Gupta and I. Hen, Elucidating the interplay between non-stoquasticity and the sign problem, arXiv:1910.13867.

[35] E. Farhi, J. Goldstone, and S. Gutmann, Quantum adiabatic evolution algorithms with different paths, arXiv:quant-ph/0208135.

[36] E. Crosson, E. Farhi, C. Yen-Yu Lin, H.-H. Lin, and P. Shor, Different strategies for optimization using the quantum adiabatic algorithm, arXiv:1401.7320.

[37] L. Hormozi, E. W. Brown, G. Carleo, and M. Troyer, Nonstoquastic Hamiltonians and quantum annealing of an Ising spin glass, Phys. Rev. B **95**, 184416 (2017).

[38] Y. Seki and H. Nishimori, Quantum annealing with antiferromagnetic fluctuations, Phys. Rev. E **85**, 051112 (2012).

[39] B. Seoane and H. Nishimori, Many-body transverse interactions in the quantum annealing of the p-spin ferromagnet, J. Phys. A: Math. Theor. **45**, 435301 (2012).

[40] Y. Seki and H. Nishimori, Quantum annealing with antiferromagnetic transverse interactions for the Hopfield model, J. Phys. A: Math. Theor. **48**, 335301 (2015).

[41] H. Nishimori and K. Takada, Exponential enhancement of the efficiency of quantum annealing by non-stoquastic Hamiltonians, Frontiers in ICT **4**, 2 (2017).

[42] T. Albash, Role of nonstoquastic catalysts in quantum adiabatic optimization, Phys. Rev. A **99**, 042334 (2019).

[43] E. Farhi, J. Goldstone, and S. Gutmann, Quantum adiabatic evolution algorithms versus simulated annealing, arXiv:quant-ph/0201031.

[44] S. Boixo, V. N. Smelyanskiy, A. Shabani, S. V. Isakov, M. Dykman, V. S. Denchev, M. H. Amin, A. Y. Smirnov, M. Mohseni, and H. Neven, Computational multiqubit tunnelling in programmable quantum annealers, Nat. Commun. **7**, 10327 (2016).

[45] M. A. Nielsen and I. L. Chuang, *Quantum Computation and Quantum Information: 10th Anniversary Edition* (Cambridge University Press, Cambridge, United Kingdom, 2010).

[46] E. Farhi, J. Goldstone, S. Gutmann, and M. Sipser, Quantum computation by adiabatic evolution, arXiv:quant-ph/0001106.

[47] W. van Dam, M. Mosca, and U. Vazirani, How powerful is adiabatic quantum computation?, in *Proceedings of the 42nd IEEE Symposium on Foundations of Computer Science*, p. 279, FOCS '01 (IEEE Computer Society, Newport Beach, CA, USA, 2001).

[48] D. Aharonov, W. van Dam, J. Kempe, Z. Landau, S. Lloyd, and O. Regev, Adiabatic quantum computation is equivalent to standard quantum computation, SIAM J. Comput. **37**, 166 (2007).

[49] J. D. Biamonte and P. J. Love, Realizable Hamiltonians for universal adiabatic quantum computers, Phys. Rev. A **78**, 012352 (2008).

[50] S. P. Jordan, D. Gosset, and P. J. Love, Quantum-Merlin-Arthur–complete problems for stoquastic Hamiltonians and Markov matrices, Phys. Rev. A **81**, 032331 (2010).

[51] K. Fujii, Quantum speedup in stoquastic adiabatic quantum computation, arXiv:1803.09954.

[52] I. Ozfidan, C. Deng, A. Y. Smirnov, T. Lanting, R. Harris, L. Swenson, J. Whittaker, F. Altomare, M. Babcock, and C. Baron, Demonstration of nonstoquastic Hamiltonian in coupled superconducting flux qubits, arXiv:1903.06139.

[53] M. M. Rams, M. Mohseni, and A. del Campo, Inhomogeneous quasi-adiabatic driving of quantum critical dynamics in weakly disordered spin chains, New J. Phys. **18**, 123034 (2016).

[54] M. Mohseni, J. Strumpfer, and M. M. Rams, Engineering non-equilibrium quantum phase transitions via causally gapped Hamiltonians, New J. Phys. **20**, 105002 (2018).

[55] E. Farhi, J. Goldstone, D. Gosset, S. Gutmann, H. B. Meyer, and P. Shor, Quantum adiabatic algorithms, small gaps, and different paths, Quantum Inf. Comput. **11**, 181 (2011).

[56] N. G. Dickson and M. H. S. Amin, Does adiabatic quantum optimization fail for NP-complete problems?, Phys. Rev. Lett. **106**, 050502 (2011).

[57] N. G. Dickson and M. H. Amin, Algorithmic approach to adiabatic quantum optimization, Phys. Rev. A **85**, 032303 (2012).

[58] Y. Susa, Y. Yamashiro, M. Yamamoto, and H. Nishimori, Exponential speedup of quantum annealing by inhomogeneous driving of the transverse field, J. Phys. Soc. Jpn. **87**, 023002 (2018).

[59] Y. Susa, Y. Yamashiro, M. Yamamoto, I. Hen, D. A. Lidar, and H. Nishimori, Quantum annealing of the p-spin model under inhomogeneous transverse field driving, Phys. Rev. A **98**, 042326 (2018).

[60] A. Hartmann and W. Lechner, Quantum phase transition with inhomogeneous driving in the Lechner-Hauke-Zoller model, Phys. Rev. A **100**, 032110 (2019).

[61] T. Lanting, A. D. King, B. Evert, and E. Hoskinson, Experimental demonstration of perturbative anticrossing mitigation using nonuniform driver Hamiltonians, Phys. Rev. A **96**, 042322 (2017).

[62] J. I. Adame and P. L. McMahon, Inhomogeneous driving in quantum annealers can result in orders-of-magnitude improvements in performance, arXiv:1806.11091.

[63] A. Perdomo-Ortiz, S. E. Venegas-Andraca, and A. Aspuru-Guzik, A study of heuristic guesses for adiabatic quantum computation, Quantum Inf. Process. **10**, 33 (2011).

[64] N. Chancellor, Modernizing quantum annealing using local searches, New J. Phys. **19**, 023024 (2017).

[65] M. Ohkuwa, H. Nishimori, and D. A. Lidar, Reverse annealing for the fully connected p-spin model, Phys. Rev. A **98**, 022314 (2018).

[66] Y. Yamashiro, M. Ohkuwa, H. Nishimori, and D. A. Lidar, Dynamics of reverse annealing for the fully connected p-spin model, Phys. Rev. A **100**, 052321 (2019).

[67] A. D. King, J. Carrasquilla, J. Raymond, I. Ozfidan, E. Andriyash, A. Berkley, M. Reis, T. Lanting, R. Harris, F. Altomare, K. Boothby, P. I. Bunyk, C. Enderud, A. Fréchette, E. Hoskinson, N. Ladizinsky, T. Oh, G. Poulin-Lamarre, C. Rich, Y. Sato, A. Y. Smirnov, L. J. Swenson, M. H. Volkmann, J. Whittaker, J. Yao, E. Ladizinsky, M. W. Johnson, J. Hilton, and M. H. Amin, Observation of topological phenomena in a programmable lattice of 1,800 qubits, Nature **560**, 456 (2018).

[68] C. R. Laumann, R. Moessner, A. Scardicchio, and S. L. Sondhi, Quantum adiabatic algorithm and scaling of gaps at first-order quantum phase transitions, Phys. Rev. Lett. **109**, 030502 (2012).

[69] H. Nishimori and G. Ortiz, *Elements of Phase Transitions and Critical Phenomena* (Oxford University Press, Oxford, United Kingdom, 2011).

[70] S. Sota and S. Yunoki, private communication (2019).

[71] K. Takada, Y. Yamashiro, and H. Nishimori, Mean-field solution of the weak-strong cluster problem for quantum annealing with stoquastic and non-stoquastic catalysts, arXiv:1912.09189, to be published in J. Phys. Soc. Jpn.

[72] J. J. Hopfield and D. W. Tank, Computing with neural circuits: a model, Science **233**, 625 (1986).

[73] A. Lucas, Ising formulations of many NP problems, Frontiers in Phys. **2**, 1 (2014).

[74] R. Harris, J. Johansson, A. J. Berkley, M. W. Johnson, T. Lanting, S. Han, P. Bunyk, E. Ladizinsky, T. Oh, I. Perminov, E. Tolkacheva, S. Uchaikin, E. M. Chapple, C. Enderud, C. Rich, M. Thom, J. Wang, B. Wilson, and G. Rose, Experimental demonstration of a robust and scalable flux qubit, Phys. Rev. B **81**, 134510 (2010).

[75] R. Harris, M. W. Johnson, T. Lanting, A. J. Berkley, J. Johansson, P. Bunyk, E. Tolkacheva, E. Ladizinsky, N. Ladizinsky, T. Oh, F. Cioata, I. Perminov, P. Spear, C. Enderud, C. Rich, S. Uchaikin, M. C. Thom, E. M. Chapple, J. Wang, B. Wilson, M. H. S. Amin, N. Dickson, K. Karimi, B. Macready, C. J. S. Truncik, and G. Rose, Experimental investigation of an eight-qubit unit cell in a superconducting optimization processor, Phys. Rev. B **82**, 024511 (2010).

[76] O. V. Lounasmaa, *Experimental Principles and Methods below* 1 K (Academic Press, London, United Kingdom, 1974).

[77] A. J. Leggett, S. Chakravarty, A. T. Dorsey, M. P. A. Fisher, A. Garg, and W. Zwerger, Dynamics of the dissipative two-state system, Rev. Mod. Phys. **59**, 1 (1987).

[78] P. Pfeuty, The one-dimensional Ising model with a transverse field, Ann. Phys. **57**, 79 (1970).

[79] G. G. Cabrera and R. Jullien, Role of boundary conditions in the finite-size Ising model, Phys. Rev. B **35**, 7062 (1987).

[80] J. Tsuda, Y. Yamanaka, and H. Nishimori, Energy gap at first-order quantum phase transitions: An anomalous case, J. Phys. Soc. Jpn. **82**, 114004 (2013).

[81] N. Metropolis, A. W. Rosenbluth, M. N. Rosenbluth, A. H. Teller, and E. Teller, Equation of state calculations by fast computing machines, J. Chem. Phys. **21**, 1087 (1953).

[82] T. Jörg, F. Krzakala, J. Kurchan, A. C. Maggs, and J. Pujos, Energy gaps in quantum first-order mean-field–like transitions: The problems that quantum annealing cannot solve, Europhys. Lett. **89**, 40004 (2010).

[83] V. Bapst and G. Semerjian, On quantum mean-field models and their quantum annealing, J. Stat. Mech.: Theor. Exp. **2012**, P06007 (2012).

[84] G. A. Durkin, Quantum speedup at zero temperature via coherent catalysis, Phys. Rev. A **99**, 032315 (2019).

[85] M. Filippone, S. Dusuel, and J. Vidal, Quantum phase transitions in fully connected spin models: An entanglement perspective, Phys. Rev. A **83**, 022327 (2011).

[86] T. Holstein and H. Primakoff, Field dependence of the intrinsic domain magnetization of a ferromagnet, Phys. Rev. **58**, 1098 (1940).

[87] A. Garg, Application of the discrete Wentzel–Kramers–Brillouin method to spin tunneling, J. Math. Phys. **39**, 5166 (1998).

[88] A. Garg, E. Kochetov, K.-S. Park, and M. Stone, Spin coherent-state path integrals and the instanton calculus, J. Math. Phys. **44**, 48 (2003).

[89] M. Ohkuwa and H. Nishimori, Exact expression of the energy gap at first-order quantum phase transitions of the fully connected p-body transverse-field Ising model with transverse interactions, J. Phys. Soc. Jpn. **86**, 114004 (2017).

[90] D. S. Rokhsar and S. A. Kivelson, Superconductivity and the quantum hard-core dimer gas, Phys. Rev. Lett. **61**, 2376 (1988).

[91] R. Moessner and K. S. Raman, Quantum dimer models, arXiv:0809.3051.

[92] R. Moessner, S. L. Sondhi, and P. Chandra, Two-dimensional periodic frustrated Ising models in a transverse field, Phys. Rev. Lett. **84**, 4457 (2000).

[93] R. Moessner and S. L. Sondhi, Ising models of quantum frustration, Phys. Rev. B **63**, 224401 (2001).

[94] S. Sachdev, *Quantum Phase Transitions*, 2nd ed. (Cambridge University Press, Cambridge, United Kingdom, 2011).

[95] S. R. White, Density-matrix algorithms for quantum renormalization groups, Phys. Rev. B **48**, 10345 (1993).